TECHNISCHE UNIVERSITÄT WIEN

DIPLOMARBEIT

Crystallization Experiments with Enzymes of the Flavonoid Metabolism

zur Erlangung des akademischen Grades

Diplom-Ingenieur

im Rahmen des Studiums

Masterstudium Technische Chemie

eingereicht von

Matthias Hackl
Matrikelnummer 01304757

ausgeführt am Institut für Verfahrenstechnik, Umwelttechnik und technische Biowissenschaften
der Fakultät für Technische Chemie der Technischen Universität Wien
(in Zusammenarbeit mit der Fakultät für Chemie am Institut für Biophysikalische Chemie der Universität Wien)

Betreuung
Betreuer/in: Associate Prof. Dipl.-Ing.in Dr.in techn. Heidi Halbwirth
Mitwirkung: Senior Scientist Dipl.-Ing. Dr.rer.nat. Christian Haselmair-Gosch

Wien, Februar 2025

(Unterschrift Verfasser/in) (Unterschrift Betreuer/in)

Table of Content

Abstract

A polyphenol oxidase (PPO) of the wild strawberry (*Fragaria vesca)*, was successfully heterologously expressed as a fusion protein with GST-Tag or His6-Tag in *Escherichia choli*, respectively. The latter could be purified, after cleavage of the His6-tag, utilizing immobilized metal affinity chromatography (IMAC) and anion exchange chromatography (AEX) to a purity of more than 90 %. The purity was assessed with dynamic light scattering (DLS) and sodium dodecyl sulphate polyacrylamide gel electrophoresis (SDS-PAGE). The goal of this thesis was the determination of protein crystallization conditions that leads to the formation of crystals and to contribute to the protein structure determination with X-ray crystallography. Based on the protein structure an *in-silico* search of natural inhibitors of the enzyme, that decreases the shelf life of processed strawberry food significantly, should be performed.

The molecular weight of the purified enzyme was estimated to be 55 kDa based on a clear single band in SDS-PAGE. Two isosbestic points were identified for the measurement of DOPAchrome at the wavelengths at 524 nm (ε_{524} = (1200 ± 277) $M^{-1}\,cm^{-1}$) and 412 nm for the utilized buffer in the activity assays. The latent enzyme could be classified as tyrosinase, since it exhibited activity for the substrates tyramine with 16.3 U mg^{-1} and dopamine in the presence of SDS. The proenzyme was also activated in the absence of detergents utilizing serine proteinases and in the presence of Mg^{2+} and Ca^{2+} ions, unambiguously.

The results of stability tests, which were based on SDS-PAGE, of thermal shift assays, copper quantifications and DLS indicated that the enzyme´s stability is limited. Therefore, an immediate execution of crystallization experiments after the purification of the latent PPO without a tag identified a promising condition (50 mM sodium citrate, 13 % (w/v) PEG 8000, pH 6.77 (at 22°C)), that produced a crystalline object after 16 days. This very promising candidate was lost in the course of sample preparation for the X-ray crystallization. Further crystallization did not result in the growth of protein crystals and therefore, within the scope of this thesis the protein structure could not be allocated.

Kurzfassung

Ein Isoenzym der Polyphenol Oxidase (PPO) aus der Wald-Erdbeere (*Fragaria vesca)* konnte im Rahmen dieser Arbeit erfolgreich als Fusionsprotein heterolog in *Escherichia choli* exprimiert werden, einerseits mit einem GST-Tag und andererseits mit einem His6-Tag. Die Aufreinigung des Proenzyms nach Abspaltung des His6-Tags erfolgte mittels Immobilisierten-Metallionen-Affinitätschromatographie (IMAC) und Anionenaustausch-chromatographie (AEX). Dies führte zu einer Reinheit von mehr als 90 %, welche mit dynamischer Lichtstreuung (DLS) und Natriumdodecylsulfat-Polyacrylamidgelelektrophorese (SDS-PAGE) beurteilt wurde. Das Ziel der Arbeit war die Auffindung einer Kristallisationsbedingung, die Kristalle für die Strukturaufklärung mittels Röntgenkristallographie erzeugt. Dies sollte in weiter Folge zur *in-silico* Auffindung von potenziellen natürlichen Inhibitoren von Erdbeer-Polyphenol Oxidasen beitragen.

Die Größe des Proteins wurde mit SDS-PAGE auf 55 kDa geschätzt. Im Zuge von Aktivitätstests konnten zwei isosbestische Punkte identifiziert werden. Die isosbestischen Punkte 524 nm (ε_{524} = (1200 ± 277) $M^{-1}\,cm^{-1}$) and 412 nm konnten für den Puffer 50 mM TRIS, pH 7.75 (295.15 K) bei 298.15 K ermittelt werden. Die Tyrosinase-Aktivität der Polyphenol Oxidase konnte für die Substrate L-DOPA, Dopamin und Tyramine (16.3 U mg^{-1}) in der Anwesenheit von SDS bestätigt werden. Das Proenzym zeigte ebenfalls Aktivität in der Abwesenheit von SDS, wenn die zweiwertigen Ionen Mg^{2+} and Ca^{2+} zugegeben wurden, sowie wurde nach dem Einsatz von Proteinase K Aktivität verzeichnet.

Stabilitätstests, der Einsatz von Methoden wie DLS, Thermofluor Assays und die Kupferquantifizierung führten alle zu dem Schluss, dass das Protein eine eingeschränkte Stabilität besitzt. Dies zeigte sich auch in den Kristallisationsversuchen, in denen erst eine potenzielle Bedingung identifiziert werden konnte, nachdem das Protein unmittelbar zur Kristallisation herangezogen verwendet wurde. Nach 16 Tagen Inkubation konnte ein kristallines Objekt in 50 mM Natriumcitrat, 13 % (w/v) PEG 8000 bei pH 6.77 (at 22°C) gefunden werden, dass bei der Messung mittels Röntgenstrahlung verloren gegangen ist. Weitere Kristallisationsversuche führten zu keinen Kristallen im Rahmen dieser Arbeit.

Acknowledgment

Foremost, I want to thank everybody who accompanied and supported me during my studies.

This work was carried out in cooperation of Technische Universität Wien, Universität Wien and was part of a project supported by HiStabJuice. The latter is a European intersectoral and interdisciplinary network, which is relevant to the entire food industry worldwide.

I am very grateful to *Associate Prof. Dipl.-Ing.in Dr.in techn. Heidrun Halbwirth* for the suggestion of the theme of the thesis and the possibility to execute it under her guidance in the *Research Group for Phytochemistry and Biochemistry of Natural Compounds*.

I want to thank *Prof. Dr. rer. nat. Rompel Annette* for her guidance and for the possibility to work in the *Department of Biophysical Chemistry*.

DI. Dr. Matthias Pretzler provided an excellent introduction in the field of crystallization for which I want to thank him. As an early-stage researcher of HiStabJuice *Msc. Zavarise Alberto* had a great impact on this thesis, especially as a guide in protein purification.

Although working on such an intriguing topic the organization included some challenges, when the practical execution of the work had been distributed in between multiple laboratories, which were located at three campuses. However, the unprecedently coordination between the research group, including the measurement and analysis of samples with LC-MS in the research group of *Univ.-Prof. Dr. Christopher Gerner* and the X-ray analysis at the *Core Facility Crystal Structure Analysis* of the University of Vienna, must be emphasized and was something that I really appreciated.

Since the list of people would be too long and there is always danger to forget one name, brevity is the source of wit: I want to thank all members of all research groups, which were present during my work!

Danksagung

An dieser Stelle möchte ich mich bei einem besonderen Menschen in meinem Leben bedanken. Franciska, vielen Dank für deine Unterstützung und für deine liebenswerte Art die mich stets nach vorne schauen lässt. Diese Arbeit wäre ohne dich und all jenen, die mich zu dem Menschen gemacht haben, der ich heute bin, nicht möglich gewesen. Danke Mama, dass du mich stets motiviert und unterstützt hast.

1. Introduction

1.1. The Relevance of Metals in Biological Systems

Metals and metalloids are present in small quantities in living tissue and take a vital role throughout life and death, while latter happens not only in excess but also in absence of metals. Trace metals emerge in different forms as macro or microelements. They act as structural components, signal transmitters, electron donors, participate in stabilisation of nucleotide bases and resemble the cell´s ion balance [1], [2], [3].

The highly flexible coordination spheres, the strong Lewis acid character, a redox activity and the ability to activate nucleophilic amino acid residues and substrate molecules underline the importance of metals as catalysts in protein systems. Metal ions are often located in the active site of the biocatalysts and are coordinated by amino acid residues and by water molecules. The latter usually participates in the catalytic reaction, in which also a change of the metal oxidation state occurs [4]. The functionality of approximately one third of all enzymes depends on metal ions [5].

1.1.1. Copper Proteins

The advent of copper and also iron in the biosphere happened when an enrichment of O_2 in the atmosphere took place in history. This event could provide an explanation to the development of many copper enzymes that use O_2 as substrate and therefore, has enabled living systems to manage a potentially noxious gas. Copper is also strongly involved in iron absorption, transport, and metabolism[6]. Both metals are related to oxygen transport based on the findings in hemocyanin (copper) and hemoglobin/hemerythrin (iron) [7].

Copper proteins, can introduce O_2 in substrates as oxygenases, exhibit antioxidant activity as superoxide dismutase or can cause pigmentation [6]. They play a critical role in aerobic respiration and photosynthesis, where copper is found in the electron transport chain, in cytochrome c oxidase. In the course of the electron transport the copper ions switch between the two oxidation states that are possible in biological systems Cu(+I) and Cu(+II) [8]. Complex IV transports overall 4 electrons over a binuclear Cu_A center to a Cu_B -cytochrome a_3(Fe) binding site, that tethers O_2 [9]. The ligand composition and geometry of the metal center leads to a differentiation between Cu_A , Cu_B and Cu_Z centers. A further classification of cuproproteins is based on spectral signals in electron paramagnetic resonance (EPR) and UV/Vis measurements into Type I (EPR and UV/Vis signal), Type II(no UV/Vis signal) and Type III copper (no EPR signal) centers [10].

1.1.2. Type III Copper Center

In contrast to type I and type II, the type III copper center is binuclear, consisting of two copper ions labeled as Cu(A) and Cu(B) [11]. Both metals form a three-dimensional active site with the imidazole nitrogen of three coordinated histidine residues[12]. The Cu ions in the active center can have oxidation states between +I and +II and Cu(A) and Cu(B) are in a proximity of 2.8-4.6 Å depending on the state of the active center in the *deoxy*, *met* or *oxy* form as it is shown in Figure 1. The *met*-form is referred to the resting state of the protein before reacting with an *o*-diphenol, followed by a conversion to the *deoxy*-form. The presence of molecular oxygen leads to the formation of the *oxy*-form, which exhibits a characteristic charge transfer band at 345 nm (O_2^{2-} (π_{σ}^{*}) → Cu^{2+} (d_{x2-y2})) and one at 580 nm (O_2^{2-} (π_{ν}^{*}) → Cu^{2+} (d_{x2-y2})) with an approximated 20-fold weaker absorption. The active site is surrounded by 4 alpha helices, which are conserved among all members of type III copper proteins. Prominent examples are hemocyanines and laccases, as well as polyphenol oxidases [13].

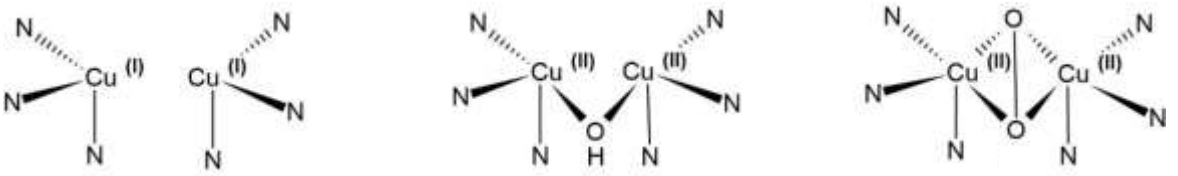

Figure 1 From left to right: deoxy-, met- and oxy-form of type III copper center. Based on [13]. Graphic created with [14].

1.2. Polyphenol Oxidase (PPO)

The term polyphenol oxidase (PPO) comprises the oxidoreductases tyrosinase (EC 1.14.18.1), catechol oxidase (EC 1.10.3.1), aureusidin synthase (EC 1.21.3.6) [15], [16], [17]. The enzymes in this group possess a dinuclear copper center, which is classified as type III copper center [13].

In the presence of molecular oxygen tyrosinases exhibit monophenolase activity by catalysing the hydroxylation of monophenols to *ortho*-diphenols, but also diphenolase activity, when the respective *o*-diphenols are subsequently oxidised to the respective *o*-quinones. Catechol oxidases possess only diphenolase activity [13]. Aurone synthase shows monophenolase activity towards chalcone substrates and is therefore functionally different compared to the other two oxidoreductases. It takes an role in the formation of aurones, the yellow plant flavonoid [18]. An overview of the tyrosinase and catechol oxidase reaction is depicted in Figure 2.

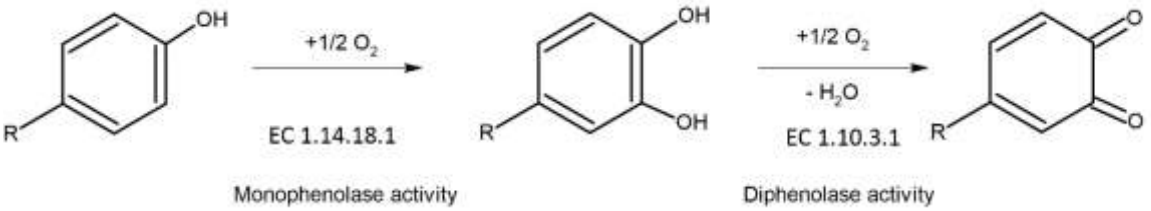

Figure 2 Overview of tyrosinase and catechol oxidase general reaction: The *ortho* hydroxylation of a monophenol is catalysed by tyrosinase, as well as the oxidation of the respective *ortho*-diphenol to the *ortho*-quinone. Catechol oxidase can only catalyze the oxidation to the *ortho*-quinone utilizing *ortho*-diphenols as substrate. Based on [13]; Graphic created with [14].

1.2.1. Structure of Latent PPOs

When PPOs are expressed *in vivo*, they are latent pro-enzymes consisting of three domains: a signal peptide at the N-terminus (usual size of approx. 4-9 kDa), a catalytical domain (approx. 40 kDa) containing the active site and a shielding domain located at the C-terminus (approx. 19 kDa) [13].

The majority of plant PPOs possess a chloroplast transit peptide and a thylakoid transfer domain at the N-terminus, which are assumed to mediate the transport of the protein to the chloroplast and to the thylakoid membrane [15]. While a N-terminal signal peptide is typical for PPOs, Aguilera et al. [11] describes two ancient gene duplication events that have led to the introduction of cysteine rich segments in this domain. This changes its interaction behavior with proteins, or its restitution, so that the location of the PPO in the cell can be redirected. Although PPOs are membrane associated, they are not integrated into it [19].

The shielding domain generally hinders the substrate of accessing the active site and therefore plays an important role in the enzyme´s activity and the activation of the mature pro-enzyme, respectively [20]. The blocking of the active center is subject to many theories including the “blocker residue”, meaning that the presence of a phenylalanine in the proximity of Cu(A) is preventing the access of the substrate [21]. Bijelic et al. [22] suggests that amino acid residues in the proximity of about 8 Å of the active center, influence the substrate binding. Panis et al. [23] could show that the tyrosinase activity of PPO in walnut leaves can be altered to catechol oxidase activity by the mutation of non conserved activity controlling amino acids and the blocker residue. The residues of the substrate binding site around the copper center vary among the PPO family, indicating that individual natural substrates occur for many of the PPOs in different species [13].

1.2.2. Activation of PPO

The *in vitro* activation of the proenzyme PPO can be achieved by different strategies. Serine proteinases (e.g. Proteinase K) can be used to remove the C-terminus and activate the pro-enzyme [24]. Acidic conditions, the addition of fatty acids or detergents like sodium dodecyl sulphate (SDS), but also enzymatic stress lead to activation [20], [25]. Detergents like SDS only changes the steric structure of the latent form at a certain concentration, allowing the substrate to access the active site of the PPO [20].

The *in vivo* function of plant PPOs in the thylakoid membrane, their activation and natural substrates in plants remain unclear. The theory of peptide induced self cleavage, the spontaneous self activation has been suggested [20], [21]. However, the location of PPOs in the cell results in a spatial separation of the polyphenolic substrates [26]. When the cell membrane looses it´s integrity due to tissue degradation, aging or mechanical stress, PPOs can access polyphenolic substrates, which leads to the formation of brown pigments [27].

1.3. Natural Browning Process

The formation of brown pigments is observed in plants, animals and fungi. This common strategy has been developed in order to prevent the organism from harmful ultraviolet rays emitted by the sun. UV-B (315 nm to 280 nm) leads to direct damage of DNA and it is a major exogenous source of reactive oxygen species (ROS) such as superoxide anions (O_2^-) and hydrogen peroxide (H_2O_2). Once the antioxidant capacity of a cell is exhausted, oxidative stress occurs by lipid peroxidation (membrane damage), oxidation of amino acids and oxidation of enzyme substrates (protein inactivation) [27], [28]. While animals are associated with melanin, in plants flavonoids can act as UV-protectants. Both originate from phenylalanine as it can be seen in the synthetic metabolic pathways in Figure 3 and Figure 5 [28].

1.3.1. Melanin

The brown pigment melanin is a heterogeneous compound consisting of polyphenolic species and acts photo-protective by scattering and absorbing UV radiation in the epidermal layer in animals. The *in vivo* synthesis of eumelanin occurs in the cytosol and is then transported via a conjugated glutathione-S-transferase to the specific cell compartment. Three main compounds (L-DOPA; DOPA-quinone and DOPAchrome) and three enzymes (tyrosinase (TYR), tyrosinase-related protein 1 (TRYP1) and dopachrometautomerase (DCT)) are participating in the synthesis as depicted in Figure 3. Proteins, peptides, amino acids, water, anthocyanins (in plants) and other polyphenols engage in the formation of melanin by interacting with the highly reactive *ortho*-quinone and trigger Michael addition reactions [27], [29], [30]. Melanin species are differentiated based on the used substrate in tyrosinase reaction leading to a black/brown eumelanin (substrate: DOPA-quinone) and yellow/reddish pheomelanin (dopamine and cysteine), but also neuromelanin (5-CysDOPA), pyomelanin and allomelanin [28], [31], [32]. The analysis of the reaction is challenging, including but not limited to the difficulties in isolating high molecular weight melanin species and monitoring the high number of substrates involved in the formation [29].
The *in vitro* formation of melanin can be observed when PPOs and dopamine react under the formation of DOPAchrome, which can be detected spectrophotometric [33], [34]. The formation of DOPAchrome can also be observed non enzymatically in the reaction between dopamine and an oxidation agent like $NaIO_4$. In the course of the reaction the molar extinction coefficient of the red colored intermediate DOPAchrome (ε_{480} = 3300 M^{-1} cm^{-1}) can be determined before the formation of the dark colored reaction product polydopamine, an eumelanin similar [34], [35].

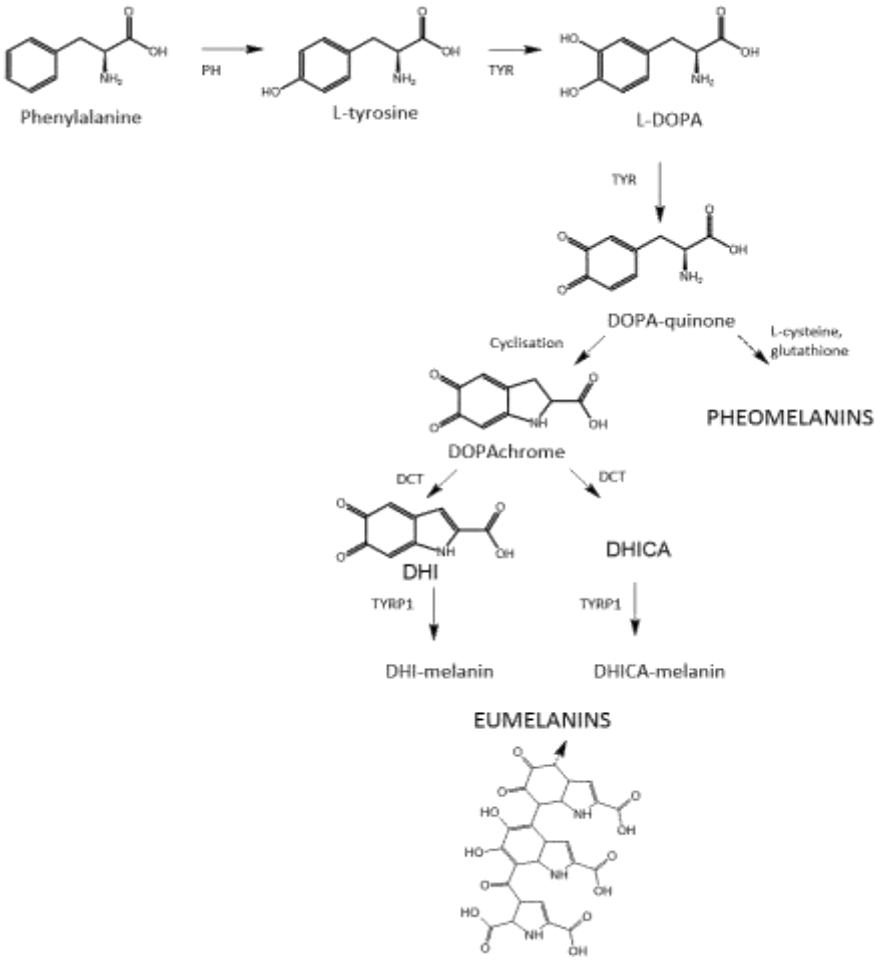

Figure 3 Overview of synthetic metabolic pathway of melanin. Enzymes and intermediates are reported in this letter code: PH, phenylalanine hydroxylase; TYR, tyrosinase; DCT, dopachrometautomerase; DHI, 5,6-dihydroxyindole; DHICA dopachrometautomerase; DHICA, indole-5,6-quinone carboxylic acid; DOPA, L-3,4- dihydroxyphenylalanine; TYRP1, tyrosinase-related protein 1. Based on [28], [36]. Graphic created with [37].

1.3.2. Flavonoids

Flavonoids are a widely distributed group of secondary metabolites in plants. Flavonoids emerge of the phenylpropanoid pathway and possess two aromatic rings (A and B ring), which are linked by a heterocyclic pyrane ring (C ring). The classification is based on the oxidation degree of the C ring in Figure 4, including flavonols, flavan-3-ol and anthocyanins. Another layer of structural diversity is introduced with modification of the aromatic cycles, due to methylation, glycosylation, acylation and prenylation, leading overall to more than 9000 bioactive structural variants allocated over the plant kingdom [28], [36].
They play an important role in the development and defense of the plant, due to their function as signal molecules, phytoalexins and as UV-protectants. The latter function is also hold by pigments, that attract pollinators, contributing to the plant's reproduction [38], [39].

1.3.2.1. Pigments

Besides chlorophyll and carotenoids, pigments of plants are also constituted by flavonoids, which are anthocyanins (red, orange, blue, and purple pigments), chalcones/aurones (yellow pigments) and flavonols/flavones (white and pale-yellow pigments) [38]. Phlobaphenes are reddish colored pigments found in different plants and are believed to be related to the co-occurrance of the colorless proanthocyanindins, which is formed when flavan-3-ols are condensed [40]. Proanthocyanindines are also called condensed tannins, and are of polymeric nature, sharing similarity to melanin (eumelanin in Figure 3 and proanthocyanidins in Figure 5). Laccases and polyphenol oxidases initiate the formation of proanthocyanidin derivatives, the brown pigments in plants [28].

1.3.2.2. Color Stability of Anthocyanins

Anthocyanins, but also proanthocyanidins, are edible pigments that exhibit an influence as taste regulating components in food and wine [38]. The anthocyanin´s color depends on hydroxylation, methylation, glycosylation and other substitutions of the flavylium cation (Figure 4) at different pH values [41]. The color stability is influenced by self-association (condensation of anthocyanins) and also the co-pigmentation, which leads to the formation of compounds that are more stable than the anthocyanin monomer. In addition, temperature, metal ions, light, oxygen, non-enzymatic browning reactions and L-ascorbic acid influence color stability as well [42]. However, the two enzymes, PPO and peroxidase (POD), have been related to be mainly responsible for the color destabilization of anthocyanins in fruits [43], but the typical glycosylation of the more than 600 hundred types of the phenolic anthocyanins on the 3-C carbon (Figure 4), sterically hinders the approach to the active site[29], [44]. The glycosidic bond is broken in the presence of β-glycosidases, making the corresponding anthocyanidin available as substrate [43].

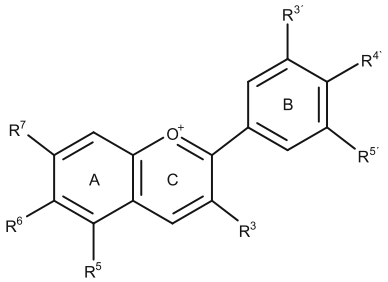

Figure 4 Basic Structure of anthocyanins: flavylium cation with possible substitution positions, whereas R^3 is typically glycosylated. Based on [41]. Graphic created with [14]

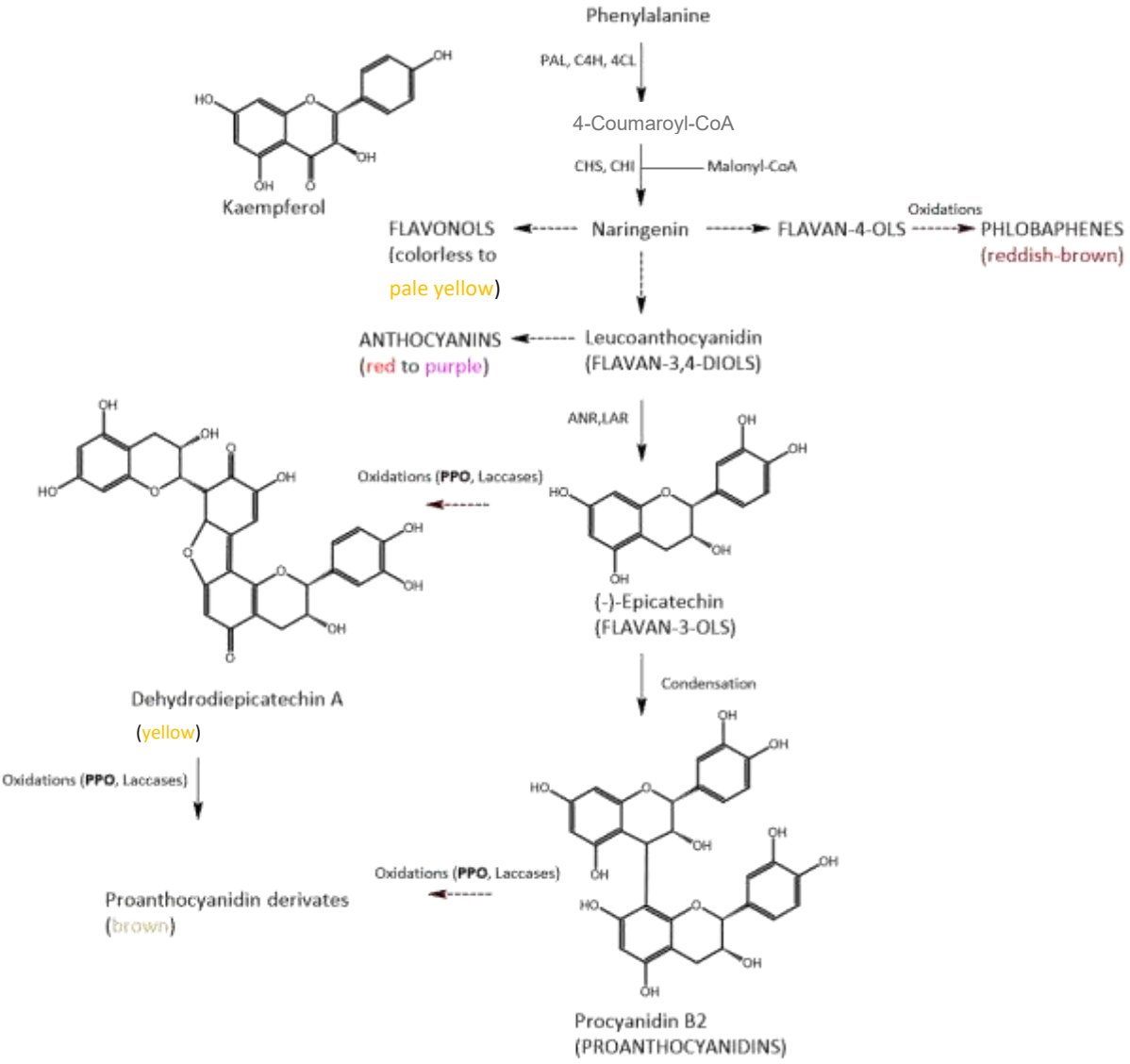

Figure 5 Overview of synthetic metabolic pathway of Flavonoids. Enzymes are reported in this letter code: PAL, phenylalanine ammonia lyase; C4H, cinnamic acid4 hydroxylase; 4CL, 4-hydroxycinnamoyl-CoA ligase; CHS, chalcone synthase; CHI, chalcone isomerase; ANR, anthocyanidin reductase; LAR, leucoanthocyanidin reductase; PPO, polyphenol oxidase; Flavonoid classes are reported in capital letters and their respective color, if not colorless. The chemical structures of representatives of a flavonoid group or intermediates that lead to the formation of brown pigments are depicted.
Graphic adapted from [28], [36]. Created with [37].

1.4. Strawberry *Fragaria* x *ananassa*

Cultivated strawberries (*Fragaria* x *ananassa*) are the result of natural hybridization between the strawberries *F. virginiana* and *F. chiloensis* from the 1700s. Since then, it has been an economically important soft fruit species, which is grown commercially around the world [45]. Strawberries develop their color during ripening by the formation of bright red pelargonidin and dark red cyanidin. The content of the predominant 3-*O*-glucoside form of these two pigments varies in between varieties as it can be seen in Table 1. In addition, at least 13 other anthocyanins at lower concentrations, other polyphenolic compounds have been identified in strawberries [42]. Interestingly, the total polyphenolic content in strawberry leaf is 122-fold higher than in the fruit [46].

Table 1 Polyphenol content of strawberries [47], [48], [49].

Flavonoid class	**Compound name**	**mg per 100 mg fresh weight**
Anthocyanins	pelargonidin 3-*O*-glucoside	20.28 – 68.27
	cyanidin 3-*O*-glucoside	0.63 – 6.67
Flavanols	(+)-Catechin	1.57 – 18.74
	(-)-Epicatechin 3-*O*-gallate	0.00 – 0.66
	(-)-Epigallocatechin	0.00 – 0.15
	(+)-Gallocatechin	0.00 – 0.12
	(-)-Epicatechin	0.00 – 0.02
Total Content of Polyphenols		72.5 – 444.4

It is common that fruits of high quality are used directly as fresh fruits for marketing reasons, while lower quality fruits are further processed. For this reason, companies that process strawberries use varieties that are optimized for the fresh market. This leads to products with a short shelf life, whereas the color is either lost in the processing steps already or over days to weeks of storage. The once intensive red turns into blunt brown [42]. The enzymes PPO and also peroxidase (POD) (EC 1.11.1.7) are mainly responsible for in the formation of brown pigments in fruits [50]. However, in strawberries peroxidase is autoregulated by by-product inhibition with dehydrodiepicatechin A (structure in Figure 5) and the main contribution to enzymatic browning derives from polyphenol oxidase [51].

1.4.1. Strawberry PPOs

PPOs in strawberry are encoded by a gene family [19]. The diploid organism *Fragaria vesca* can be used as a model for the octoploid cultivar *Fragaria x annassa* and also for the whole *Rosacea* family [52]. An analysis of the *Fragaria vesca* genome (Chapter 4.1 PPO Member Identification in Strawberry Genome) revealed the presence of 6 possible *PPO* genes. The structural organisation of the latent form of *Fv*PPO (accession number XP_004293563.1), as well as it´s homology model is depicted in Figure 6.

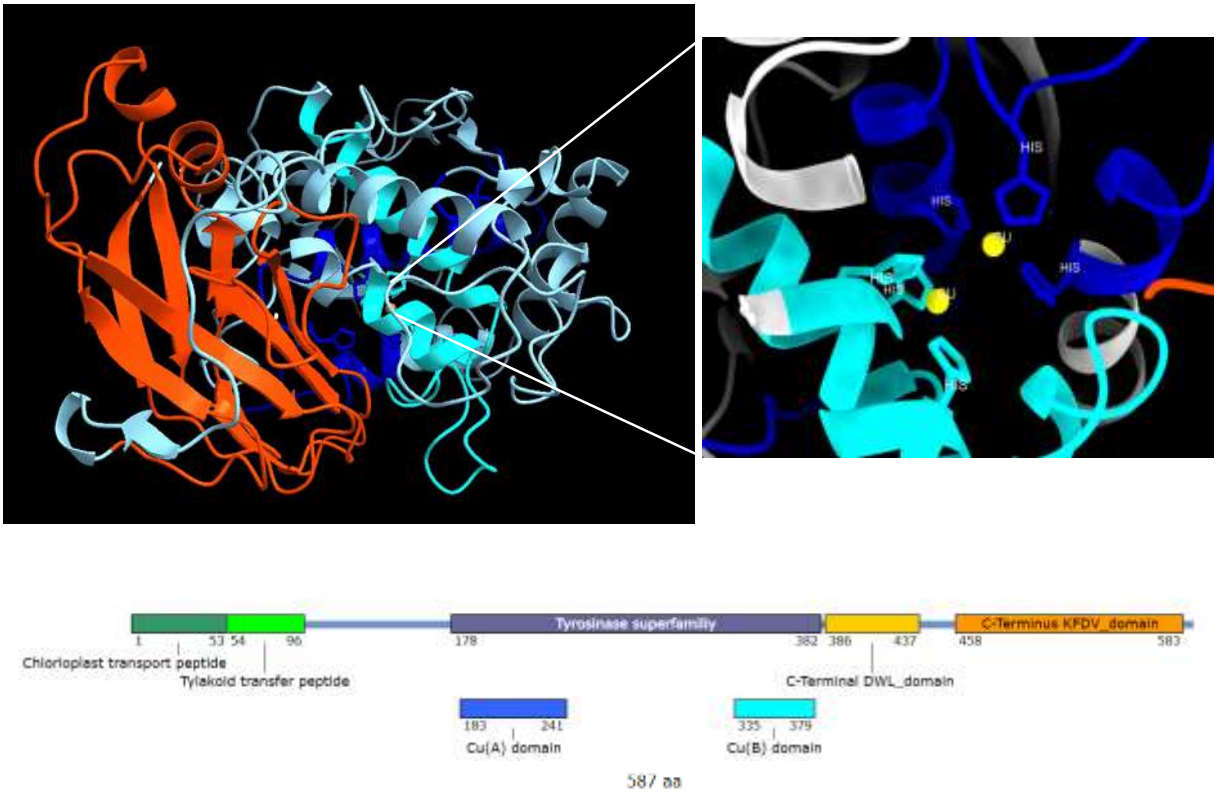

Figure 6 Structural details of L-*Fv*PPO (accession number XP_004293563.1) (Top) Homology model without the signal peptide and DWL_Domain. The active center is magnified, containing two copper ions in yellow, which are coordinated by three histidine residues, respectively. (Bottom) Overview of the structural organisation of the protein. Graphics created with SnapGene Viewer (www.snapgene.com)) and [53]. Regions identified based on [15], [54], [55].

1.5. Inhibition of PPO

The discoloration and the loss of nutritional properties of fruits leads to low acceptance amongst customers, and therefore to less marketability. An estimated loss of more than 50 % of food is caused by enzymatic browning, linked with high economic losses for the food producers and the food-processing industry. Therefore, the motivation is high to identify methods for polyphenol oxidase inhibition [56].

Inhibition can be achieved either with physical or chemical approaches. Physical-based methods are commonly thermal treatment, storage at low temperatures and at modified atmospheres, prevention of oxygen and irradiation [56]. The compounds, which are used as additives to influence the enzymatic browning, are classified based on the inhibition mechanism as complexing, reducing or chelating agents, or as acidulants. Ascorbic acid is the most frequently used substance, although its inhibitory effect is only temporary due to reactions with pigments and metal ions as copper [57]. Most of the methods lead to negative consequences either for the product or for the costumer's health including sulphur-containing agents like cysteine sodium metabisulfite and glutathione(reduced) [56], [58]. This is why researchers are seeking for natural extracts from fruits, vegetables, herbal and animal by-products as inhibitors [56]. It has been demonstrated by Tian et al. [59] that it is possible to screen for possible natural inhibitors based on the PPO (*Agaricus bisporus*) protein structure utilizing machine learning and molecular docking.

1.6. Protein Structure Determination

Several methods for structure determination are currently used, including X-ray crystallography, nuclear magnetic resonance (NMR) spectroscopy, and electron microscopy. X-ray diffraction patterns, information on the local conformation and the distance between atoms, and images of the shape of the protein represent the respective data of each method, that is required to allocate a protein´s structure [60]. The limitation of each method is primarily based on the requirement of protein crystallization, the size limitation of the protein with 50 kDa and the accessibility of high-end electron microscopes, respectively. Statistics of the Protein Data Bank (PDB, http://www.rcsb.org), reflect that more than 80 % of the 197 125 solved protein structures (05.12.2024) have been elucidated based on X-ray diffraction patterns, making X-ray crystallography the most frequently used method [60].

1.7. Protein Crystallography

1.7.1. Theory

The formation of protein crystals is an unlikely phenomenon since proteins are highly flexible and dynamic. These are properties that define their functionality, but do not contribute to their ability to form crystals. Crystal formation is driven by few weak and non-covalent interactions between the protein molecules that holds them together in the crystal. The highly specific surface characteristics result from charged and polar amino acids that are solvent exposed and define the required few intermolecular contacts between the protein molecules in a crystal [61]. The voids in between the protein molecules are filled with mother liquor, the buffer of the reservoir and leads to the fragility of a protein crystal compared to a salt crystal. It must be highlighted that if the intermolecular contacts can not interact, the protein is probably not crystallizable and requires modifications [62].

Single protein crystals are formed in supersaturated solutions. Supersaturation leads to the creation of metastable zones in the crystallization phase diagram (Figure *7*), in which the system is comprised to relax in equilibrium. This state can be introduced by the addition of precipitants, removal of water due to evaporation, solvent exchange by dialysis, change of pH and others. Overcoming the kinetic energy barrier in the formation of a nucleus or by the addition of an external one leads to a phase separation of saturated protein in solution and a protein-rich phase such as excess protein as precipitate or crystal in solid state [62].

Therefore, nucleation resembles a first order phase transition from disordered to an ordered state, respectively the transition from a liquid to a solid state. This leads to a decrease of protein concentration in the liquid phase and the system is shifted to a part of the metastable zone where the crystal can grow [61].

When the crystal growth is considered from a perspective of free crystallization energy $\Delta G^0_{crystal}$, it is depended on the enthalpy $\Delta H^0_{crystal}$, the temperature and entropy term $-T\Delta S^0_{crystal}$ of the crystallization, whereas $\Delta G^0_{crystal} < 0$ is required for crystal growth. The enthalpic contributions, which resemble the heat formation in the crystal growth, are insignificant, so the free energy of the crystal formation is influenced mainly by entropy. Although entropy increases in the first order transition, it can be derived where the remaining stabilizing energy originates, if the total free enthalpy is formulated as [62]:

$$\Delta G^0_{crystal} = \Delta H^0_{crystal} - T(\Delta S^0_{protein} - \Delta S^0_{solvent}) \quad (1)$$

The entropy of the solvent $\Delta S^0_{solvent}$ increases when water molecules are released from hydrophobic and polar surface residues during crystal formation. This explains why even very small changes in chemical conditions, but also environmental changes can influence the crystallization success [62]. The objective of the crystallographer is the identification of conditions that drive the system in zones that are favorable for crystallization [61].

1.7.2. Vapor Diffusion (VD)

The most frequent used technique to obtain single crystals is vapor diffusion (VD) either in the hanging-drop (VD-HD) or sitting-drop (VD-SD) set up. VD-HD and VD-SD are both comparable methods which are only differentiated by the location of the drop and the resulting accessibility of the crystals, when they are required to be removed of the drop. While the crystals are more difficult to access in VD-SD, the experimental set-up can be automated by pipetting robots. Both methods contain a drop with the protein solution and a crystallization precipitant cocktail that is equilibrated against the reservoir containing the latter, in a closed system [63]. An equilibrium between the drop and the reservoir is achieved, when water evaporation of the drop in the aerial space results in the diffusion of the water vapor into the reservoir. This leads to an increase of protein and precipitant concentration in the drop and enables the movement in the crystallization diagram to favorable crystallization zones in Figure *7* [61].

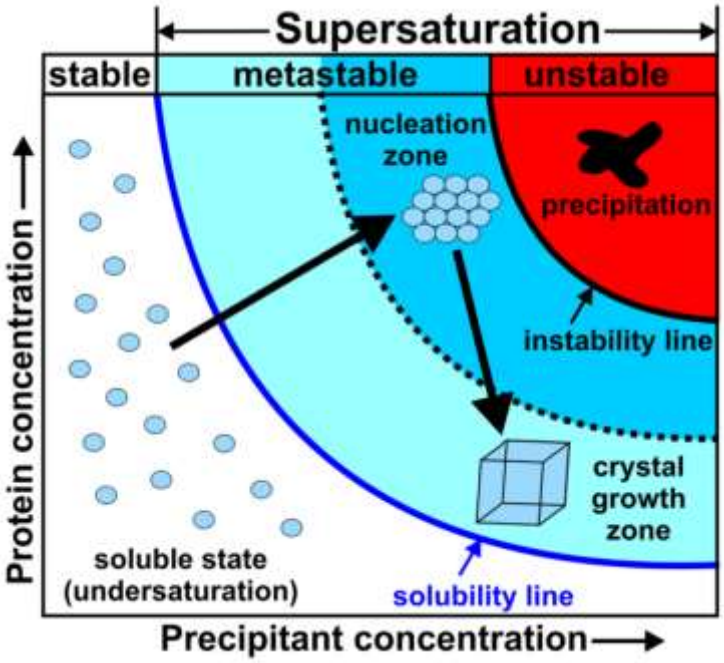

Figure 7 Crystallization phase diagram. Crystal growth in the course of vapor diffusion is indicated by the arrows. When water evaporates in the drop the protein and precipitant concentration increases until the system reaches the nucleation zone within the metastable zone. Then a phase transition from liquid to solid leads to a decrease of protein concentration in the liquid phase during the growth of the protein crystal. It can be seen if the system reaches the condition in the unstable zone, respectively no nucleus has formed or this condition is chosen, that the protein will precipitate. From [61].

1.7.3. Screening Approaches

To simplify the sheer number of parameters, crystallization experiments are usually started with initial screening, that leads to some kind of protein crystal. Initial screens are designed as sparse matrix screens, which are biased samplings of crystallization parameters. They are chosen based on conditions that have led most frequently to crystallization successes according to published structures [64]. Commercially available crystallization kits contain these conditions. They are often based on polyethylene glycols (PEGs) with a mean molecular weight ranging from 2000 to 8000 g mol^{-1}, which are reported to be the most successful precipitants for crystallization, besides ammonium sulphate [65], [66].
Once a protein crystal has grown, optimization is often required to improve the crystal´s quality. In a grid screen, the parameters of the drop with the protein crystal, or also called "hit" are varied systematically around the condition [64]. For example, if the protein crystal is found at a certain condition with a pH of 7, the pH can be varied systematically in some defined steps between 6 to 8, while the other parameters are not changed in this grid screen.

1.7.4. Additives in Crystallization

Two types of additives are used in crystallization. One type consists of molecules that influence the protein´s physiological properties, e.g. substrates, inhibitors, cofactors or other effectors. Another type participates in the stabilization of certain protein conformations when particular ions are added; or acts as chaotrope or kosmotrope by altering the solubility or affecting interactions between macromolecules and solvents. A promising group of additives are polyoxometalates that provide reversible crosslinks within a protein or in-between protein molecules, that lead to the formation of new protein-protein contacts [61].

1.7.4.1. Polyoxometalates (POMs)

This class of inorganic anionic clusters of oxygen and early transition metal atoms M (Mo, W, Nb, Ta, Mo, W) in their highest oxidation state posses a high number of structures in different sizes. Their properties and diverse functions lead to the application in many different fields within biology, biotechnology, medicine, catalysis, nanosicience and crystallography [61], [67]. Their structure comprises either isopolyanions with the general formula $[M_mO_y]^{n-}$ or heteropolyanions with $[X_xM_mO_y]^{n-}$. The heteroatom X is not restricted to be a transition metal. POMs often consist of octahedral $\{MO_6\}$ units, which are self assembled around *x* heteroatoms in the center. Although POMs are originally introduced as phasing tool, hexatungstotellurate (TEW) $[TeW_6O_{24}]^{6-}$ has turned out to be also a suitable crystallization additive among other properties. It has contributed to the crystallization of two structurally unknown polyphenol oxidases (mushroom tyrosinase from *Agaricus bisporus*) and aurone synthase from *Coreopsis grandiflora*) [61].

2. Aims

The browning process of food is a major problem leading to the waste of processed fruits that are no longer appealing to the costumer. Compared to other fruits like apples or banana, strawberries exhibit less extensive browning. However, the color degradation and browning of strawberries in processed products is a technology problem. The identification of natural inhibitors of the responsible polyphenol oxidases, which could be used as food additives, is therefore of high interest.

The goal of this thesis is the structure determination of the latent form of one isozyme of the wild strawberry's polyphenol oxidases. The method of choice is protein crystallography. The protein is heterologously expressed in *Escherichia coli* (*E. coli*), and standard methods of protein crystallization should be applied to grow a crystal of diffraction quality without the presence of an affinity tag in the protein. This should eventually lead to the allocation of the structure and to the formation of a basis to identify natural inhibitors *in silico*.

Although the protein tag is cleaved before crystallization, its impact on the expression and purification of the heterologous protein arouses interest in this work. Therefore, the His6 tag of the fusion protein should be replaced with a glutathione-S-transferase (GST) tag. The expression system *Escherichia coli* with the target sequence for the expression of L-*Fv*PPO with the His6 tag has been provided for this work, whereas the gene sequence has been codon optimized. Methods of molecular cloning are applied to change the His6 tag to a GST tag. The cloning method is based on sticky end ligation [68]. The sequences of the primers and L-*Fv*PPO are attached in the appendix (9.2 Sequences). Immobilised metal affinity chromatography (IMAC) and affinity chromatography (AC) should be utilized for capturing the fusion protein. The L-*Fv*PPO batches without an affinity tag would be united, and a suitable purification method should be developed that meets the required purity of the protein for crystallization. This purity should be assessed with methods of SDS-PAGE, dynamic light scattering, copper quantification and thermal shift assays. Protein quantification is performed either spectrophotometric or with a Lowry assay. The latter quantification method is used as a reference in protein crystallization. Crystallization is either automated in a vapour diffusion sitting drop (VD-SD) set up or manually performed in a vapour diffusion hanging drop (VD-HD) set up. In Figure 8 a decision tree is depicted, that summarises the decision making for crystallization of the protein during this work.

During the growth of the protein crystals, findings of the purification that influence the activity of the polyphenol oxidase should be investigated. The stability of the measurable species DOPAchrome should be determined for the used storage buffer and its respective molar extinction coefficient.

The latent form of the enzyme must be activated for enzymatic activity. This represents a basis in functional behaviour of the enzyme and can possibly reveal information that contributes to the identification of inhibitors. The activation can be achieved in different ways. Possible influences on the activation should be evaluated, to assess their contribution to the characterisation of the PPO´s kinetic parameters.

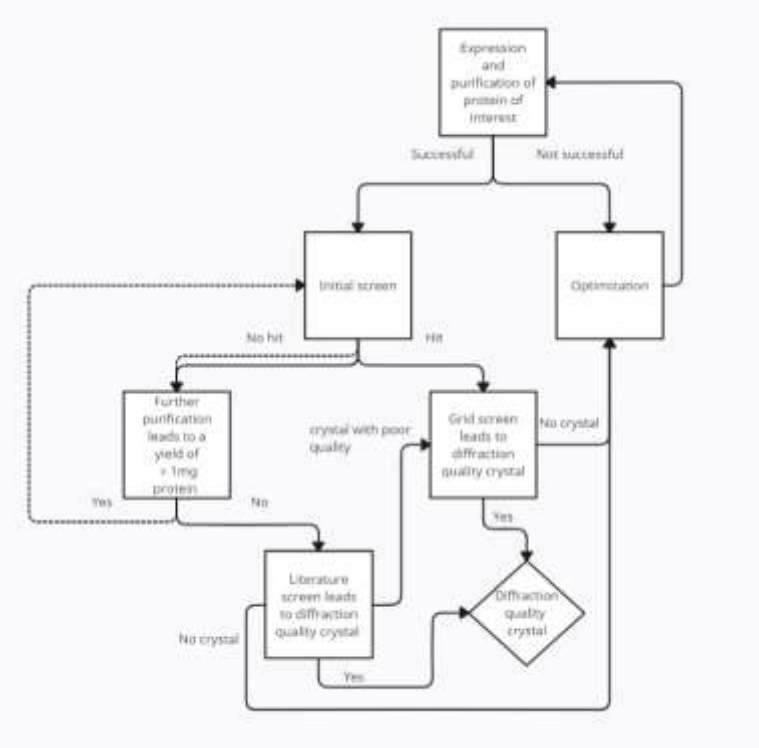

Figure 8 Decision tree in crystallization experiments, whereas the dotted arrows represent the repetition of an experiment.

3. Materials

Table 2 Chemicals used in this work and their respective supplier.

Chemical	Supplier
2,2´Biquinolinic acid	Thermofisher Scientific
Acetic acid (99%)	VWR
Agar-agar	Roth
Ammonium sulphate	Sigma
Ampicillin	Sigma
APS	Merck
ATP*2Na	Roth
Benzamidine	Roth
Bovine serum albumin	Thermofisher Scientific
Citric acid	Sigma
Coomassie Brilliant Blue R-250	Sigma
$CuSO_4 \cdot 5H_2O$	Sigma
Dopamine Hydrochloride	Merck
Ethanol (abs.)	Supelco
Glycerol (98%)	Roth
Glycine	Roth
HEPES	Roth
Imidazole	Roth
IPTG	Roth
Kanamycin	Roth
KH_2PO_4	Merck
K_2HPO_4	Merck
L-DOPA	Merck
L-Glutathione	Roth
Lysozyme from chicken egg white	Sigma
Methanol (≥ 99.9 %)	Fisher Scientific
$MgCl_2 \cdot 6H_2O$	Roth
$MgSO_4 \cdot 7H_2O$	Merck
$NaIO_4$	Roth
NaOCl	Lactan
$NiSO_4 \cdot 6H_2O$	Merck
Peptone	VWR
PMSF	Roth
Polyethylene glycols	Sigma
Proteinase K from *Tritirachium album*	Sigma
SDS	Roth
SOC Medium	Thermofisher Scientific
Sodium ascorbate	Roth
Sodium chloride	VWR
Sodium formiate	Merck
SYPRO orange	Sigma
TCEP · HCl	Thermofisher scientific
TEMED	Roth
TRIS	VWR/Roth
Tryptone	Roth
Tyramine	Merck
Urea	AppliChem
Yeast Extract	Roth
$YCl_3 \cdot 6H_2O$	Merck

4. Methods

4.1. PPO Member Identification in Strawberry Genome

The program hmmsearch (Version 3.3.2 (Nov 2020)) was used to screen the target genome of *Fragaria vesca* subsp. *vesca* (RefSeq GCF_000184155.1) for possible tyrosinases based on a query file (PF00264.hmm [69]). In total 6 possible Tyrosinases were identified with an expected value of smaller than $1.4 \cdot 10^{-30}$ (March 5th 2024). The PPO with the accession number XP_004293563.1 was analysed with the BLAST tool CDD (https://www.ncbi.nlm.nih.gov/cdd) revealing conserved domains: tyrosinase super family, PPO1_DWL and PPO1_KFDV domains. Further, the online tool TargetP - 2.0 revealed the N-terminal signal peptides (Chloroplast and thylakoid guiding sequence) [55]. The sequence without the signal peptides was codon optimized and used for molecular cloning.

4.2. Homology Modeling of L-*Fv*PPO

SWISS model was used for creating a model based on the protein sequence [70]. Following the manual of the website, the program suggested multiple templates and models fitting for L-*Fv*PPO. The model with the highest sequence coverage, ligand inclusion and based on a crystal structure (PDB,http://www.rcsb.org; 6els.1: Structure of latent apple tyrosinase (MdPPO1)) was chosen.

4.3. Molecular Cloning of L-*Fv*PPO with GST tag

Solutions: Forward Primer (FL, FS) and Reverse Primer (RL, RS)
Vector pGEX-6P-1 (GE Healthcare, Munich, Germany)
GoTaq®G2 and buffer(5x) (Promega Corporation, Wisconsin, United States)
10mM dNTPs (Thermo Fisher Scientific, Vienna, Austria)
Serva DNA Stain Clear G (SERVA Electrophoresis GmbH, Heidelberg, Germany)
Quick-Load® Purple 1 kb Plus DNA Ladder
(New England Biolabs, Massachusetts, USA)
Q5 High Fidelity Polymerase (M0491) and Buffer (New England Biolabs, Massachusetts, USA)
T4 ligase and buffer (New England Biolabs, Massachusetts, USA)
TAE buffer and Nuclease free water
SOC medium (Thermo Fisher Scientific Inc. (NYSE: TMO), Massachusetts, USA)

Materials: Stellar chemically competent *E. coli* (Takara Bio, Saint-Germain-en-Laye, France)
Agarose gel (1%) mixed with 5 µL Serva DNA Stain Clear G
innuPREP DOUBLEpure Kit (Innuscreen GmbH, Berlin, Germany)
innuPREP Plasmid Mini Kit 2.0 (Innuscreen GmbH, Berlin, Germany)
LB Agar plates with ampicillin
sterile Toothpick
1.5 mL sterile tubes (Eppendorf SE, Hamburg, Germany)
PCR tubes (VWR, Vienna, Austria)

Devices: Mastercycler® epgradient Thermo Cylcer (Eppendorf SE, Hamburg Germany)
SPECTROstar Nano (BMG LABTECH, Ortenberg, Germany)
standard thermo mixer

This cloning method is based on sticky end PCR [68], which enables the generation of sticky end DNA (*Bam*HI and *Eco*RI) ready for ligation into linearized pGEX-6P1 expression plasmid. For that, the primer combinations FS + RL and FL + RS were used in two separate polymerase chain reaction (PCR) reaction mixtures with the plasmid harbouring the target sequence L-*Fv*PPO as template according to Table 3. The sequences of the primers and L-*Fv*PPO are attached in the appendix (9.2 Sequences). The PCRs were performed with the settings listed in Table 4. Each PCR product was mixed with 2 µL 6 x loading dye and loaded on an agarose gel (1%). After electrophoresis (40 min, 100 V), the bands of interest were cut out with a clean scalpel. The extraction of the DNA was performed with the innuPREP DOUBLEpure Kit according to the manual provided by the manufacturer (Innuscreen GmbH, Berlin, Germany) with the alteration that the incubation took place at 60 °C for 10 min on the thermo mixer after 650 µl gel solubilizer solution (part of the kit) was added. The DNA concentration of the PCR products and the linearized vector pGEX-6P-1 (lab collection) were determined by measuring the absorption at 260 nm of 2 µL aliquots in the SPECTROstar Nano.
Same ng amounts of the two PCR product were mixed and denatured at 95°C for 5min, before re-annealing at RT for 10 min. This results in a total of four different re-annealing products, whereas only 1/4 of that represented the sticky end DNA (*Bam*HI and *Eco*RI) for ligation into pGEX-6P-1. In a final volume of 10 µL, 4 µL (300 ng) of the re-annealing products were mixed with 4 µL (100 ng) pGEX-6P1, 1 µL 10 x T4 ligase buffer and 1 µL T4 ligase. The ligation was performed at 15 °C for 3 h, 4°C over night and 10 min at 65°C.

Table 3 Reaction mixture of sticky end PCRs

	Forward Primer	Reverse Primer	Plasmid pUC19_ L-*Fv*PPO	dNTPS	Q5 Buffer	Q5 Polymerase	Nuclease free water	Total
Concentration	10 µM	10 µM	50 ng µL^{-1}	10 mM				
Volume (µL)	1.25	1.25	0.5	0.5	5	0.25	16.25	25

Table 4 PCR program setting for the sticky end PCR.

Step	Temperature °C	Duration	Cycles
Initial Denaturation	98	30	-
Denaturation	98	10	30
Annealing	65	30	
Extension	72	45	
Final extensions	72	120	-
Hold	4	∞	-

For transformation, an aliquot of 25 µL chemically competent *E. coli* cells (Stellar) and 500 ng plasmid pGEX-6P-1_L-*Fv*PPO were mixed in a sterile 1.5 mL Eppendorf tube. After incubation on ice for 10 min, they were carefully mixed by snipping the tube. The cells were incubated on ice for another 30 min until they were placed in a preheated water bath for 30 seconds at 42 °C. The mixture was immediately chilled on ice for 5 min again, before a volume of 225 µL preheated SOC medium (37 °C) was added and the tube was placed horizontally in a thermal mixer (60 min, 37 °C, 500 min^{-1}). Volumes of 10 µL and 100 µL of the transformed cells were then spread out on an ampicillin agar plate respectively and incubated at 37°C over night.

Ten colonies were chosen and transferred to a new agar plate with a sterile toothpick. The respective toothpick of each colony was then thoroughly pressed against the bottom of the inside of a PCR tube used for "colony PCR" (Table *5* and Table 6). The PCR samples were then loaded on an agarose gel (1%) for electrophoresis (30 min, 100 V).

When only one band with the corresponding size of approximately 1.5 kb was visible in the agarose gel under UV-light, liquid cultures were prepared of the respective *E. coli* clone. Each containing 5 mL LB medium, 50 g L^{-1} ampicillin. They were incubated overnight (37 °C, 180 rpm). The plasmid extraction was performed according to the manufacturer (Innuscreen GmbH, Berlin, Germany) protocol using 4 mL culture suspension. The concentration of the plasmid pGEX-6P-1_L-*Fv*PPO was determined on the SPECTROstar Nano. The required plasmid concentration and sequencing primers were sent to an external company (Microsynth AG, Balgach, Switzerland) for sequencing.

Plasmids with the correctly sequenced insert were used for transformation in the expression strain *E. coli* BL21(DE3) by heat shock method and the success of transformation was verified by colony PCR again as described before.

For the production of permanent cultures, overnight cultures were mixed with glycerol to a final concentration of 50 % (v/v). The permanent cultures were shock frozen with liquid Nitrogen and stored at -80°C. These were used for expression of the L-*Fv*PPO with an GST-tag.

Table 5 Reaction mixture for Colony PCR.

	Forward Primer FL	Reverse Primer RL	dNTPS	Taq Buffer	Taq Polymerase	Nuclease free water	Total volume
Concentration	10 µM	10 µM	10 mM				
Volume µL	1	1	0.4	4	0.2	13.4	20

Table 6 PCR Program for colony PCR.

Step	Temperature °C	Duration	Cycles
Initial Denaturation	95	120	-
Denaturation	94	30	30
Annealing	65	90	
Extension	72	90	
Final extensions	94	30	-
Hold	65	∞	-

4.4. Recombinant Protein Production

4.4.1. Heterologous Protein Expression

Solutions: Expression medium (TB-medium)
1 M ITPG (Isopropyl-β-thiogalactosid)
1 M $CuSO_4$
Kanamycin or Ampicillin stock solutions (500 mM)
Periplasm buffer (50 mM HEPES, 200 g L^{-1}, 1 mM EDTA, pH 7.9(22°C))
5 mM $MgSO_4$
Materials: sterile 1 L and 2 L Erlenmeyer flasks
Device: Shaking incubator CERTOMATMAT®BS-1
(B. Braun Austria GmbH, Maria Enzersdorf, Austria)
UV spectrophotometer Shimadzu UV-1800 (Shimadzu, Kyōto, Japan)

A volume of 0.1 L expression media was prepared in a sterile 1 L Erlenmeyer flask adding the respective antibiotics in a concentration of 50 mg L^{-1}. For inoculation of the expression medium, cells from the permanent culture were transferred with a sterile toothpick into the 1 L Erlenmeyer flask, whereas the permanent culture was immediately frozen again in liquid nitrogen and stored at -80°C. The pre-culture was incubated over night in a shaking incubator (37 °C, 250 rpm). An aliquot of 15 mL of this pre-culture was added to 500 mL sterile expression medium that was prepared in a 2 L Erlenmeyer flask with an antibiotic concentration of 50 mg L^{-1}. Multiple batches were prepared simultaneously at 37 °C and 250 rpm. The OD_{600} of the flasks is measured every 1 to 2 hours until a value of 0.6 - 0.8 was reached. The induction of the expression was started by adding IPTG first, followed by copper sulphate ($CuSO_4$) to a final concentration of 1 mM, respectively. 1 M $CuSO_4$ needed to be added dropwise while constantly shaking the flask manually, since bacterial cells can otherwise enter a state of viability, but being not culturable [71]. The cultures were incubated in a shaking incubator at a temperature of 18 °C and 250 rpm agitation for 16 hours over night. The cell culture was centrifuged (5000 rpm, 3 °C, 20 min) and the supernatant discarded.

The periplasm membrane of the *E.coli* cells can be separated, which facilitates the lysis and increase the yield of the following capturing of the His6 (6 x histidine) tagged fusion protein [72]. The freshly harvested cell pellet was resuspended in 5 mL periplasm buffer per gram pellet on ice using a glass rod. The suspension was centrifuged 2 times at 7000 x g for 30 min at 4°C and the supernatant was discarded. The texture of the pellet became softer, and the pellet was not adhesive to the wall of the vessel like before.

Then it was resuspended in precooled (4 °C) 5 mM $MgSO_4$ and incubated on ice for 10 min in a shaking rack. The suspension was centrifuged at 4000 x g for 30 min and the supernatant was discarded. The pellet was either shock frozen with liquid nitrogen and stored at -80 °C or it was used directly for cell lysis.

4.4.2. Cell Lysis

Solutions: Lysis buffer
Materials: Glass rod
Device: Sonicator, Lance model CL-18 (Qsonica L.L.C, Newtown, USA)
Shaking rack KS 125 basic (IKA-Werke GmbH & CO. KG, Staufen, Germany)
Magnetic stirrer and bar
Avanti® Centrifuge J-26 XP (Beckman Coulter, Inc., California, United States)

The protease inhibitors benzamidine and PMSF were both added to reach a final concentration of 1 mM in the lysis buffer. This was critical for PMSF due to its stability in the presence of water. The frozen pellet was thawed at room temperature and resuspended in 5 mL lysis buffer per gram pellet by using preferably a glass rod or by pipetting. Thoroughly mixing of the pellet with the lysis buffer was required to prevent the formation of clumps that are not lysed. The suspension was stirred with a magnetic stir bar, while an ultrasonic lance (Pulse: 15 seconds, Pause: 45 seconds, Amplitude: 15 %) was running for a total of 3 pulses, until the periplasm membrane was separated. If not, the time was extended to at least 40 pulses. The cell debris were separated by centrifugation (48 384 x g, 40 min, 4 °C) and the supernatant was decanted and used directly for purification at the FPLC. The cell debris were discarded.

4.5. Protein Purification

4.5.1. Sample Preparation

Materials: Whatman 0.2 µM filter paper (Merck, Darmstadt, Germany)
Device: 1 L Vacuum flask

If no precipitates or dust were observed in the supernatant of the lysate or in the sample that has already passed a purification step, it was only centrifuged (12000 rpm, 10 min, 4 °C) before loading. Otherwise, it was vacuum filtered using a Whatman 0.2 µM filter. Glycerol in the sample was not considered to be disturbing in the purification steps and has not been buffer exchanged if a sample has been thawed.

4.5.2. Fast Protein Liquid Chromatography (FPLC)

Material: Amicon® Ultra Centrifugal Filter, 30 kDa MWCO (Merck, Darmstadt, Germany)
Eppendorf™ 96-Well Protein LoBind Deep Well (Eppendorf SE, Hamburg, Germany)
Whatman 0.2 µM filter paper (Merck, Darmstadt, Germany)
Device: Amersham ÄKTA Explorer consisting of fraction collector Frac-950, Pump P-900, UV/Vis Detector UV-900, pH-Conductivity detector pH/C-900 and system Box 900 (GE HealthCare Technologies, Chicago, USA)
FPLC columns (Cytiva Europe GmbH, Freiburg, Germany)
MonoQ 5/5 1 mL (GE HealthCare Technologies, Chicago, USA)
Allegra™ 2IR Centrifuge (Beckman Coulter, Inc., California, United States)
1 L Vacuum flask and Ultrasonic bath

The buffers in Table *7* were vacuum filtered through Whatman 0.2 µM filter paper and degassed in an ultrasonic bath for 10 min and then they were stored at the working temperature of the FPLC. The chaperone wash buffers were freshly prepared and used at the same day. The regenerated and/or cleaned columns were equilibrated based on the recommendations of the respective manufacturer, but in any case, until the signals of pH, conductivity and A_{280} remains constant in the UNICORN software. The sample was loaded either with a sample pump (more than 200 mL), a loop (50 mL or 1 mL) or directly with a syringe (< 1 mL) depending on the sample volume. For the elution of the target protein different buffers and elution profiles are used and they are listed in Table 8 and Table 9. During elution 1 mL fractions were collected in 96 Well plates. The fractions of interest were either selected based on the A_{280} and A_{345} signal of aromatic amino acids in the chromatogram or based on an activity assay (5 mM tyramine, 1 mM SDS) according to the chapter 4.6 Activity Assay. Then they are pooled in a centrifugal filter with a cut-off of 30 kDa. They were concentrated or the buffer of the solution was exchanged by ultracentrifugation (4000 x g) until the elution buffer concentration was reduced by a factor of 10^3. The factor was increased to 10^5, if the sample contains the strong PPO inhibitor glutathione.

For long term storage of the protein solution, glycerol was added to a final concentration of 20 % (v/v) then it was shock frozen in liquid nitrogen and placed at -80 °C. For short time storage, the buffer was exchanged to 30 mM TRIS pH 8 (22°C) and placed in the refrigerator at 4°C.

Table 7 Required buffers in the protein solution before the respective purification step.

Step	Concentration of TRIS (mmol L^{-1})	Concentration of NaCl (mmol L^{-1})	Concentration of $(NH_4)_2SO_4$ (mol L^{-1})	pH (at 22 °C)
IMAC 2	30	500	-	8
AEX		-	-	9
HIC		-	1.5	8

4.5.2.1. Immobilized Metal Affinity Chromatography (IMAC 1 and 2)

The columns used in this step were HisTrap HP His tag protein purification columns (Cytiva Europe GmbH, Freiburg, Germany). They were loaded according to the manual of the manufacturer with Ni^{2+} ions. If the same protein was purified, they were used multiple times. Two separate columns were used for IMAC 1 and IMAC 2 to prevent that residues of tagged protein would eventually be present after IMAC 2.

As the initial capturing step, the fusion protein was bound to the column due to an affinity of the His6 tag to the Ni^{2+} ions on the Nitrilotriacetic acid (NTA) Sepharose resin. Since other proteins of the expression system share this affinity, the total bound protein was washed on the column to eliminate protein presence with only a weak bond to the metal ions. This was done with 5 to 10 column volumes (CV) mobile phase, 10 CV chaperone wash buffer 1 and then again with 10 CV mobile phase. Then the elution was initiated according to the elution profile in Table 9.

In IMAC 2, the His6 tag was not fused to the protein anymore due to the removal of the tag as described in the chapter 4.5.3 Removal of the Protein Tag. The protein solution´s buffer was exchanged to the buffer in Table *7*. Therefore, the target protein was not going to bind to the column anymore and was expected to be in the flow through, while most of the non target proteins bind again on NTA-Ni^{2+} Sepharose resin.

4.5.2.2. Affinity Chromatography (AC)

For capturing the fusion protein L-*Fv*PPO with a GST-tag in the supernatant, the cell lysate was loaded on an equilibrated 5 mL FF GSTrap™ (Cytiva Europe GmbH, Freiburg, Germany) with 3 mL min^{-1} flow rate. The bound protein was washed with 10 CV of mobile phase, 5 CV of the chaperone wash buffer 2 containing Urea, and then again with 10 CV of mobile phase. The elution was performed according to Table 9. The fractions of interest were buffer exchanged and the GST tag was removed according to the chapter 4.5.3 Removal of the Protein Tag.

4.5.2.3. Anion Exchange Chromatography (AEX)

The protein was separated based on the interaction of it´s negative charge, that result of the pH value at 9 and the positive charge of the resin in the MonoQ 5/5 1 mL (Cytiva Europe GmbH, Freiburg, Germany). The separation on a cooled FPLC system at 4 °C increased the separation success. Since the pH value of TRIS buffer is temperature dependent, opening the refrigerator during the elution influences the elution behaviour and was therefore avoided. Once the protein was loaded on the column, it was washed with 10 CV of mobile phase and eluted according to Table 9.

4.5.2.4. Hydrophobic Interaction Chromatography (HIC)

An aliquot of 50 µL protein solution of a non concentrated AEX fraction was placed in a well of an activity assay and 200 µL of 2 M $(NH_4)_2SO_4$ was added dropwise. The precipitation behavior was followed though the microscope. Since no precipitation was observed, the concentration of $(NH_4)_2SO_4$ in the sample was adjusted to 1.5 M and the pH value was adjusted to 7.99 (at 22°C).

This method was applied for capturing AEX fractions that contain L-*Fv*PPO. The protein solution was filtered through a Whatman 0.45 µm filter. The sample was loaded and washed with 40 CV mobile phase and then eluted according to Table 9.

Table 8 Overview of columns and buffer systems that were used for capturing and purification of the enzyme of interest.

Method	IMAC	AC	AEX	HIC
Flow Rate (mL min^{-1})	3	3	1	1
Column	5 mL HisTrap HP His tag protein purification column	5 mL FF GSTrap™	MonoQ 5/5 1 mL	HiTrap 1 mL Butyl HP
Mobile Phase and washing buffer	A1	A2	A3	A4
Elution buffer	B1(A1+500mM imidazole)	B2(A2+15 mM imidazole)	B3	B4
Additional Washing buffer	Chaperone wash buffer 1	Chaperone wash buffer 2	-	-
Working temperature	RT	RT	4 °C	RT

Table 9 Elution profiles of the applied capturing and purification methods.

	IMAC		AEX	
Step	Concentration of eluent B1 (%)	CV	Concentration of eluent B2 (%)	CV
1	6.0	10	9.8	20
2	6.0-35.0	4	10.0	20
3	35.0	5	10.0-10.8	50
4	100.0	15	10.8-20.0	10
5	-	-	100.0	15
	AC		**HIC**	
Step	Concentration of eluent B3 (%)	CV	Concentration of eluent B4 (%)	CV
1	100.0	8	100.0	20

4.5.3. Removal of the Protein Tag

Solutions: HRV3C protease with His6-tag or GST-tag
0.5 M tris(2-carboxyethyl)phosphine (TCEP)

Depending on the used tag, either His6-tagged or GST-tagged HRV3C protease was added to the protein solution after IMAC 1 or AC. Both proteases were heterologous expressed and purified in-house (lab collection) and were stored at -80 °C at a concentration of 10 g L^{-1}.

The respective protease was added to the protein solution in a ratio of 1:50 (protease:protein), in the presence of the reducing agent TCEP in a final concentration of 2.5 mM. Increasing the concentration of TCEP to 5 mM would have led to precipitation of the protein. The reaction was placed in the refrigerator at 4 °C over night. After centrifugation of the reaction mixture (17 000 x g, 10 min, 4 °C) the sample was loaded on an IMAC or AC column. Since complete cleavage of the protein tag might not be achieved in the reaction over night, tagged protein will bind to the column. Even though these pooled fractions can be proteolytically digested again, they are not added to the main fraction due to the introduction of additional non target protein species to the sample. The untagged protein was used for further purification as described in the chapter 4.5.2.3 Anion Exchange Chromatography (AEX).

4.6. Activity Assay

Solutions: 500 mM Tyramine | 500 mM Dopamine | 500 mM L-DOPA
100 mM SDS
150 mM TRIS pH 7.82 (25°C)
Materials: 96 Flat Bottom Transparent Polystyrene Plate
Device: Infinite® 200 PRO Tecan plate reader (Tecan Group Ltd., Männedorf, Switzerland)

This assay was designed as an initial rate assay, where the substrate was added in excess. The formation of DOPAchrome, a red-orange intermediate (Structure in Figure 3) after the polyphenol oxidase reaction (Figure 2) is the basis for the continuous colorimetric assay and is monitored by measuring the transmission of the reaction (λ = 480 nm, ε_{480} = 3300 M^{-1} cm^{-1}, 25 °C) [34]. The absorbance was then calculated by a Tecan plate reader. The reaction mixture had a final concentration of 1 mM SDS, 30 mM TRIS buffer (pH 7.75), 5 mM substrate and a certain amount of

enzyme with a total volume of 200 µL, if not stated otherwise. The reaction was initiated by adding substrate to the reaction.

One unit (U) is defined as the amount of enzyme that is required for the catalyzation of the reaction to 1 µmol product per min under the standard assay conditions. The specific activity was determined as unit per milligram enzyme in the assay (µmol min^{-1} mg^{-1}), whereas the protein concentration was determined according to the chapters 5.7.1 Absorption at 280 nm and 4.7.24.7.1. Lowry Protein Quantification. The volumetric activity is specified as unit per milliliter of enzyme solution (µmol min^{-1} mL^{-1}).

Due to the tyrosinase activity of L-*Fv*PPO either monophenolic tyramine or diphenolic dopamine or L-DOPA can be used as substrate. Tyramine exhibits a higher latency and is more suitable for quantitative activity measurement. As a diphenolic substrate dopamine is mainly utilized for a qualitative assessment of protein activity.

The activity assay for the active form of *Fv*PPO was performed as described before for the latent form, but without the addition of a detergent SDS.

4.6.1. Determination of the Isosbestic Point

Solutions: 500 mM Dopamine
200 mM $NaIO_4$ (f = 1.001)
150 mM TRIS pH 7.82 (25°C)
Materials: PS 1.5 mL semi-micro (12.5 x 12.5 x 45mm)
Device: UV spectrophotometer Shimadzu UV-1800 (Shimadzu ,Kyōto, Japan)

The concentration of the educt dopamine, the excess of $NaIO_4$ and the temperatures were varied to determine potential isosbestic points in the measurement dopachrome. First the educt concentration and the $NaIO_4$ excess were varied until the signal of the absorbance spectrum (850-200 nm) exhibited a sufficient high over a time period of 10 min. Then the temperature was varied in order to determine any temperature influences on the signal. Based on the pretests the reaction mixture was prepared according to Table 10 directly in the cuvette with a final volume of 1.5 mL, but the reaction was started by adding $NaIO_4$ at last. Multiple spectra of the reaction with this specific buffer were measured in time intervals of 70 seconds.

In order to determine the molar absorption coefficient at the wavelength of the isosbestic point, the absorption was measured at different concentrations of dopamine in the reaction mixture, which was varied from 500 to 400, 300, 200 and 100 µM utilizing Lambert Beer´s Law. The slope of the regression curve represents the molar absorption coefficient.

Table 10 Summary of the measurement conditions and final concentrations of the reaction mixture for the determination of the isosbestic point. The Dopamine concentration is varied from 500 to 400, 300, 200 and 100 µM when the molar absorption coefficient is evaluated.

	Final concentration (mmol L^{-1})
$NaIO_4$	10
Dopamine	0.5
TRIS	50
Temperature: 298.15 K	
pH 7.75 (22°C)	

4.7. Determination of Protein Concentration

4.7.1. Absorption at 280 nm

Solutions: 13% NaClO solution (LACTAN, Graz, Austria)
Materials: QS 10.00 mm quartz cuvette (Volume 70 µL, layer thickness 10 mm VWR)
Precision wipes (e.g. Kimwipes®)
Device: UV spectrophotometer Shimadzu UV-1800 (Shimadzu ,Kyōto, Japan)

The protein solution were recovered after the measurement in quartz cuvettes, which were cleaned thoroughly before usage as follows. NaClO solution, isopropanol, water and buffer were added to the cuvette in this order. The first solution was incubated for 5 min, while the others were added and immediately withdrawn by suction. The baseline was measured with deionised water. The spectrum of the buffer was measured and was used a blank that was subtracted when evaluating the results. All measurements were performed at room temperature. For sample dilutions of up to 1:70, the buffer was presented first and then the sample was diluted directly in the cuvette. Air bubbles can arise and interfere with the measurement. They were removed by stirring the solution with the pipette tip. The outside of the cuvette was cleaned with isopropanol and dust free wipes. Although the concentration determination only requires the absorption at 280 nm, the whole spectrum (900 – 200 nm) was measured in order to make a quality assessment of the sample and identify possible impurities. The A_{280} signal was divided by the theoretically Absorbance value at 0.1% (=1 g/L) calculated by the online tool ProtParam [73].

4.7.2. Lowry Protein Quantification

Solutions: Solution A (0.1 M NaOH with 2 % Na_2CO_3 and 0.5 % SDS)
Solution B (1 % $CuSO_4 \cdot 5H_2O$ in H_2O)
Solution C (2 % Trisodium citrate in H_2O)
1:1 dilution Folin-Ciocalteau´s phenol solution (Merck, Darmstadt, Germany)
BSA stock solution in ddH_2O (1 g L^{-1})
Materials: PS 1.5 mL semi-micro (12.5 x 12.5 x 45 mm)
Device: SPECTROstar Nano (BMG LABTECH, Ortenberg, Germany)

Solution ABC was prepared by mixing 10 mL solution A, 100 µL solution B and 100 µL solution C. Triplicates containing 10, 20, 30, 40 and 50 µg BSA per mL solution ABC were prepared to determine a standard curve. The samples of unknown concentration were prepared in the same way so that the concentrations were going to lie within the range of the standard curve. All samples were vortexed before and after the addition of 100 µL Folin-Ciocalteau´s phenol solution to a volume of 1.1 mL and then incubated in the dark (closed shelf) for 45 min. The measurement were performed at 750 nm.

4.8. Sodium Dodecyl Sulfate Polyacrylamide Gel Electrophoresis (SDS-PAGE)

The method of Laemmli was used for the determination of the size of the protein and for an assessment of the purity of a protein sample [74].

4.8.1. Preparation of Hand Cast SDS-PAGE Gels

4.8.1.1. SDS-PAGE Gel with Fixed Polyacrylamide Gel Concentration

Solutions: 10 % (w/v) APS (freshly prepared)
10 % (w/v) SDS
TEMED
1.5 M TRIS pH 8.8 (RT)
1.0 M TRIS pH 6.8 (RT)
ROTIPHORESE®Gel 30 (37.5:1), ready-to-use
(Carl Roth GmbH + Co. KG, Karlsruhe, Germany)
Isopropanol

Materials: Mini-PROTEAN® Tetra Handcast Systems (Bio-Rad Laboratories, Inc, Hercules, USA)

First, the comb, the spacer plates and the short plates that form a cassette sandwich with 1 mm integrated space when assembled, were cleaned with deionized water and isopropanol. The resolving gel solution was prepared according to Table 11, whereas the SDS, APS and TEMED solutions were added in this order. The mixture was thoroughly mixed without generating foam and subsequently a volume of 4.5 mL of it was pipetted in one assembled cassette. To prevent conus formation and the access of inhibiting oxygen to the resolving gel a layer of isopropanol was added on top of it. After 15 min the apparatus is tilted, and the isopropanol was decanted as completely as possible while soaking it in a paper towel. While the isopropanol residues evaporate, the stacking gel was prepared and again the SDS, APS and TEMED solution were added in this order. The solution was pipetted up to the top of the cassette. After 15 min hardening time, the cassette was washed with deionized water to remove the spilled stacking gel of the glass plates. Drying was not required, since the cassette was packed in wet paper towels and sealed in a plastic bag. The bag was placed over night in the fridge to finish the polymerization. Storage of gels more than two weeks is not recommended.

Table 11 Pipetting scheme for a volume of 5 mL stacking and resolving gel respectively with fixed gel concentrations.

Gel	**Resolving**			**Stacking**
Separation range (kDa)	20-80	12-60	10-43	-
Gel concentration	10 %	12 %	15 %	5 %
	Volume			
deionised water	7.9 mL	7.9 mL	7.9 mL	7.9 mL
ROTIPHORESE®Gel 30 (37.5:1)	6.7 mL	6.7 mL	6.7 mL	6.7 mL
10 % (w/v) SDS	200.0 µL			200.0 µL
1.0 M TRIS pH 6.8(RT)	-			-
1.5 M TRIS pH 8.8(RT)	5.0 mL			5.0 mL
10 % (w/v) APS	200 µL			200 µL
TEMED	20 µL			20 µL

4.8.1.2. SDS-PAGE Gel with a Gradient of Polyacrylamide Gel Concentration

Materials: Measuring pipette (5 mL)

The preparation of gradient gels was similar to the preparation of the hand cast gels for SDS-PAGE with a fixed concentration as described before. The gradient in the resolving gel was achieved by the mixing of two gel concentrations. Both were prepared separately according to Table *12*, again by adding last the SDS, APS and TEMED solutions in this order. Since polymerisation already started, the following steps were executed fast. The light solution (10 %) is pipetted up with a 5 mL measuring pipette. Then the heavy solution (15 %), that contains glycerol (15 %) was carefully taken up in the same pipette. A phase separation can be seen in between the solutions, which is interrupted by intentionally sucking air up, that wanders through the solution as bubbles. After 3 bubbles passed through the solution, it was immediately pipetted in the cassette. Then the gel was prepared as described before, which also includes the preparation of the stacking gel (5%) according to Table 11. Although the volume of the stacking gel was decreased by 0.5 mL, since it was sufficient for stacking of the protein.

Table 12 Pipetting scheme for a volume of 2.5 mL for the light and heavy solution that will be mixed for resolving gel with a gradient of 10-15 %.

Gel	**Light solution**	**Heavy solution**
Gel concentration	10 %	15 %
	Volume	
deionised water	1000.0 µL	333.5 µL
ROTIPHORESE®Gel 30 (37.5:1)	833.3 µL	1250.0 µL
87 % (v/v) Gylcerol	-	250.0 µL
10 % (w/v) SDS	25.0 µL	
1.5 M TRIS pH 8.8 (RT)	625.0 µL	
10 % (w/v) APS	15.0 µL	
TEMED	1.5 µL	

4.8.2. Performing SDS-PAGE

Solutions: 10 x Running buffer (192 mM glycine, 25 mM Tris pH 8.27 (22°C), 1 g L^{-1} SDS)
Laemmli sample buffer (250 mM Tris pH 6.8 at 25 °C, 3 % (w/v)
SDS,20 % (v/v) Glycerin, 0.02 %(w/v) bromophenol blue, 7.5 %(v/v) 2-Mercaptoethanol)
Materials: hand cast SDS-PAGE gel
Devices: PowerPac™ Basic Power Supply (Bio-Rad Laboratories, Inc, Hercules, USA)
Mini-PROTEAN Tetra Vertical Electrophoresis Cell
(Bio-Rad Laboratories, Inc, Hercules, USA)
SPROUT® PLUS (Heathrow Scientific, Illinois, USA)

4.8.2.1. Reducing SDS-PAGE

If not stated otherwise, 5 µg of the protein of interest or an aliquot of a few microliters of a purification step were mixed with 4 µL Laemmli buffer. Deionised water was added to a final volume of 20 µL. The closed tube was then placed in a heating block at 95 °C for 10 min. After the sample cooled down to room temperature, it was centrifuged on a tabletop centrifuge for 2 min until no condensed water was visible.

Samples of the chaperone wash buffer 1 were loaded while hot (95 °C) to prevent the formation of insoluble potassium salts of SDS, which are commonly known for the extraction and purification of SDS solubilized proteins and DNA structures [75].

The glass plates containing the hand cast gel were cleaned with deionised water and isopropanol. Then the electrophoresis cell was assembled, and the 1x SDS running buffer was poured into it. The samples were applied on each lane, including a reference protein marker.

The current in the two sections of the gel was 80 V in the stacking gel for 15 min and was then increased to 120 V, which was hold until the blue colored solvent front reaches the end of the gel.

4.8.2.1.1. SDS-PAGE Staining

Solutions: Destaining solution (45 % (v/v) methanol, 10 % (v/v) acetic acid)
Staining solution (Destaining solution + 0.25 % (w/v) coomassie brilliant blue R-250)

After the protein samples were separated on the reduced SDS-PAGE gel after electrophoresis as described before, the glass plates were removed and the gel was rinsed with deionised water. Then it was washed under mild agitation. Starting and ending with deionised water and in between it was soaked with destaining solution each for 10 min. The staining solution was added to the gel and it was soaked over night.

The staining solution can be reused up to 5 times. After rinsing with deionised water, the purple gel was covered with destaining solution. Again, every step was performed under mild agitation. Once the destaining solution was purple, it was recycled by filtering it through a funnel that contains filter paper filled with activated carbon. When the first bands were visible, the solution was changed to deionised water. When the background of the gel is not violet anymore, a picture of the gel was made. The gel can be stored in a sealed plastic bag at 4°C.

4.8.2.2. Non-reducing SDS-PAGE

This method differs from the reducing SDS-PAGE in the preparation of the sample. The reducing agent 2-mercaptoethanol was not added to the sample buffer. The reference protein marker that was used in the reduced SDS-PAGE can not be used to assess the size of the protein. The same current profile as in the reduced SDS-PAGE was used (80 V for 15 min and then hold at 120 V).

4.8.2.2.1. Activity Staining

The staining of non-reduced PAGE gels is based on the tyrosinase activity of L-*Fv*PPO. After electrophoresis the gel was rinsed and then washed with deionised water in a plastic container for 10 min under mild agitation. The water was discarded and the activity staining of the PPO was initiated when a tyramine solution (5 mM tyramine hydrochloride in dH_2O) was added. After approximately 10 min the first brown bands appeared. It was washed thoroughly with deionised water, in order to prevent further reaction and therefore dying of the whole gel in brown color. The gel was stored in a sealed plastic bag at 4 °C.

4.9. Western Blot

4.9.1. Loading of the Membrane

Solutions Blocking solution (20 mL PBS (1 x) with BSA (20mg L^{-1}))
Materials Trans-Blot Turbo Mini Transfer Packs (Bio-Rad Laboratories, Inc, Hercules, USA)

Blot roller (Bio-Rad Laboratories, Inc, Hercules, USA)

Device — Trans-Blot Turbo (Bio-Rad Laboratories, Inc, Hercules, USA)

The device´s bottom cassette (anode) and top cassette (cathode), as well as the SDS-PAGE gel were rinsed with deionised water. The anode reservoir stack with the blotting membrane on top was placed on the wet bottom cassette without touching the membrane. Trapped air bubbles were carefully removed with the moisturized blot roller. The SDS-PAGE gel was placed on top of the membrane and air bubbles were again removed once the cathode reservoir stack has been placed on top of it. The top cassette was placed on top and the sealing mechanism locks the cassette. The preprogrammed protocol MIXED MW (settings: 1.3 A constant, up to 25 V; 5-150 kDa; 7 min) of the device allowed a quick transfer of the protein bands on to the membrane. Protein bands of the ladder and the sample with a molecular weight greater than 150 kDa were transferred to the membrane too, despite it was not recommended by the manufacturer.

The success of the transfer onto the membrane was verified by the identification of the protein marker on the membrane. It was rinsed with deionised water and a volume of 20 mL blocking solution was added to the membrane in a closable container. Air bubbles beneath the membrane were removed by thoroughly shaking the container. The closed container was incubated under mild agitation for at least 90 min or over night. The membrane was now blocked and was processed based on the protein tag of interest.

4.9.1.1. Western Blot Protocol

4.9.1.1.1. His6-Tag

Solutions — Washing solution 1 (1x PBS, 0.2 % (v/v) Tween 20)
Alkaline phosphatase buffer (100 mM NaCl, 0.1 M Tris and 5 mM MgCl2, pH 9.5 (RT))
Anti-His6 -tag Antibody (organism: Mouse) (Bio-Rad Laboratories, Inc, Hercules, USA)
50 mg mL^{-1} BCIP
50 mg mL^{-1} NBT

The blocking solution was discarded and the membrane was washed two times with 10 mL washing solution for 10 minutes. The Anti-His6 -tag antibody was added to 15 mL PBS in a ratio of 1: 5000, and then the membrane was incubated for 90 minutes on a shaking rack. The membrane was rinsed two times with 10 mL washing solution 1. The development of the bands with the color reaction was started by adding 10 mL AP buffer, 35 µL BCIP and 66 µL NBT in this order. Once the first faint violet bands appeared, the solution was discarded and the membrane was washed with deionised water multiple times.

The developed membrane can be stored at -20 °C between a sandwich of Whatman filters and cardboards in a closed plastic bag for at least 2 months.

4.9.1.1.2. GST-Tag

Solutions: PBS buffer (1 x)
Washing solution 2 (1 x PBS, 1 % (v/v) Tween 20)
Antibody solution I (Anti-GST antibody in washing solution 2 (1:2000))
Antibody solution II (goat x rabbit-Poly-HRP in washing solution 2 (1:2500))
SuperSignal™ West Pico PLUS Chemiluminescent substrates
(Thermo Fisher Scientific Inc. (NYSE: TMO), Massachusetts, USA)
Device: ChemiDoc Imager (Bio-Rad Laboratories, Inc, Hercules, USA)

The blocking solution was discarded and the membrane was washed 3 times with 20 mL washing solution 2 for 10 minutes. A total of 20 mL antibody solution I was added and the membrane was incubated for 1 hour on a shaking rack. Then it was washed two times with 15 mL washing solution 2. After another incubation step with antibody solution II for 1 hour, the membrane was washed 2 times with 20 mL washing solution 2 and 2 times with PBS buffer for 5 min each. The membrane was carefully rinsed a few times with deionised water before a volume of 1 mL of both chemiluminescent substrates were added. After incubating it a few moments while shaking it manually, the membrane was measured using the settings: “Blot”, “Chemic highest sensitivity” and “signal accumulation mode 1-30 s, 30 images”.

4.10. Activation of L-*Fv*PPO

4.10.1. Activation with Proteinase K

Solutions: Proteinase K (stock solution with 1.26 g L^{-1})
400 mM PMSF in Ethanol (fresh prepared)
150 mM TRIS pH 8.00 (22°C)
40 mM Sodium ascorbate
Materials: 1.5 mL Eppendorf protein LoBind® tube (Eppendorf SE, Hamburg, Germany)

The protease reaction was performed in a 1.5 mL Eppendorf protein LoBind® tube. For each time point 13 µg protein were required, whereas 2 x 5 µg protein were applied to reducing and non-reducing SDS-PAGE and 3 µg were used for an activity assay (50 mM TRIS pH 7.75 (22°C), 1 mM PMSF, 5 mM tyramine, 0.07 mM sodium ascorbate). The addition of sodium ascorbate increased the latency of the reaction. The ratio of protease to enzyme was chosen to be 1:4 (w/w) with a reaction duration of 25 min. The sampling times were 1, 2, 3, 4, 7, 8, 15 and 25 min. The protease reaction was prepared according to Table 13. The final volume of 200 µL was reached by adding deionised water. Finally, the protein solution with L-*Fv*PPO was added to start the reaction by mixing thoroughly.

The sample tubes for SDS-PAGE were prepared with 2 µL PMSF (400 mM) before taking a sample for a specific timepoint to facilitate the workflow. The wells for the activity assay contained PMSF in order to stop the reaction, and also 0.07 mM sodium ascorbate.

Table 13 Final concentration of the educts in the activation reaction of L-*Fv*PPO with proteinase K in a volume of 200 µL.

	Final concentration
Sodium ascorbate	5.00 mM
TRIS (final pH 7.75 (22°C))	50.0 mM
L-*Fv*PPO	1.00 g L^{-1}
Proteinase K	0.25 g L^{-1}

4.10.2. Activation with Cations

Solutions 50 mM TRIS pH 7.00 (22°C)
2 M stock solutions: KCl | $CaCl_2$ | NaCl | $MgCl_2$
500 mM dopamine
Materials BRANDplates® microtitration plate, 96-well, pureGrade™ S, F-bottom (BRAND GMBH + CO. KG, Wertheim, Germany)

The wells were prepared according to Table 14. The final volume of each well was 200 µL and the formation of the red orange dopachrome or melanin was documented qualitative by pictures after 1, 10, 20 and 50 min.

Table 14 Final concentrations in the experiment to assess the salt influence on the activation of L-*Fv*PPO.

Well	**1**	**2**	**3**	**4**			
Row	**KCl** (mmol L^{-1})	**$CaCl_2$** (mmol L^{-1})	**NaCl** (mmol L^{-1})	**$MgCl_2$** (mmol L^{-1})	**TRIS** (mmol L^{-1})	**Dopamine** (mmol L^{-1})	L-*Fv*PPO * (mg L^{-1})
A	50				48.50	2	14
B	100				47.25		
C	350				41.00		
D	500				37.25		
E	800				29.75		
F	1000				24.75		
G	1200				19.75		
H	1500				12.25		
***Purity of more than 80 % (chapter 5.13.2.2.1)**							

4.11. Quality Assessment of Protein Solution for Crystallization

4.11.1. Stability Test

Protein solutions of L-*Fv*PPO with a final glycerol concentration of 1, 2, 5, 10, 15 and 20 % were prepared. The stability of the protein with different glycerol concentrations were assessed with reducing SDS-PAGE (according to chapter 4.8.2.1) after the storage of the samples in the refrigerator at 4 °C for two weeks.

Without the addition of glycerol the stability of L-*Fv*PPO with a purity of more than 90 % was assessed after the storage at 4 °C in the fridge for 4 weeks.

4.11.2. Liquid Chromatography Coupled with Mass Spectrometry (LC-MS)

Bands of interest in the SDS-PAGE were cut out with a clean scalpel. Tryptic digests of the bands were prepared and analysed with LC-MS by the group of Univ.-Prof. Dr. Christopher Gerner (Department of Analytical Chemistry, University of Vienna). The samples were separated with 1260 Infinity LC System with nanopump, cappump and binpump (Agilent) and quantified with a 6490 triple-quadrupole mass spectrometry (Agilent) including MS/MS fragmentation.

4.11.3. Thermal Shift Assay (TSA)

Solutions: SYPRO orange (5000x)
Materials: Axygen® PCR Strip Tubes and Caps, 0.2 mL, clear (Corning, Arizona, USA)
Device: Eppendorf Realplex2 Mastercycler EP Gradient S (Eppendorf SE, Hamburg, Germany)

SYPRO Orange, the buffer of interest and the protein L-*Fv*PPO with a final concentration of 10 µM were added to a PCR tube. The working concentration of SYPRO orange was evaluated to be either 4-fold or 10-fold, since no significant increase in the signal intensity could be observed for L-*Fv*PPO. If necessary, deionised water was added to reach the final volume of 50 µL. Finally, the respective aliquot of SYPRO Orange dilution (50 x) was added to the reaction. Once the solution was mixed well in the PCR tube, it was closed and placed in the thermocycler. The temperature program started at 4 °C and was increased in 0.5 °C intervals until a temperature of 94 °C was reached. The fluorescence of the dye was measured during the temperature increase.

4.11.4. Dynamic Light Scattering (DLS)

Material: Glass cuvette (square cell with cap) (Malvern Panalytical GmbH, Kassel, Germany)
Whatman® UNIFLO® PVDF membrane, pore size 0.22 µm(Merck, Darmstadt, Germany)
Device: Zetasizer nano ZS (Malvern Panalytical GmbH, Kassel, Germany)

The measurement is non invasive and therefore, the protein solution can eventually be used for crystallization experiments. Therefore, cleanliness was important in this process. Dust in the cuvette or apparatus can influence the measurement. The cuvette was cleaned (according to chapter 4.7.1 Absorption at 280 nm), in order to recover the protein solution without additional impurities introduced. To get rid of dust particles, the buffer was filtered and then used to clean the cuvette one more time.

The system was switched on 1 hour before usage in order to reach a constant laser output and temperature. The measurement of filtered buffer reveals, whether particles are present and if not, it can be proceeded to the measurement of the protein solution. An estimation of the hydrodynamic radius of the target protein was required in order to choose a minimal protein concentration in accordance with the manufacturer manual. The hydrodynamic radius was estimated with the program HYDROPRO (Ver. 10, Sep 2011) in accordance with A. Ortega et al. whereas a model of the protein is used [76]. The pdb.file was created with AlphaFold v2 [77]. The hydrodynamic radius of L-*Fv*PPO was calculated to be 7.69 nm (with the parameters used in the calculation: 0.01 poise, 0.702 $cm^3\ g^{-1}$, 1.0 g cm^{-3}, 20 °C). According to the manual of the device the minimal protein concentration in the measurement was 0.5 mg mL^{-1}. The settings for the refractive indices of the buffers and cuvette, as well as the back scattering measure mode were chosen in the ZETASIZER Software (Ver.7.12). The sample was centrifuged (12 000 x g, 10 min, 4 °C) and when is was pipetted in the cuvette, the outside of the cuvette was cleaned with a dust free wipe. The measurement was started in backscatter mode and the attenuator was selected automatically. The size distribution was calculated by the software based on three measurements of the same sample and was resembled in one curve.

4.11.5. Copper Quantification

Solutions: 2 M Sodium ascorbate
0.5 g L^{-1} 2,2´Biquinolinic acid in glacial acid
30 mM Tris pH 8.00 (22°C)
deionised water

Materials: QS 10.00 mm quartz cuvette (Volume 70 µL, layer thickness 10 mm VWR)
Whatman® UNIFLO® PVDF membrane, pore size 0.22 µm
(Merck, Darmstadt, Germany)

Device: UV spectrophotometer Shimadzu UV-1800 (Shimadzu ,Kyōto, Japan)

This method is used for the determination of Cu(I) in the sample and is based on Hanna et al. [78]. All buffers were filtered before usage. A mixture of 2,2´biquinolinic acid and sodium ascorbate in a final concentrations of 0.3 g L^{-1} and 0.1 M respectively was prepared in an Eppendorf tube. A volume of 10 µL L-*Fv*PPO (17.26 g L^{-1}) was added last to the solution for a final volume of 200 µL and initiated a pink color in the solution, due to the formation of the (biquinoline)Cu(I) complex. The reaction solution was mixed thoroughly by pipetting and vortexing. After a reaction time of 10 min the mixture was vortexed again and the sample´s absorbance at 546 nm was determined. The blank contained buffer (30 mM TRIS (pH 8.00)) and was like the sample measured in triplicates.

4.12. Protein Crystallization

4.12.1. Overview of Batches Used for Crystallization

Although it was not anticipated, the purification of L-*Fv*PPO resulted in different batches at different purification levels, which are summarized in Table 15. These batches were used in the crystallization experiments.

Table 15 Overview of the batches used for crystallization and their reference in this work as batch with a purity of either more than 80 % or 90 % purity, or concentrated with HIC.

Batch label	Purification steps	Purity assessment	Buffer composition
More than 80 % purity	2x HisTrap, 1x AEX	Chaperones present	50 mM Tris, 500 mM NaCl pH 8.01 (25 °C)
Concentrated with HIC	2x HisTrap, 3x AEX, 1x HIC	High purity, no chaperones	30 mM Tris, 0.65 mM $(NH_4)_2SO_4$ pH 8.35 (22°C)
More than 90 % purity	2x HisTrap, 1x AEX	High purity, no chaperones	30 mM Tris, pH 8.00 (22°C)

Aliquots of protein solution with more than 80 % purity must be thawed before crystallization, since they were stored at -80 °C. The glycerol must be buffer exchanged 4 times with 30 mM TRIS, 500 mM NaCl at pH 8.01 (25°C) by centrifugation (10 000 x g, 10min; Filter; Vivacon 500, 30kDA (Sartorius AG, Göttingen, Germany)). The batch that was concentrated with HIC and the one with a purity of more than 90 % were stored at 4 °C without glycerol. All samples were centrifuged at 12 000 x g for 10 min before using for crystallization.

4.12.2. Vapor Diffusion

4.12.2.1.1. Hanging Drop (HD)

4.12.2.1.1.1. General Description

Material: 15 well EasyXtal plates (Qiagen, Hilden, Germany)

To decrease the risk of water evaporation of the buffers during storage, they were prepared freshly one day before usage. A volume of 500 µL buffer was added into the reservoir of every experiment. The respective cap was turned upside down and up to five drops with a volume of up to 1 µL buffer were pipetted in a circular arrangement. The evaporation of water in the drop influences the final protein concentration of the drop. The final volume of the drop was dictated by the buffer volume. When these factors were considered, the calculated volume of the protein was added to the drops respectively and mixed by pipetting. Once the cap was loaded, it was flipped fast and the well was closed tight by screwing. According to the manual of the plate manufacturer no grease is required for sealing. The plates were stored in a tempered shelf at 291.15 K.

4.12.2.1.1.2. Literature Search

Six conditions for the successful crystalized PPOs which were found in literature are listed in Table 16. Deviating pH values of the used buffers in these experiments were in *italics* in Table 16. They were prepared for L-*Fv*PPO with a purity of more than 90 % and for the batch that was concentrated with HIC in VD-HD. Three drops per well were arranged according to Table 17.

Table 16 Literature references for successful crystallization experiments of polyphenol oxidases of different species. These conditions were used in crystallization experiments as stated in the text, and the deviations in the pH value of the conditions are marked in *italics*. The start and end concentrations were referred to the state of the drop before and after equilibration of the drop.

Protein	Buffer	Additive	Protein concentration in drop, start (g L^{-1})	Protein concentration in drop, end (g L^{-1})	Temperature (K)	PDB entry number	Reference
Latent tyrosinase from apple (*Malus domestica*)	100 mM TRIS 13 % (w/v) PEG 8000 pH 8.25 *pH 8.26 (at 22°C)*		7.5	15	293.15	6ELS	[79]
Tyrosinase from walnut (*Juglans regia*)	100 mM MES 30 % (w/v) PEG 5000 MME pH 6.5 *pH 6.39 (at 22°C)*	200 mM $(NH_4)_2SO_4$	20	10	293.15	5CE9	[22]
Latent aurone synthase from calliopsis (*Coreopsis grandiflora*)	60 mM sodium citrate 15 % (w/v) PEG 4000 pH 7.4	100 mM $MgCl_2$	7	14	293.15	4Z14	[80]
Polyphenol oxidase (apo-form) from tomato (*Solanum lycopersicum*)	50 mM sodium citrate 13 % (w/v) PEG 8000 pH 6.8 *pH 6.77 (at 22°C)*		5	10	293.15	6HQJ	[25]
Catechol oxidase from Grenache (*Vitis vinifera*)	100 mM sodium citrate 30% (w/v) PEG 4000 pH 5.6 *pH 5.61 (at 22°C)*	200 mM ammonium acetate	5	10	291.15	2P3X	[81]
Catechol oxidase from sweet potato (*Ipomoea batatas*)	50 mM Hepes 12% (w/v) * PEG 6000 pH 7.0	500 mM NaCl	14**	14**	277.15	1BT1	[82]

*** equilibrated against a solution of 20% w/v PEG 6000**
****starting and end concentration in drop not clearly stated in literature**

Table 17 Overview of the drop composition utilizing VD-HD.

L-*Fv*PPO protein batch	More than 90 % purity			Concentrated with HIC		
Protein concentration (g L^{-1})	5.23			17.63		
Composition of reservoir	Literature conditions of Table 16 with the respective adjusted pH values in *italics*					
Volume of drop (µL)	1.50	2.00	2.50	1.25	1.56	2.00
Volume of reservoir solution in drop (µL)	1.00					
Protein concentration in drop, start (g L^{-1})	1.74	2.62	3.14	3.53	6.33	8.82
Protein concentration in drop, end (g L^{-1})	2.62	5.23	7.85	4.41	9.87	17.63
Incubation temperature (K)	291.15					

4.12.2.1.1.3. Grid screen

In the grid screen the following condition were used: 50 mM sodium citrate, 13 % (w/v) PEG 8000 and pH 6.8 were varied systematically in VD-HD set up. The buffer concentration was hold constant and the PEG concentration was chosen to be 11 %, 13 % or 15 % (w/v) and five different pH values were chosen in a range of ± 0.5 units. The variations are summarized in Table 18. In contrast to the literature search, all solutions besides the protein solution, were filtered through a PES 2 µm syringe filter before usage. Five drops were pipetted per well according to Table 19.

Table 18 Summary of the grid screen conditions utilizing VD-HD. The buffer composition was 50 mM sodium citrate and Incubation temperature was 291.15 K.

Row	Well	pH	PEG 8000 concentration (%)
A	1	6.36	11
	2	6.61	
	3	6.86	
	4	7.11	
	5	7.36	
B	1	6.36	13
	2	6.61	
	3	6.86	
	4	7.11	
	5	7.36	
C	1	6.36	15
	2	6.61	
	3	6.86	
	4	7.11	
	5	7.36	

Table 19 Overview of the drop composition in the grid screen utilizing VD-HD.

L-*Fv*PPO protein batch	More than 90 % purity				
Protein concentration (g L^{-1})	5.00				
Composition of reservoir	conditions of Table 18				
Volume of drop (µL)	1.40	1.60	2.00	2.20	4.00
Volume of reservoir solution in drop (µL)	1.00				
Protein concentration in drop, start (g L^{-1})	1.43	1.88	2.50	2.73	3.75
Protein concentration in drop, end (g L^{-1})	2.00	3.00	5.00	6.00	15.00
Incubation temperature (K)	291.15				

4.12.2.1.1.4. Precipitation Approach with TEW and YCl_3

Solutions: 50 % (v/v) PEG 2000
40 % (w/v) PEG 8000
10 mM TEW in ddH_2O (prepared in the lab)
10 mM YCl_3 in ddH_2O

The drops that were prepared according to Table 20 and Table 21 the precipitation behaviour of L-*Fv*PPO with purity of more than 80 % should be evaluated after 24 hours equilibration. The TEW and YCl_3 solutions were filtered with a PES 2 µm syringe filter. A final concentration of 1 mM YCl_3 was anticipated in the drops after 24 h. TEW was added once the drops have been equilibrated for 24 hours at 291.15 K to a final concentration of 1 mM after another day. The PEG solutions 50 % (v/v) PEG 2000 and 40 % (w/v) PEG 8000 were prepared the day before usage [83].

Table 20 Overview of the drop composition in the precipitation approach. Deionised water was added to the final volume of the drops. After 24 h equilibration, TEW was added to a final concentration of 1 mM. The experiment was performed in VD-HD.

L-*Fv*PPO protein batch	**More than 80 % purity**													
Protein concentration (g L^{-1})	24.36													
Composition of reservoir	50 % (v/v) PEG 2000													
Volume of drop (µL)	4													
Volume of reservoir solution in drop (µL)	1													
Volume of deionized water in drop (µL)	2.8	2.7	2.6	2.5	2.4	2.3	2.2	2.1	2.0	1.9	1.8	1.6	1.4	0.9
Final Protein concentration in drop (g L^{-1})	4	8	10	12	15	18	20	22	24	28	30	35	40	50
Incubation temperature (K)	291.15													

Table 21 Overview of the drop composition in the precipitation approach with a final concentration of 1 mM YCl_3. The experiment was performed in VD-HD.

L-*Fv*PPO protein batch	**More than 80 % purity**					
Protein concentration (g L^{-1})	14.76					
Composition of reservoir	40 % (w/v) PEG 8000					
Volume of drop (µL)	5					
Volume of reservoir solution in drop (µL)	0.25					
Volume of YCl_3 solution in drop (µL)	1.5					
Volume of deionized water in drop (µL)	3.1	3.0	2.7	2.6	2.4	2.2
Final Protein concentration in drop (g L^{-1})	8	16	32	40	48	60
Incubation temperature (K)	291.15					

4.12.2.1.2. Sitting Drop (SD)

Solutions: JBSCreen Classic 1-10 (Jena Bioscience, Thuringia, Germany)
Crystallization Basic Kit for Proteins (Sigma Aldrich, Buchs, Swiss)

Materials: CRYSTALQUICK RW PLATE, 96 WELL, COC, LBR (RW: round wells; COC: concave bottom; LBR: low birefringence) (Greiner Bio-One GmbH, Frickenhausen, Germany)
Sealer VIEWseal (Greiner Bio-One GmbH, Frickenhausen, Germany)
Eppendorf™ 96-Well Protein LoBind Deep Well Plates, 1mL
(Fisher Scientific GmbH, Schwerte, Germany)
PCR Tubes (VWR, Vienna, Austria)

Device: CRYSTAL GRYPHON (Art Robbins Instruments, Sunnyvale, USA)

Either commercially available kits or manually prepared buffer systems were used in an automated approach utilizing a pipetting robot. The used kits in these assays were stored at 4 °C and at the day before usage, they were placed at room temperature. The containers with the buffers were inverted multiple times before usage. The other manually prepared buffers were used directly after preparation. All buffers were pipetted manually in a 96 well plate.
A tank of ddH_2O was connected with the tubes and the pumps were switched on. The system was flushed until no bubbles were visible in the transparent pipes. The 96 well plate containing the buffers and the, yet empty crystallization plate were placed at the proper positions of the device. A minimum volume of 150 µL protein solution was presented in a PCR Tube to avoid the formation of protein foam in the pipe, when it was aspirated.
The program was started, beginning with a washing step of the syringes and the aspiration needle with deionized H_2O. In total 96 reusable syringes were used for dispensing 100 µL buffer into the reservoir and then for placing drops with a volume of 0.2 µL on the platforms of the respective experiment. The used crystallization plates have 96 reservoirs each containing three wells. On each well either 0.2, 0.4 or 0.8 µL of the protein solution with more than 80 % purity were added by the aspiration needle. Once the crystallization assay was prepared it was sealed with clear transparent sealing tape and stored at the respective temperature.
The set up of the plates in a sparse matrix screen or grid screen summarized in Table 23 and the respective drop composition for each plate is depicted in Table 22. The plates were either stored at 277.15 K in the fridge or in a tempered shelf at 291.15 K.

Table 22 Composition of the drops in the VD-SD protein crystallization assay. The plate numbers refer to Table 23, that lists the buffer composition. The respective drop in each well is abbreviated with I, II and III.

Plate	Protein concentration in the stock (g L^{-1})	Respective Well in Reservoir	Volume of drop (µL)	Ratio of drop (protein:reservoir)
1	17	I	0.4	1:1
		II	0.6	2:1
		III	1	4:1
2		I	0.4	1:1
		II	0.6	2:1
		III	1	4:1
3	30	I	0.4	1:1
		II	0.6	2:1
		III	1	4:1
4	39.69	I	1	4:1
		II	0.6	2:1
		III	0.4	1:1

Plate	Protein concentration in the stock (g L^{-1})	Respective Well in Reservoir	Volume of drop (µL)	Ratio of drop (protein:reservoir)
5		I	0.4	1:1
		II	0.6	2:1
		III	1	4:1
6		I	0.4	1:1
		II	0.6	2:1
		III	1	4:1

Table 23 Summary of the protein crystallization experiments with L-*Fv*PPO performed with the pipetting robot in VD-SD.

Plate	Row	Well	Buffer	Buffer Concentration	Precipitant	Precipitant concentration (%)	Additive and concentration	pH	T (K)
1	A-H	1-12	JBSCreen Classic 1-4						277.15
2	A-H	1-12	JBSCreen Classic 1-4						291.15
3	A	1-3	TRIS	100 mM	PEG 8000	10, 13, 16		8.25	291.15
		4-6				10, 13, 16		8.0	
		7-9				10, 13, 16		7.5	
		10-12				10, 13, 16		7.0	
	B	1-3		50 mM		10, 13, 16		8.25	
		4-6				10, 13, 16		8.0	
		7-9				10, 13, 16		7.5	
		10-12				10, 13, 16		7.0	
	C-F	1-12	JBSCreen Classic 5-6						
	G	1-12	JBSCreen Classic 3						
	H	2-12							
	H	1	TRIS	50 mM	PEG 8000	16		7.0	
4	A-H	1-12	JBSCreen Classic 7-10						291.15
5	A	1-4	TRIS	50 mM	PEG 4000	20, 15, 10, 5		8.0	291.15
		5-9						7.5	
		10-12						7.0	
	B	1-4		100 mM		20, 15, 10, 5		8.0	
		5-9						7.5	
		10-12						7.0	
	C	1-4				20, 15, 10, 5	100 mM $MgCl_2$	8.0	
		5-9						7.5	
		10-12						7.0	
	D	1-4				20, 15, 10, 5	50 mM $MgCl_2$	8.0	
		5-9						7.5	
		10-12						7.0	
	E	1-4				20, 15, 10, 5	100 mM MgCl2 100 mM NaCl	8.0	
		5-9						7.5	
		10-12						7.0	
	F	1-4				20, 15, 10, 5	50 mM $MgCl_2$ 50 mM NaCl	8.0	
		5-9						7.5	
		10-12						7.0	
	G	1-4				20, 15, 10, 5	100 mM NaCl	8.0	
		5-9						7.5	
		10-12						7.0	
	H	1-4				20, 15, 10, 5	50 mM NaCl	8.0	
		5-9						7.5	
		10-12						7.0	
6	A	1-4	Citrate-phosphate buffer	50 mM	PEG 4000	30, 25, 20, 15		7.6	291.15
		5-9						6.6	
		10-12						5.2	
	B	1-4				30, 25, 20, 15	500 mM NaCl 100 mM HCOONa	7.6	
		5-9						6.6	
		10-12						5.2	
	C	1-4				30, 25, 20, 15	500 mM NaCl	7.6	
		5-9						6.6	
		10-12						5.2	
	D	1-4				30, 25, 20, 15	100 mM HCOONa	7.6	
		5-9						6.6	
		10-12						5.2	
	E	1-2	Crystallization Basic Kit for Proteins condition 49,50						
	E	3-12	Crystallization Basic Kit for Proteins condition 1-10						
	F-H	1-12	Crystallization Basic Kit for Proteins condition 11-48*						

*** Condition 17 and 20 of the kits were not used**

4.12.3. Monitoring of Protein Crystal Growth

Devices: Leica M205 C stereomicroscope (Leica Microsystems GmbH, Wetzlar, Germany)
Suitable polarity filter

The protein crystal growth was monitored regularly with a stereomicroscope. Since it is always helpful to have an idea what can be expected in a drop, before it is observed, the model of Zeelen Johann Phillip depicted in Figure 9 can be used for comparison [83]. The protein drops were examined first daily in the first week, then weekly. The usage of a stereomicroscope with polarity filter facilitates this task. A crystal with birefringence has a different color compared to the background as it is seen in Figure 9 in Plate 20.

For an uniform assessment of the crystalization progress and also to simplify the documentation, an evaluation system based on this orientation aid by Zeelen Johann Phillip [83] was applied for documentation of the crystal growth. Each observed condition received a number. The documentation can be adjusted if not every crystallization state can be observed. The respective number assignment can be found in the chapter 6.2.1.2 Evaluation of VD-SD Experiments and in 6.2.2.2 Evaluation of VD-HD Experiments.

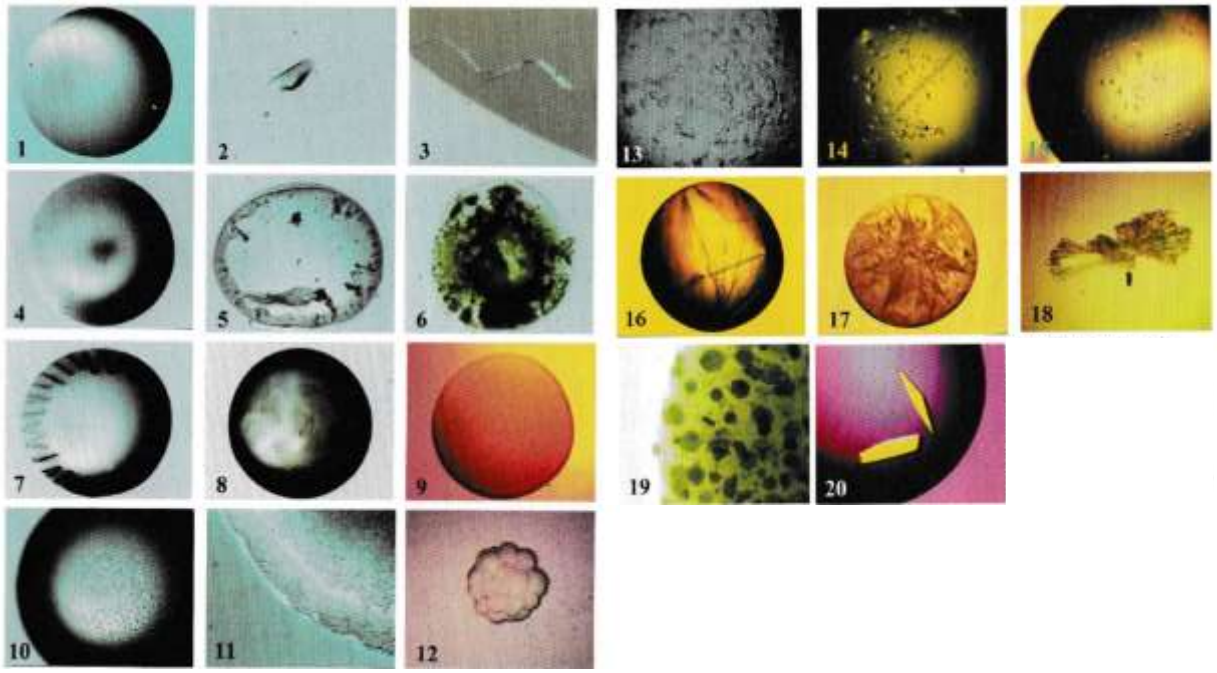

Figure 9 Different crystallization states or impurities and their respective number assignment in brackets by Zeelen Johann Phillip: Plate 1, Drop is clear (0); Plate 2, Piece of glass with irregular shape (1); Plate 3, Fiber from clothes, they are colorful in polarized light (1); Plate 4, Drop is mostly clear (2); Plate 5, Protein precipitated upon mixing with a viscous well solution. Visible as a clear region with dark edge (3); Plate 6, The protein is fully precipitated. The color of the precipitant is dark (3); Plate 7, Drop with wrinkled skin of precipitated protein (3); Plate 8, The drop contains gelatinous protein precipitate (4); Plate 9, Gelatinous protein under polarized light(4); Plate 10, Phase separation, visible as small droplets (5); Plate 11, Spherulites (6); Plate 12, Transparent cluster(6); Plate 13, Too quickly grown crystals (6); Plate 14, Microcrystals and crystals after streak seeding (6); Plate 15, Microcrystals (6); Plate 16, Needles (7); Plate 17, Shower of needles under polarized light (7); Plate 18, Needles grown after seeing with one small needle (8); Plate 19, Hexagonal plates (8); Plate 20, Crystals under polarized light (9). Graphic from [83].

4.12.4. Differentiation between Salt and Protein Crystal

Solutions: JBS Deep Purple (Jena Bioscience, Thuringia, Germany)
100 mM dopamine
100 mM SDS
Materials: microscope slide and Siliconized glass cover slips

The decision if a protein crystal or salt crystal is present or not, can be made by utilizing destructive methods. However, these only give indications instead of conformation.

The addition of 0.5 µL JBS Deep Purple dye to a drop with a potential crystal, leads to a coloring of the solution and eventually dyes the crystal with the respective color. If no crystal coloring occurs after 30 min, a drop of the reservoir solution with a suitable volume (e. g. 2 µL) is placed on a microscope slide and the potential crystal is transferred to this drop. The transfer happens with a loop, whose diameter has been estimated based on the size of the crystal. The loop is carefully placed around the crystal and lifted so that the crystal is in the center of the formed liquid film. If this transfer and the following ones are successful can be observed under the stereomicroscope.

Two deionized water drops with a volume of 4 µL were pipetted next to the crystal and 2 µL dopamine were mixed to both. A volume of 2 µL SDS (100 mM) were added to the second drop. Then the potential protein crystal was transferred to the first drop without SDS and then to the second with SDS. Since the latent PPOs in crystalline form exhibit activity in the presence of their substrates and SDS, the addition of both can dye the crystal orange/red. This is also referred to as an in *crystallo* activity tests [84]. The protein solution in the second drop is going to become red due to PPO in the liquid film. If no dying of the crystal is observed, it is washed in the reservoir drop, before placing it into another one containing only reservoir solution.

The microscope slide containing the drops and the crystal in the reservoir solution was picked up with tweezers and rapidly passed threw the lower part of a Bunsen burner flame. The drop is inspected carefully after the so called “Trail by fire” [85]. Due to the high melting point of salt crystals, it will eventually not melt. If the crystal does not melt, it is prepared as reduced SDS sample (according to chapter 4.8 Sodium Dodecyl Sulfate Polyacrylamide Gel Electrophoresis (SDS-PAGE)) and after heating it, the crystal is again examined under the microscope and eventually applied under the microscope.

5. Results

5.13. Protein Expression and Characterisation

5.13.1. Molecular Cloning of L-*Fv*PPO-GST

The success of the molecular cloning was accessed by agarose gel electrophoresis and finally by sequencing. In Figure 10 the agarose gels with the PCR products are depicted that resulted during molecular cloning. For the sticky end ligation, the PCR products of FS + RL were required. In Figure 10A the PCR products of the primer systems FS + RL and FL + RS could be found at the expected band size of approx. 1.5 kb. The faint bands in in both lanes were not regarded as the necessary PCR products for sticky end ligation and therefore were not extracted for further cloning. The concentration of the gel extracts was determined to be 32.3 ng μL^{-1} for FS + RL and 25.02 ng μL^{-1} for FL + RS. After denaturation and annealing, four PCR products were produced, whereas only the FL/RL PCR product was ligated with the vector. After heat shock transformation of the plasmid, the transformed cells had not grown in high abundance on the agar plates over night at 36 °C. A colony PCR and agarose gel electrophoresis (Figure 10B and C) of 10 colonies of *E. coli* pGEX-6P-1_L-*Fv*PPO confirmed the transformation success, since the expected PCR product FL + RL could be identified in each colony. The sequencing results of the extracted plasmid verified that no mutations had been introduced. The extracted plasmid pGEX-6P-1_L-*Fv*PPO from colony 1 was transformed in *E. coli* BL21(DE3). Using the same approach, the transformation success was confirmed for 5 colonies with colony PCR as well, since the PCR products at 1.5 kb could be found in tested colony as it is displayed in Figure 10D.

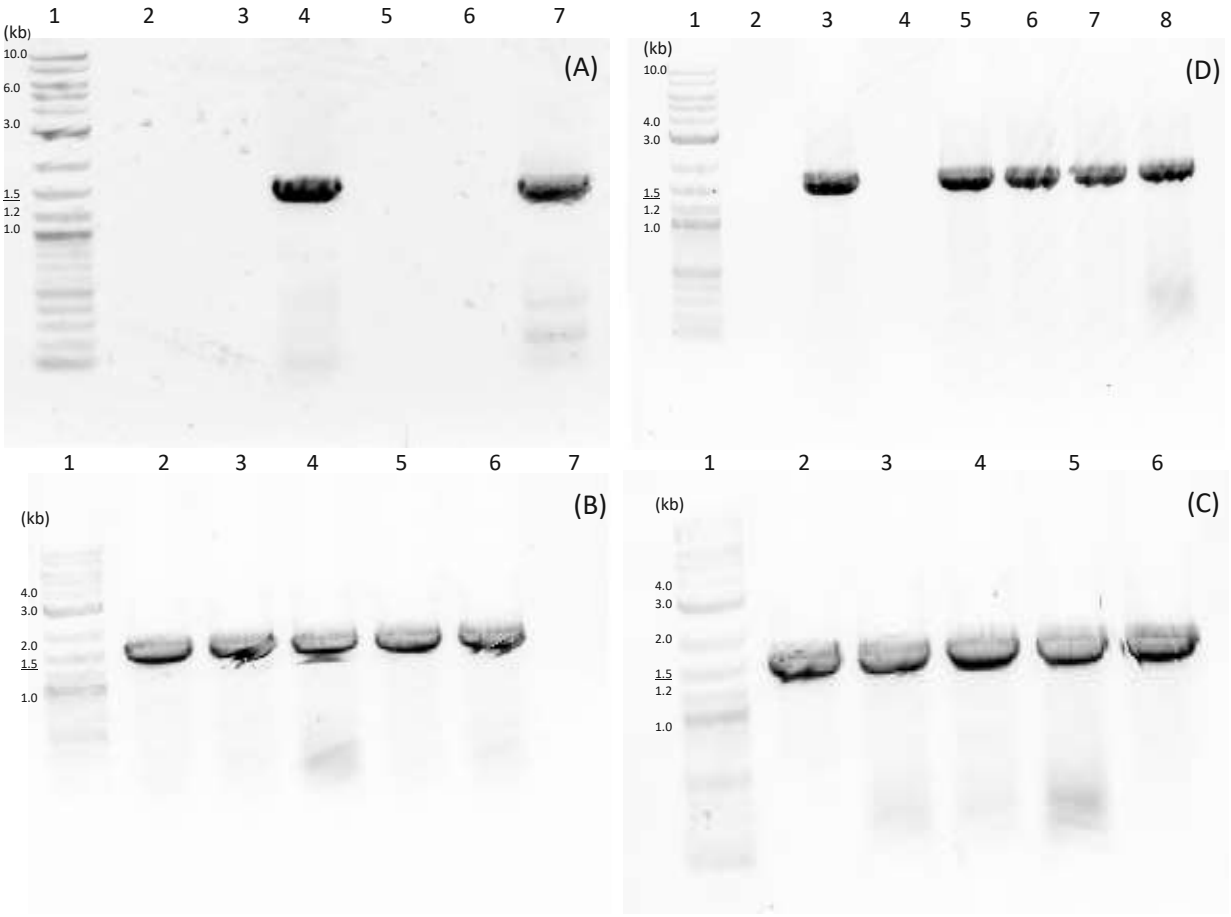

Figure 10 Images of 1 % agarose gels, where in each gel lane 1 is a reference DNA marker. PCR products of sticky end ligation FS/FR in lane 4 and FL/RS in lane 7 (A); Colony PCR of 10 colonies of *E. coli* pGEX-6P-1_L-*Fv*PPO starting with the arbitrary numbered colony 1 (B) and (C); Colony PCR of *E. coli* BL21(DE3) pGEX-6P-1_L-*Fv*PPO (D)

5.13.1.1. Purification of L-*Fv*PPO-GST-Tag

In AC 1 the flow through exhibited activity (5 mM dopamine, 1 mM SDS, 50 mM TRIS pH 8 (22°C)). Although the buffer had been exchanged (10 kDa cut off) to 30 mM TRIS pH 8.00 (22°C), the only eluted peak exhibited no activity. Regardless the absence of activity, the GST-tagged fusion protein was proteolytically digested and applied in AC 2, but no A_{280} band was detected in the flow through. The protease reaction assay and the lysate were analysed with SDS-PAGE (reduced) and western blot in Figure *11*. In the western blot bands of approximately 80 kDa match the size of the L-*Fv*PPO-GST fusion protein in the lysate. This band was not expected to be present in the proteolytically digested sample, if the digestion was complete. The absence of the band was confirmed in both SDS-PAGE and western blot. In SDS-PAGE of the proteolytically digested sample the following bands were identified at a molecular weight of 26 kDa the GST-tag, at 48 kDa the HRV3C-GST fusion protein and at the size of 55 kDa the digested L-*Fv*PPO. A distinct band at 100 kDa could not be assigned. Both the tagged protease and the GST-tag were detected in the western blot at the respective sizes. In the lysate multiple GST-tagged species were identified, however the most intensive band was higher than the expected fusion protein at approximately 80 kDa. Due to the activity in the flow though in the AC 1, it can be concluded that the fusion protein L-*Fv*PPO-GST was successfully expressed, but the active form did not bind to the column and therefore the protein was not purified.

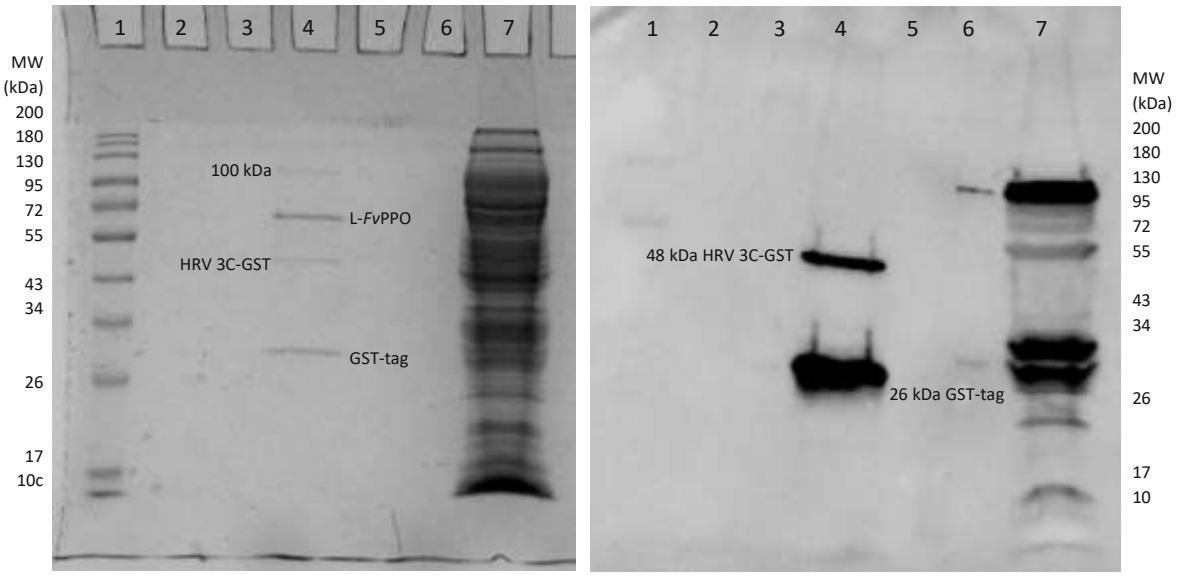

Figure 11 (left) Reduced SDS-PAGE (resolving gel 12 %, stacking gel 5 %) and (right) western blot (images untruncated); The respective lanes are: Lane 1, protein marker; Lane 4, Protease reaction mixture HRV3C-GST:L-*Fv*PPO-GST (1:50); Lane 7, supernatant of *E.coli* BL21(DE3) L-*Fv*PPO-GST lysate.

5.13.2. Expression and Cell Lysis of L-*Fv*PPO-His6

Multiple heterologous expressions of *E. coli*BL21(DE3) L-*Fv*PPO-His6 were prepared and frozen at -80 °C until further processing. Due to the usage of complex media and other factors that could influence the growth and the expression of *E. coli* each cultivation in a single shaking flask was different. The cultures had an average OD_{600} of 0.856 ± 0.058 (n=5) when induced and an OD_{600} of 0.563 ± 0.041 (n=3, dilution 1:10) when the cells were harvested. The cumulative mass of the cell pellets of batches with a total of 6 L growth medium had a mass of 83.27 g, which was reduced by 24.55 % after the removal of the periplasm membrane.

5.13.2.1. Evaluating Cell Lysis Method

In order to determine the most efficient way of cell lysis of L-*Fv*PPO-His6 three different approaches were tested: (1) freeze and thaw (pellet is resuspended in lysis buffer (adjusted to 3 mM $MgCl_2$ and 10 mM $CaCl_2$) and then shock frozen in liquid nitrogen, with subsequent thawing in warm water; in total five repetitions) and (2) french press (GEA Lab Homogenizer PandaPLUS 2000 (GEA Group AG, Düsseldorf, Germany): , 1200 bar, 11 min, 150 mL min^{-1}) as well as, (3) sonication (according to chapter 4.4.2 Cell Lysis).
The results were assessed with SDS-PAGE (reduced) (Figure 12). All lysis methods resulted in active protein. The sonicated sample showed bands higher than 250 kDa and were also found in the pocket, resembling cell debris that had not been dissolved in the loading buffer during SDS-PAGE sample preparation. Besides this preparation related bands, it could be concluded that the target protein was present in the cell pellet of each lysis method. No attempts were made to quantify the loss. Results from chapter 4.10.2 Activation with Cations led to the decision not to use the freeze and thaw method, due to $MgCl_2$ and $CaCl_2$ presence in the lysis buffer. The french press was not available anymore for the duration of this work but would be the method of choice due to the total working time of only 15 min on the specific device. Therefore, sonication was applied. The performance of sonication without the separation of the periplasm membrane had also been attempted successfully and purified protein was also included in the preparation of the batch with more than 80 % purity. However, potential impurities located in the periplasm membrane would decrease the initial purity of L-*Fv*PPO-His6 after IMAC 1.

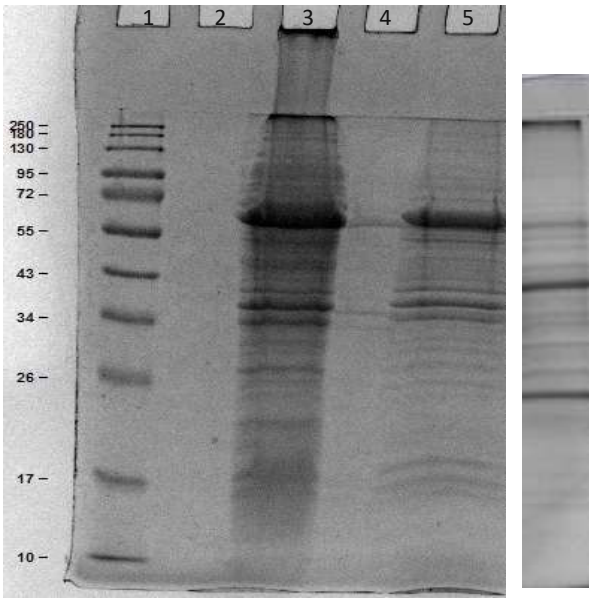

Figure 12 Reduced SDS-PAGE (resolving gel 12 %, stacking gel 5 %)(images untruncated); Lane 1, Ladder; *E. coli* BL21(DE3) L-*Fv*PPO-His6 cell pellets after lysis performed with: Sonication (Lane 3), french press (Lane 5), 5 cycles freezing and thawing (right picture). Sample volumes: 10 µL (sonication), 25 µL (french press), 5 µL (Freeze and Thaw) each from a different 6L cell lysate.

5.13.2.2. Purification of L-*Fv*PPO-His6

5.13.2.2.1. L-*Fv*PPO Purity of more than 80 %

The soluble proteins in the supernatant of the lysate were captured in the IMAC 1 due to their affinity to nickel. The absorbance signal at 280 nm of the aromatic amino acids of unbound protein was saturated and is not shown in Figure 13. Once the proteins were bound to the column, they were washed by binding buffer which commonly should contain a low concentration of imidazole. In this approach, a wash with elution buffer at 6 % B (30 mM imidazole) was performed resulting in the first peak in the chromatogram in Figure 13, containing protein with small affinity to the Ni^{2+} ions. The second peak was observed at 175 mM imidazole or 35 % B, when L-*Fv*PPO-His eluted from the column. In both peaks the characteristic charge transfer band (O_2^{2-} (π^*_σ) → Cu^{2+} (d_{x2-y2})) of the *oxy*-form was measured at 345 nm, indicating the presence of protein with a type III copper center in both peaks. The absorbance is about 20 times lower than at 280 nm and the expected absorbance at 580 nm would had been 400 times lower and was not detected [13]. The fractions of both peaks were collected and united separately. It was confirmed by western blot in Figure 14 and reduced SDS-PAGE in Figure 23, as well with an activity test, that L-*Fv*PPO-His6 was present not only in the 35 % B fractions but also in those within the 6 % B fractions. The two eluted fractions were not united, due to the low target protein concentration of approximately 10 % in the 6 % B fraction.

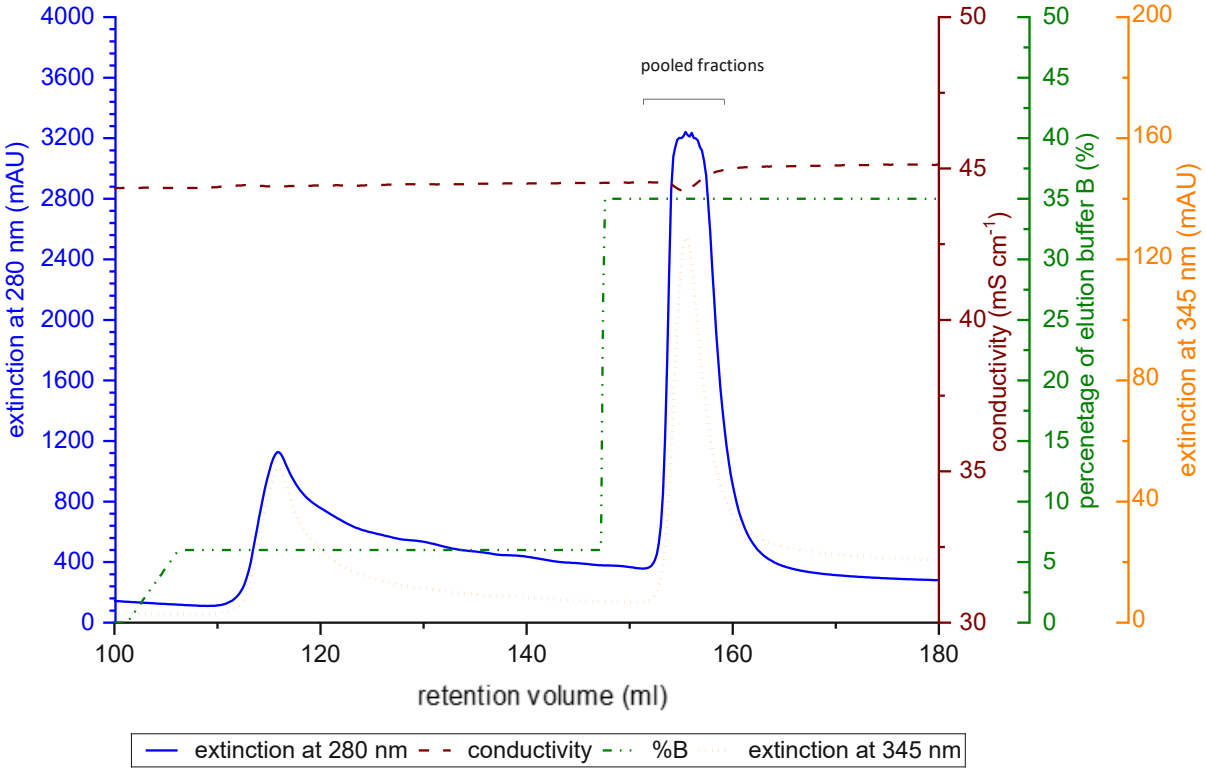

Figure 13 IMAC 1 chromatogram recorded with UNICORN software. The first peak at 6 % B resembles the fractions of proteins that have a weak bound to the stationary phase (Ni^{2+} ions). The second peak at 35 % B contains most of the L-*Fv*PPO-His6. The extinction at 345 nm is used to monitor proteins with type III copper centers. Temperature = 20 °C.

After buffer exchange, concentrating and over night protease reaction of the 35 % fractions, the protein solution was loaded on a regenerated Ni-NTA HisTrap column for IMAC 2. The chromatogram in Figure 15 depicts a typical separation of L-*Fv*PPO without a tag, which was found in the first peak, the flow through. The remaining fractions were found at 35 % B and did not contain fusion protein with an intact His6 tag as it can be seen in the western blot in Figure 14. These fractions were united and further purified.

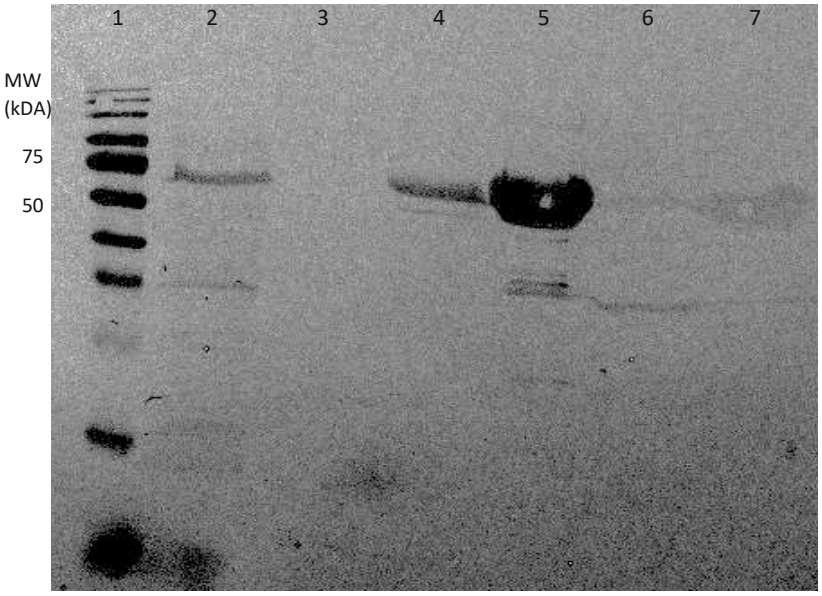

Figure 14 Western Blot for the identification of the His6-tag in the samples, until it was proteolytically cleaved off from L-*Fv*PPO-His6: Protein marker (Lane 1); lysate (Lane 2), wash with chaperone wash solution 1 in IMAC 1 (Lane 3), elution with 6 % B1 IMAC 1(Lane 4), elution with 35 % B1 IMAC 1 (Lane 5), elution with 35 % B1 IMAC 2 (Lane 6), Flow through IMAC 2 (Lane 7).

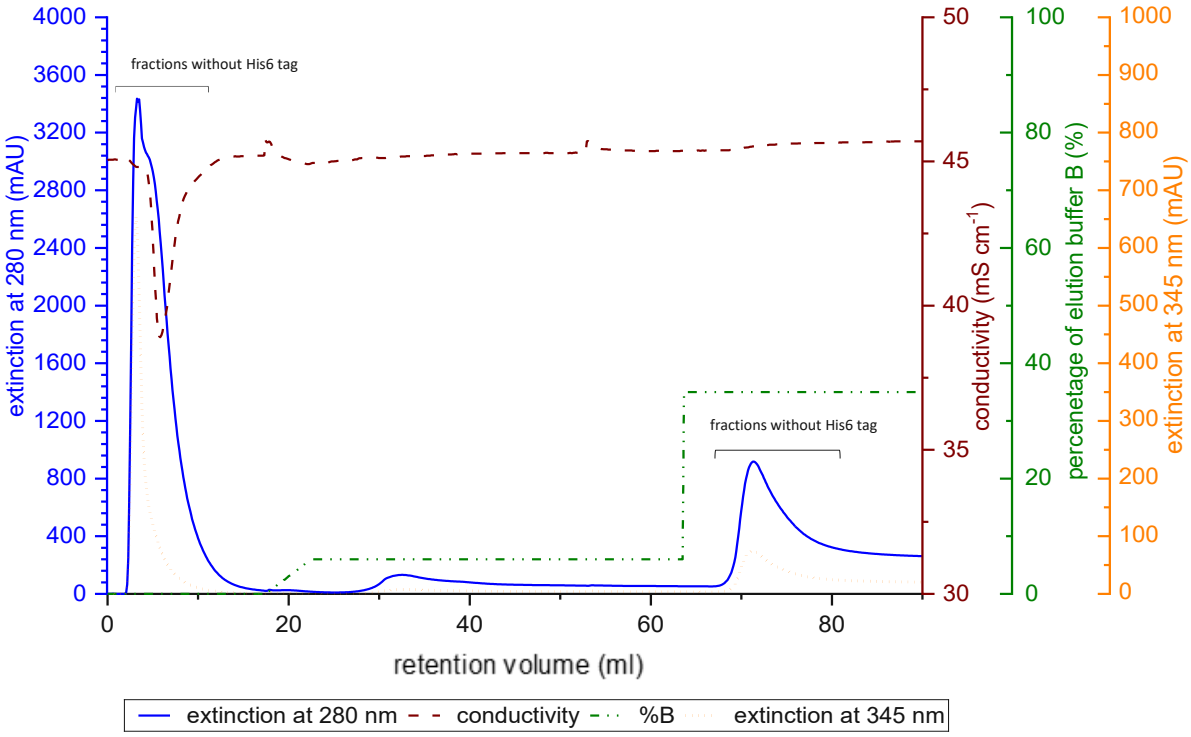

Figure 15 IMAC 2 chromatogram recorded with UNICORN software. The first peak resembles the fractions of protein that contain L-*Fv*PPO without His6 tag. The second peak at 6 % B contains non target protein. The third peak eluted at 35 % B and contained L-*Fv*PPO with an intact His6 tag. The extinction at 345 nm is used to monitor proteins with type III copper centers. Working Temperature at 20 °C.

This described purification had been repeated several times with multiple batches up to this purification stage. The protein solutions were united and purified with anion exchange chromatography (mobile phase: 50 mM TRIS pH 8.0 (RT); elution buffer: 50 mM TIRS, 1 M NaCl pH 8.0 (RT); linear gradient over 20 CV) to achieve a homogenous protein solution. The respective chromatogram in Figure 16 shows more than three peaks in the A_{280} signal. Although an SDS-PAGE gel of each peak indicated impurities at the size of 130 kDa in each peak besides number 3, the fractions of all three peaks (53-63 mL) were united. After the addition of glycerol to a concentration of 20 %, the concentration was measured to be 39.68 mg mL^{-1} based on Lowry protein quantification and is going to be referred as a batch with more than 80 % purity in the following sections.

Due to the high demands for protein for initial crystallization screens, it had been decided that the 22.96 mg of L-*Fv*PPO with low quality, would be used for further experiments, including protein crystallization. The batch was store at -80 °C after shock freezing with liquid nitrogen.

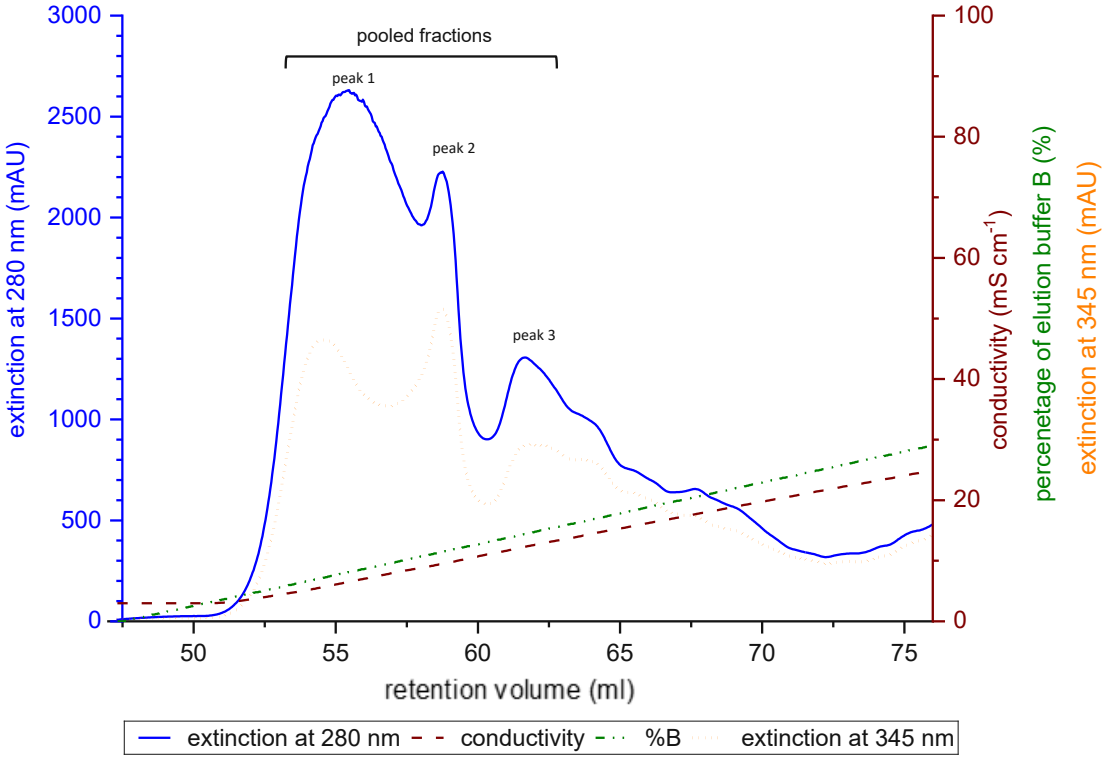

Figure 16 Anion exchange chromatogram of multiple united batches of L-*Fv*PPO was recorded with UNICORN software. The extinction at 345 nm was used to estimate the content of the recombinant expressed protein of interest. The united fractions are marked and represent the protein solution with more than 80 % purity. Working temperature at 20 °C.

5.13.2.2.2. Hydrophobic Interaction Chromatography

Additional purification steps with AEX, that primarily aimed to separate the band at 120 kDa in the reduced SDS-PAGE (Band A in Figure 23). First, AEX was repeated but at 4 °C. However, the separation was not successful and additional peaks were still observed (Figure 23). An activity assay (5 mM tyramine, 1 mM SDS) was performed of fractions with local maxima in the A_{280} signal. The highest volumetric activity of the fractions was measured in the second A_{280} peak in the chromatogram in Figure 17. Due to the distribution of the activities in the peaks the fractions 54 to 66 mL were pooled.

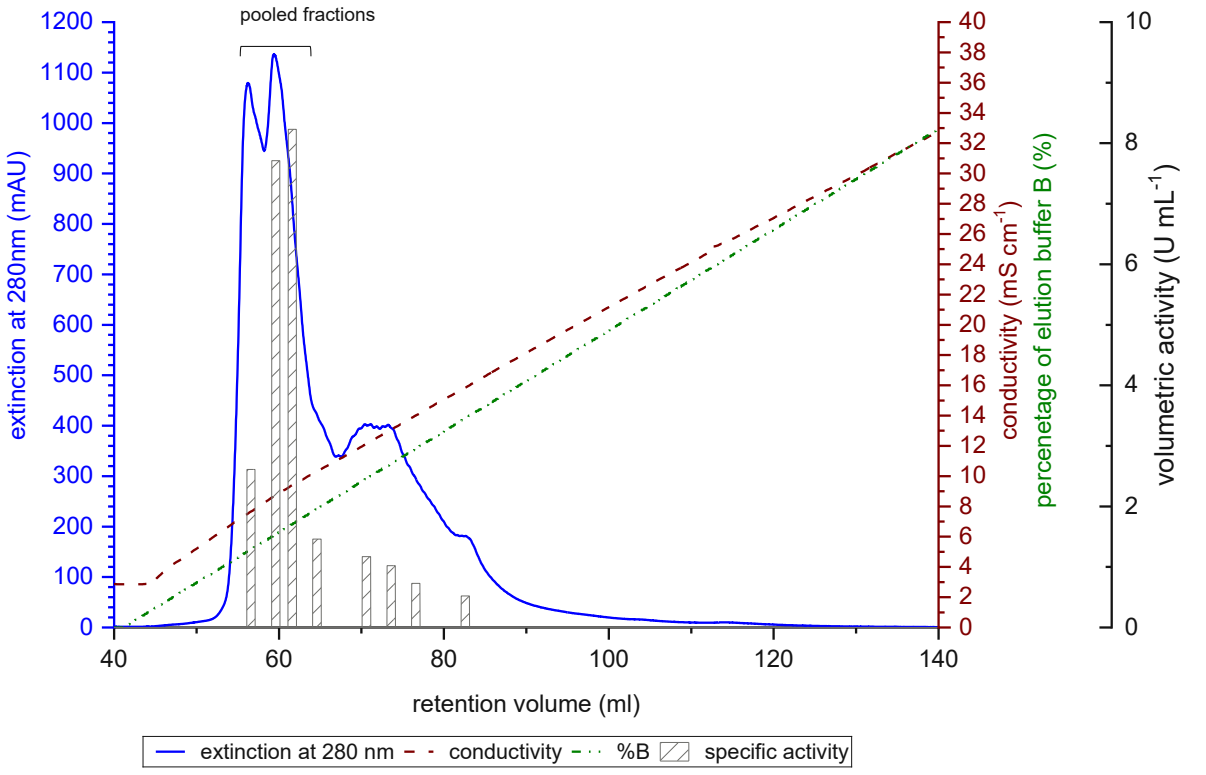

Figure 17 Anion exchange chromatogram of L-*Fv*PPO with a purity of more than 80 % recorded with UNICORN software. A high volumetric activity (5 mM tyramine, 1 mM SDS) was used to identify the fractions of interest. The united fractions are marked (55-67mL). Working temperature at 4 °C.

For further purification the concentration of the mobile phase was changed from 50 mM to 30 mM TRIS in AEX. A more distinct peak was observed in the chromatogram (Figure 18). However, when it was attempted to concentrate the peak with different filters (cut-off 10 kDa and 30kDa Vivacon 500 (Sartorius AG, Göttingen, Germany)) more than 80 % volumetric activity was recorded in the permeate. The pooled fractions from 165 to 180 mL were captured with HIC at 25 °C. Only one sharp peak eluted, when the $(NH_4)_2SO_4$ concentration was decreased to 0.63 M as it is shown in Figure 19. These fractions of the peak were successfully concentrated. The activity of the permeate could be reduced to 17.55 % of the total activity after again concentrating in a 10 kDa filter (Vivacon 500). A reduced SDS-PAGE showed that the remaining activity could be explained due to L-*Fv*PPO in the permeate in Figure 20. The pooled fractions were not buffer exchanged and are further referred to as the batch "concentrated with HIC". It was used for crystallization in the literature screen. The purification with HIC decreased the activity of L-*Fv*PPO as it is summarized in Table 24.

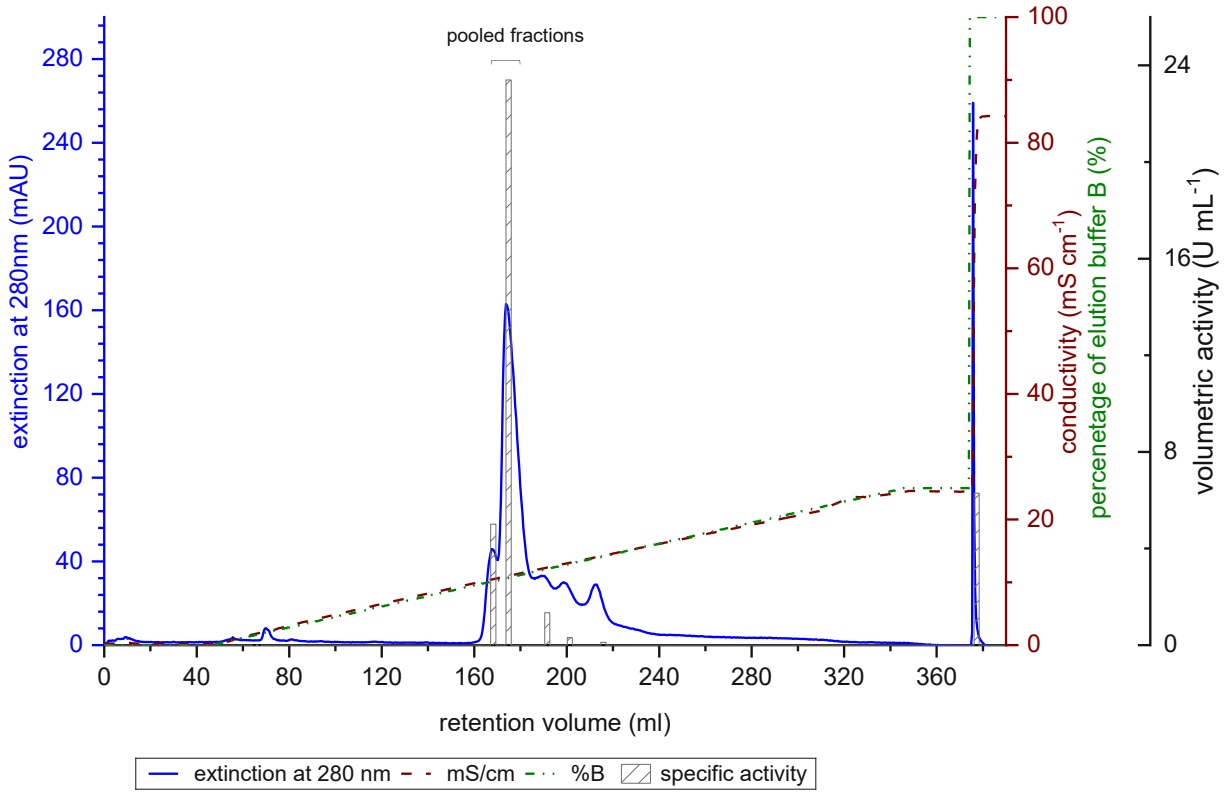

Figure 18 Anion exchange chromatogram with 30 mM TRIS of the pooled fractions of L-*Fv*PPO after 2x AEX. This was recorded with UNICORN software. A high volumetric activity (5 mM tyramine, 1 mM SDS) was used to identify the fractions of interest. The united fractions are marked (165-180mL). Working temperature at 4 °C.

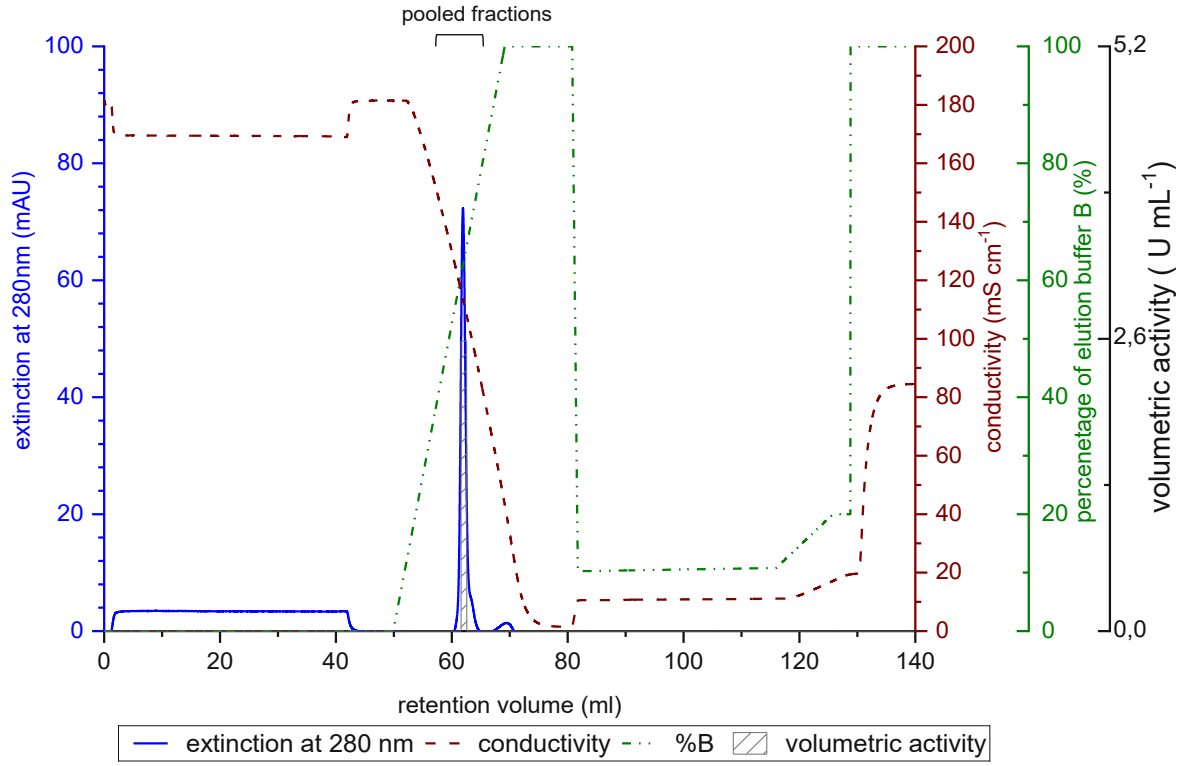

Figure 19 Hydrophobic interaction chromatogram of the pooled fractions of L-*Fv*PPO that could have not been concentrated after AEX purification. This was recorded with UNICORN software. A high volumetric activity (5 mM tyramine, 1 mM SDS) was used to identify the fractions of interest. The pooled fractions are marked (60 to 65mL). Working temperature at 25 °C.

Table 24 Purification table of L-*Fv*PPO (concentrated with HIC) including the amount of protein (mg) loaded and received after the purification. Also, the total activity (U) and specific activity (U mg^{-1}), as well as the fold purification (-) and percentage of yield (%) are listed, which are referred to the first AEX purification.

Purification step	Protein loaded (mg)	Protein after purification (mg)	Total activity (units)	specific activity (U mg^{-1})	Fold purification (-)	Percentage of Yield (%)
AEX (50mM TRIS, 20 °C)	~98.00	22.96	239.01	10.41	1.00	100
AEX (50mM TRIS, 4 °C)	16.59	6.90	94.53	13.72	1.32	39.55
AEX (30 mM TRIS, 4 °C)	6.90	0.94	21.99	23.40*	2.24°	9.2
HIC	0.90	0.26	2.30	8.87	0.85	0.96

*** after 3 days at 4°C specific activity decreased to 16.62 U mg^{-1}**
° A fold purification of 1.59 was achieved with the specific avtivity after 3 days storage

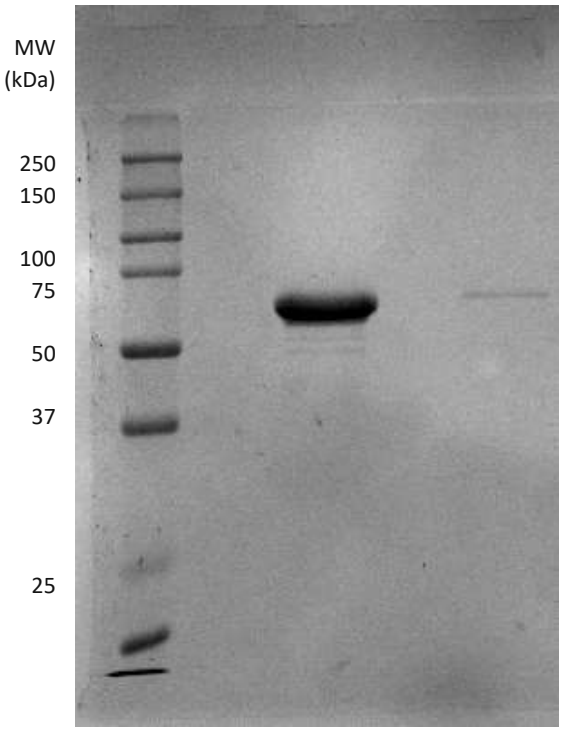

Figure 20 Reduced SDS-PAGE (resolving gel 12 %, stacking gel 5 %) (image untruncated); Lane 1, Ladder; Lane 3, Retentate of L-*Fv*PPO concentrated with a 10 kDa filter (Vivacon 500) after HIC; Lane 5, A volume of 16 µL permeate of L-*Fv*PPO concentrated with a 10 kDa filter (Vivacon 500) after HIC.

5.13.2.2.3. L-*Fv*PPO Purity of more than 90 %

The final batch is going to be referred to L-*Fv*PPO with a purity of more than 90 %. It was expressed in 6 L culture medium (12 flasks each 0.5 L). Lysis was performed with sonication, and it was captured utilizing the previously described methods of IMAC 1 and IMAC 2. The purification was performed again with AEX with a TRIS concentration of 30 mM in the buffers at a working temperature of 4 °C. More importantly the elution profile was adapted to achieve better separation. The chromatogram is shown in Figure 21 and fractions 55.6-79.6 mL were pooled since these exhibited the highest specific activity (5mM tyramine, 1 mM SDS). An increase of 3.97 % specific activity (5mM tyramine, 1 mM SDS) was recorded after the AEX purification compared to the AEX purification step of L-*Fv*PPO batch before it was concentrated with HIC as it can be seen in Table 25. The whole purification is shown in the reduced SDS-PAGE in Figure 23, without the lysate, which can be seen in Figure 12.

Table 25 Purification table of L-*Fv*PPO with a purity of more than 90 % including the amount of protein received after the purification (mg). Also, the total activity (U) and specific activity (U mg-1), as well as the fold purification (-) and percentage of yield (%) are listed, which are referred to the first IMAC 1.

Purification step	Protein after purification (mg)	Total activity (units)	specific activity (U mg^{-1})	Fold purification (-)	Percentage of Yield (%)
IMAC 1	19.06	24.85	1.030	1.00	100
AEX	0.550	9.50	17.28	16.78	38.22

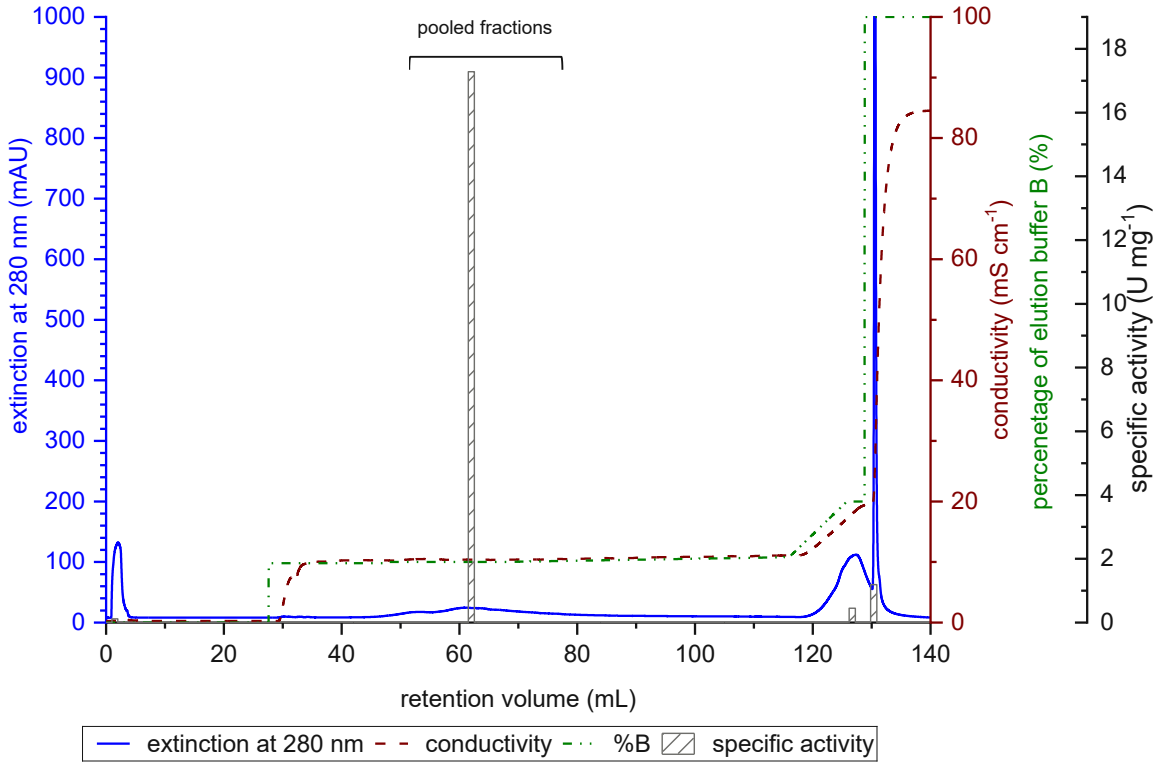

Figure 21 Anion exchange chromatogram (with 30 mM TRIS in the buffers) of the pooled fractions of L-*Fv*PPO after IMAC 2. This was recorded with UNICORN software. A high volumetric activity (5 mM tyramine, 1 mM SDS) was used to identify the fractions of interest. The united fractions are marked (55.6 to 79.6 mL). Working temperature at 4 °C.

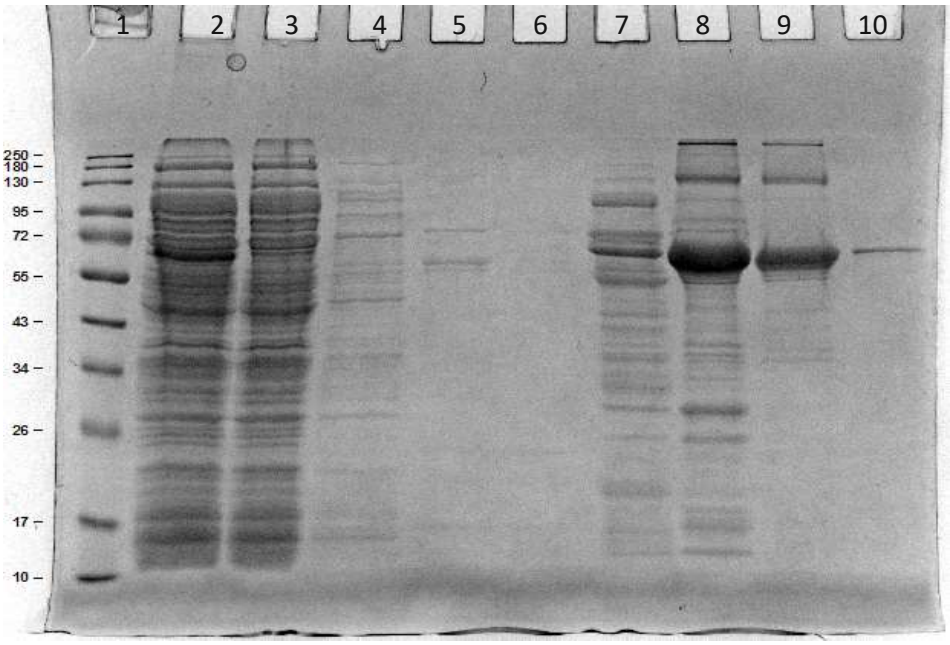

Figure 22 Reduced SDS-PAGE of the total purification of L-*Fv*PPO with a purity of more than 90 % (image untruncated): Protein marker (Lane 1); Lysate (Lane 2), IMAC 1 Flow through (Lane 3), First wash with mobile phase IMAC 1(Lane 4), Wash with chaperone wash solution 1 in IMAC 1 (Lane 5), Second wash with mobile phase IMAC 1(Lane 6), Elution with 6 %B1 (Lane 7), Elution with 35 % B1 (Lane 8), Flow through IMAC 2 (Lane 9), L-*Fv*PPO with a purity of more than 90 % after AEX (30 mM TRIS, 4 °C) (Lane 10)

5.13.3. Stability Test and Tryptic Digestion Coupled with LC-MS

The influence of glycerol on the stability of L-*Fv*PPO with a purity of more than 80 % (storage buffer: 50 mM TRIS, 500 mM NaCl, pH 8.00 (25 °C)) was evaluated after 2 weeks and for L-*Fv*PPO with a purity of more than 90 % (storage buffer: 30 mM TRIS, pH 8 (25 °C)) after 4 weeks storage at 4°C, as well. The reduced SDS-PAGE gels of the samples are depicted in Figure 23. The molecular weight of L-*Fv*PPO was estimated to be 55 kDa and was seen in each lane. However, in all samples with a purity of more than 80 %, an additional band at 130 kDa and the formation of some bands below the protein are observed. In the sample with the lowest glycerol concentration of 1 % multiple high molecular weight bands were observed. This was presumably caused by an error in sample preparation, but it cannot be ruled out that the lack of glycerol led to the formation of aggregates. For the sample of higher purity, the same additional bands at lower molecular weight could be observed after 4 weeks. Eventually, the lack of salt in the storage buffer did not have an influence on the stability of the protein based on the results of SDS-PAGE (reduced). However, the stability tests are only based on SDS-PAGE, not on activity assays. This was argued with the protein experiments, which were executed primarily at 18 °C and not at 4 °C, but based on the SDS-PAGE it could be claimed that the stability of the protein is given at 4 °C.

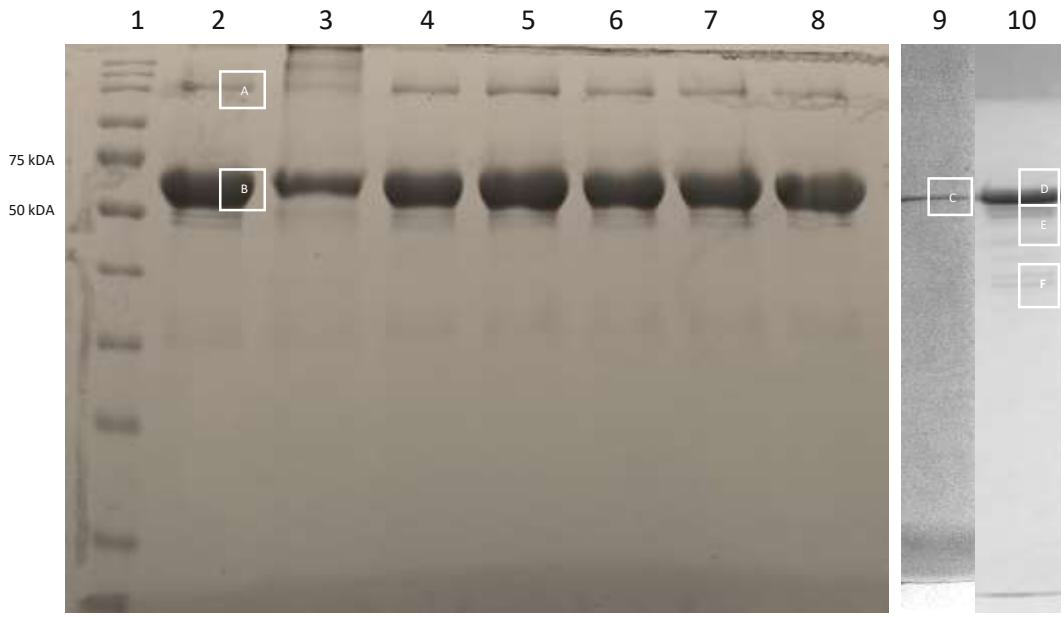

Figure 23 (left) reduced SDS-PAGE contains 20 µg of sample in lane 2-8; protein marker (Lane 1); L-*Fv*PPO with a purity of more than 80 % was stored with 20 % glycerol at -80°C (Lane 2), whereas aliquots of it in lane 3-8 were stored at 4 °C with glycerol concentrations of: 1 % (Lane 3), 2 % (Lane 4), 5 % (Lane 5), 10 % (Lane 6), 15 % (Lane 7), 20 % (Lane 8), respectively. In Lane 2 the bands are marked A and B, since they were used for mass spectrometry evaluation. (right) Reduced SDS-PAGE: protein marker (Lane 1), L-*Fv*PPO with a purity of more than 90 % immediately after purification and buffer exchange (Lane 9), after storage at 4 °C for 4 weeks (Lane 10). The bands are marked as C, D, E and F, since they were used for mass spectrometry evaluation.

The tryptic digestion products of reduced SDS-PAGE bands were analysed utilizing LC-MS by the colleagues in the research group of Univ.-Prof. Dr. Christopher Gerner. In Figure 23 the bands of interest are marked as A-F. A section of the data for band A and B is presented in Table 26 containing the log2 transformed values of the label free quantification (LFQ). The enzyme L-*Fv*PPO could be identified in each band. Based on the results in bands E and F degradation products are present. In band A not only the target protein, but also the chaperone protein DnaK was measured as shown in Table 26. It was assumed that that the chaperone was bound to the protein, since adding the molecular weight of DnaK and L-*Fv*PPO leads to approximately 124 kDa, which was also the estimated size of band A observed in Figure 23. The chaperone wash step with chaperone wash buffer 1 resulted in the elution of protein, that is shown in lane 5 of Figure 23. These bands were also analysed by means of LC-MS and it was confirmed that the eluted protein in this step was DnaK. However, the chaperone wash step did not result in the disappearance of the second band resembled by band A.

Table 26 Section of the results obtained from LC-MS data. Sample A and B are referred to the bands in a reduced SDS-PAGE lane containing L-*Fv*PPO, whereas the first one has the approximate size of 130 kDa and the latter one a size of 55 kDa.

Protein name	Sample A log2 LFQ intensity	Sample B log2 LFQ intensity	Number of peptides	Number of unique peptides	Molecular weight (kDa)
Chaperone protein DnaK	14.4	NaN	9	9	69.114
L-*Fv*PPO	25.7	28.7	53	53	54.948

5.13.4. Isosbestic Point

The time dependency of the absorbance maximum of DOPAchrome during the reaction between $NaIO_4$ and dopamine is shown in Figure 24. The absorbance at 480 nm decreased more than 8 % in the course of 10 min reaction time. The standard deviation function of the nine spectra is depicted in the top right of Figure 24. The local minima of this function are at 524 nm and 412 nm and represent the two isosbestic points for the buffer condition: 50 mM TRIS buffer at pH 7.75 (22°C) at 298.5 K, with 20-fold excess of $NaIO_4$. The absorbance at 524 nm was measured with dopamine concentrations of 100, 200, 300, 400 and 500 µM. The slope of the resulting function is equivalent to the molar absorption coefficient ε_{524} = (1200 ± 277) M^{-1} cm^{-1} for the used buffer.
Muñoz et al. [34] concluded that isosbestic points in the reaction are dependent on the substrate and the formed chinone species. Here it is shown that the isosbestic points and the respective molar absorption coefficients are also buffer dependent. This is supported by experiments performed by colleagues (data not available). It can be recommended to determine the isosbestic point for each buffer before performing kinetic studies. However, as buffer specific data were not available and this was observed at the end of the work, the general accepted molar absorption coefficient ε_{480} = 3300 M^{-1} cm^{-1} was used for activity assays performed in this work [34].

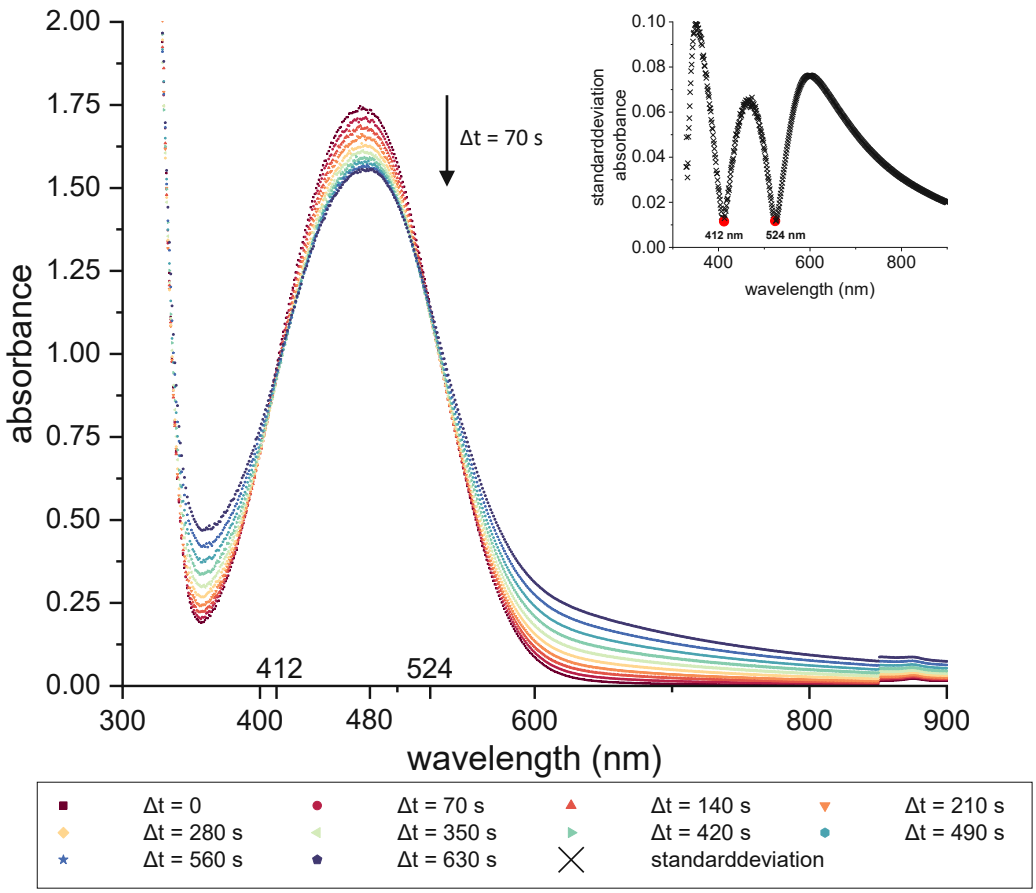

Figure 24 Recorded spectra of the reaction between 0.5 mM Dopamine and 10 mM $NaIO_4$ in time intervals of Δt = 70 s. The graph top right: standard deviation of the nine recorded spectra, whereas the isosbestic points (local minima) are marked at a wavelength of 412 nm and 524 nm.

5.13.5. Evaluation of the Activity Assay

The activity of L-*Fv*PPO was determined by utilizing the slope of the linear part of the measured curve (x-axis: time; y-axis: absorbance) if a coefficient of determination (R^2) greater than 0.95 could be recorded. First the change of the concentration over time was calculated with equation (2), whereas the optical path length (L_{opt}) had been determined to be 0.63 cm and the molar absorption coefficient ε_{480} was chosen to be 3300 M^{-1} cm^{-1} [34]. If not stated otherwise, then the total reaction volume V_{total} was 2 x 10^8 L and the total Units U were calculated according to equation (3). The Units were divided either by the known amount of protein or by the volume used in the reaction, expressed either in specific (a_{enzyme}) or volumetric activity (v_{enzyme}) according to equation 4-5.

$$\frac{dc}{dt} = \frac{k}{\varepsilon_{480} L_{opt}} = \left[\frac{mol}{Ls}\right] \tag{2}$$

$$U = \frac{dc}{dt} V_{total} = \left[\frac{\mu mol}{min}\right] \tag{3}$$

$$a_{enzyme} = \frac{\frac{dc}{dt} V_{total}}{m_{enzyme}} = \left[\frac{\frac{\mu mol}{min}}{mg} = \frac{U}{mg}\right] \tag{4}$$

$$v_{enzyme} = \frac{\frac{dc}{dt} V_{total}}{V_{enzyme}} = \left[\frac{\frac{\mu mol}{min}}{mL} = \frac{U}{mL}\right] \tag{5}$$

5.13.6. Activation of L-*Fv*PPO

5.13.6.1. Proteinase K

The volumetric activity was measured, since the mass of the enzyme did not remain constant during the reaction with proteinase K. It can be seen in Figure 25 that the activity in the presence of SDS decreased, while the activity increased in its absence. The presence of ascorbic acid and the increased SDS concentration (compared to the standard concentration of 1mM SDS) in the assay influenced the activity. It has to be noted that the activity assay in the time series was not executed in replicates. The degradation and the activation of the proenzyme respectively, is shown in both SDS-PAGE gels in Figure *26*. After 8 min only faint coomassie and activity-stained bands, that resembled the latent form, were observed. Proteinase K has a molecular weight of 28.93 kDa and was seen approximately at this size in each sample in reduced SDS-PAGE in Figure 26(left) [86]. Also, blurred bands appeared at a molecular weight higher than 75 kDa in each lane indicating that the serine protease digested the bands at approximately 130 kDa in the L-*Fv*PPO sample with more than 80 % purity (in Figure 23) immediately. As a result of the undirected digestion in the C-terminal DWL region, multiple protein fragments were created, and the active form could not be assigned to a specific band, neither in the reduced nor in the non-reduced SDS-PAGE, where two distinct bands were seen. However, based on the results it can be concluded that even though the activation was not complete, it was successful. In order to assign the bands to the active form, size exclusion chromatography could have been performed [24].

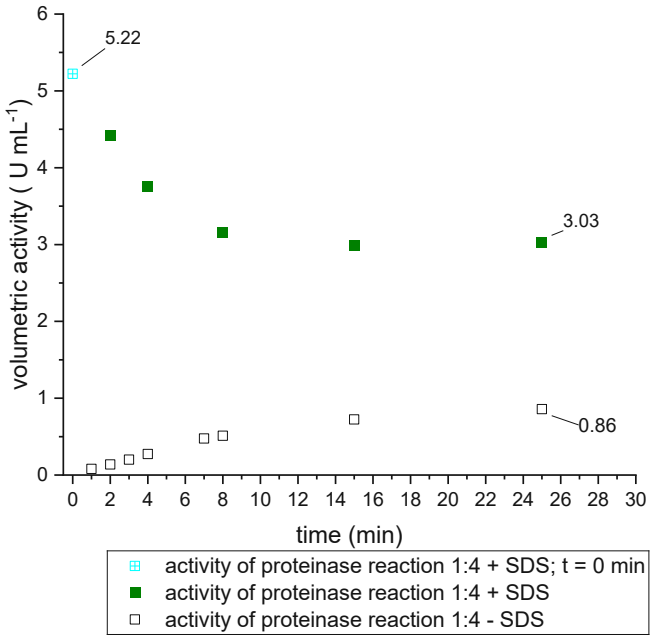

Figure 25 Activity of L-*Fv*PPO in the course of the reaction with proteinase K in a ratio of 1:4 in the presence or absence of 3 mM SDS. The assays contained 0.07 mM sodium ascorbate and 5 mM tyramine was used as a substrate.

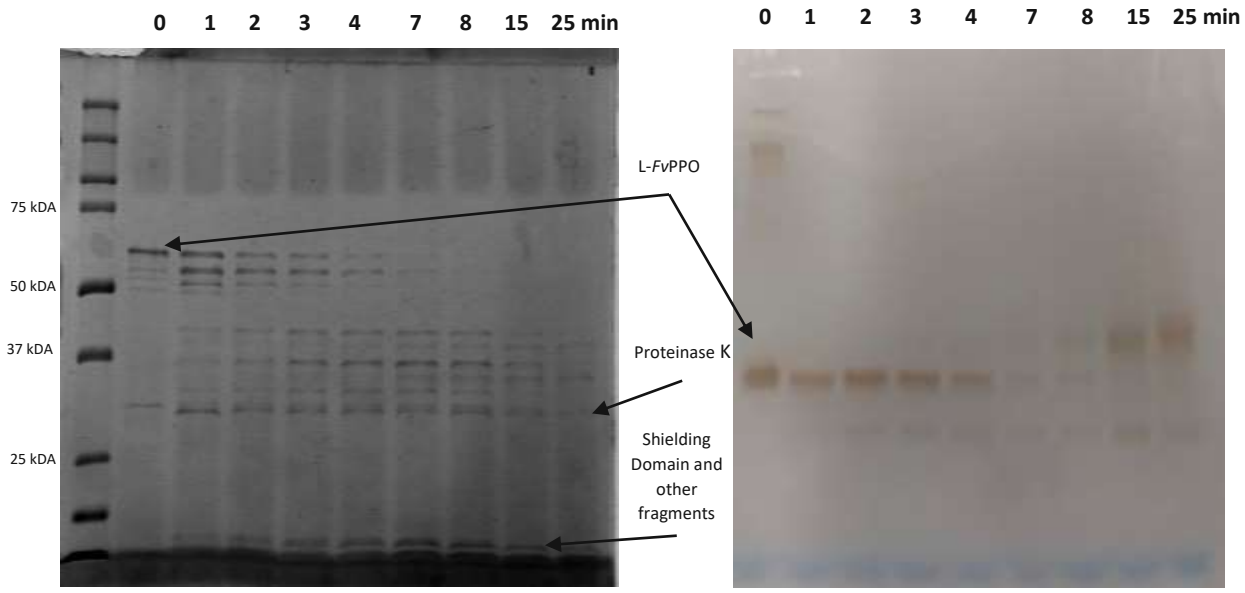

Figure 26 Time series of the digestion of L-*Fv*PPO with Proteinase K in order to achieve activation (left) reducing SDS-PAGE hand cast gradient gel (10-15 % resolving gel, 5% stacking gel), (right) activity stained (tyramine) non reducing SDS-PAGE hand cast gradient gel (10-15 % resolving gel, 5% stacking gel) after staining with 5 mM tyramine for 20 min. (images untruncated)

5.13.6.2. Cations

In the absence of detergents like SDS (Figure 27) bivalent salts led to an activation of L-*Fv*PPO with dopamine as substrate. No quantitative assessments were made for any of the tested cations. The wells with a concentration of 100 mM $MgCl_2$ and 1.2 M NaCl were not prepared. The bivalent salts $MgCl_2$ and $CaCl_2$ exhibited increased activity already after 1 min. Sodium chloride and potassium ions also influenced the activity of the L-*Fv*PPO.

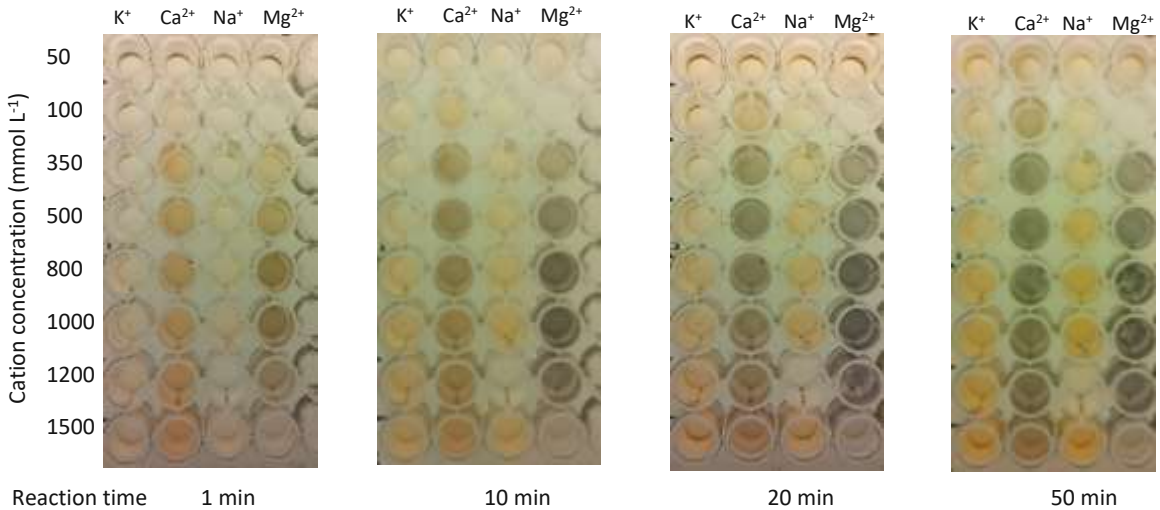

Figure 27 Time series of L-*Fv*PPO with 2 mM dopamine in the presence of the cations: K^+, Ca^{2+}, Na^+, Mg^{2+} with concentrations ranging of 50 mM, 100 mM, 350 mM, 500 mM, 800 mM, 1 M, 1.2 M, and 1.5 M. Reaction time from left to right: 1 min; 10 min; 20 min and 50 min. The wells with a concentration of 100 mM $MgCl_2$ and 1.2 M NaCl are empty.

5.13.7. Dynamic Light Scattering (DLS)

A monodisperse protein solution has an increased probability of 70-80 % to produce some kind of a crystal, whereas polydisperse solutions are less prone to crystal formation [83]. The homogeneity of L-*Fv*PPO in two different purification steps was determined, which were used in the initial screens or the literature screen in the crystallization experiments with VD-HD (chapter 6.2.2. Vapor diffusion Hanging Drop (VD-HD)). The DLS profile of protein can be temperature dependant [83]. This was not considered when measuring the protein solution first at 20°C and after further purification at 4 °C. However, based on the measured particle sizes in both samples, particle size 1 in Table 27 could be identified as L-*Fv*PPO, since the theoretical hydrodynamic radius of L-*Fv*PPO was calculated to be 7.69 nm as described in chapter 4.11.4 Dynamic Light Scattering. The intensities of the particle sizes in each sample resemble the proportion of the particle or protein in the solution and add up to 100 %. The purity of a batch is labeled as "more than 80 % purity" and "more than 90 % purity" according to the intensity of particle size 1 in Table *27*, that could be identified as the protein of interest. The batch with more than 80 % purity shows three particle sizes. It is assumed that particle size 2 resembles the impurity identified at 130 kDa and particle size 3 was either dust or aggregates formed in the solution. Further purification led to an increase of the L-*Fv*PPO proportion in the solution, whereas the significant bigger particle size 4 was formed. Particle size 2 could not be measured anymore indicating that the presumed impurity at 130 kDa was separated successfully. Similar to particle size 3, particle size 4 was assumed to be either dust or aggregates of protein. While dust can serve as crystallization seed and having a beneficial impact, protein aggregates can influence crystallization negatively. Intrinsic polydispersity was measured before and after further purification. Additionally, both samples exhibited polydispersity since the standard deviations of particle sizes 1, which had been identified as L-*Fv*PPO were greater than 15 % [87].

Table 27 Particle size distribution of L-*Fv*PPO samples after the purification with AEX (lin. gradient 0 % to 100 % B, with 3.5 % B per minute) leading to a purity of more than 80 %. And after purification with AEX (lin. gradient 10.0 % to 10.8 %, with 0.0016 % B per minute) leading to a purity of more than 90 %.

Purity level of batch	**Particle size 1**	**Particle size 2**	**Particle size 3**	**Particle size 4**
	Hydrodynamic radius in nm (Intensity % in apprentices)			
More than 80 %	7.104 ± 1.315 (80.5)	74.01 ± 14.98 (14.98)	536.9 ± 101.4 (11.7)	-
More than 90 %	7.102 ± 2.358 (91.1)	-	-	1810 ± 1036 (8.9)

5.13.8. Thermal Shift Assay (TSA)

Generally, an inactivation of polyphenol oxidase can be achieved with temperatures of 70 °C to 90 °C [88]. This leads to the denaturation of the enzyme and therefore a fluorescence increase in this region is expected. The calculation of the melting points is based on the derivative of the recorded fluorescence data (Top right in Figure 28 and Figure 29), whereas the melting point (T_m) is identified as local maximum. Multiple local maxima indicate the presence of additional protein species or degradation products in the sample. The melting points of the samples are summarized in Table 28.

Two melting points could be identified in the TSA of L-*Fv*PPO with a purity of more than 80 %. The $T_{m,3}$ at 68.25 °C almost meets the expected inhibition temperature for L-*Fv*PPO, while the $T_{m,1}$ at 48.75 °C confirms the presence of an additional species, presumably the impurity that was observed in SDS-PAGE in Figure 23 (left) with a molecular weight of 130 kDa.

After a purity of more than 90 % had been achieved for L-*Fv*PPO, still multiple melting points were present in the TSA in Figure 29. However, these were all detected in a range of 60.5 - 80.5 °C, which is closer to the expected inactivation temperature range. This fostered that the purification of the protein had been increased with the adjusted AEX protocol in chapter 5.13.2.2.3 L-FvPPO Purity of more than 90 **%**. Additional melting points presumably represent degradation products, that formed in the course of the TSA.

The addition of 500 mM NaCl led to an increase of the fluorescence signal 5 °C earlier. Also, the rather pronounced $T_{m,5}$ with 80.5 °C was decreased to $T_{m,4}$ with 74.0 °C. Furthermore, it could be observed that the protein was precipitated after the TSA, which did not happen in the absence of sodium chloride. The addition of 500 mM NaCl did not increase the stability of the protein using 30 mM TRIS as buffer at a pH of 8.0. In order to find a more suitable buffer, the pH value of the buffers should be varied too.

Table 28 Melting points (T_m) of L-*Fv*PPO with a purity of more than 80 % and more than 90 % determined in a thermal shift assay.

L-*Fv*PPO purity	**more than 80 %**	**more than 90 %**	
Buffer	50 mM TRIS, pH 8.01 (25 °C)	30 mM TRIS, pH 8.00 (22°C)	
NaCl (mM)	500	-	500
$T_{m,1}$ (°C)	48.75	-	-
$T_{m,2}$ (°C)	-	60.5	59.5
$T_{m,3}$ (°C)	68.25	70.0	69.5
$T_{m,4}$ (°C)	-	-	74.0
$T_{m,5}$ (°C)	-	80.5	-

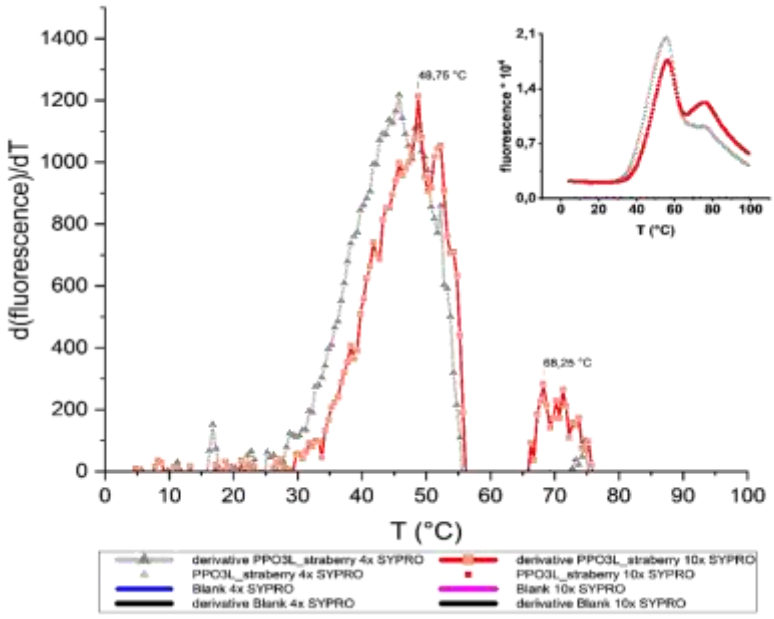

Figure 28 Thermal shift assay (TSA) of L-*Fv*PPO (10µM) in the presence of SYPRO orange with working concentrations of 4x and 10x in the top right. The derivative of the raw data is depicted in the main graph and the local maxima are marked with the respective x-values, which are the melting temperatures.

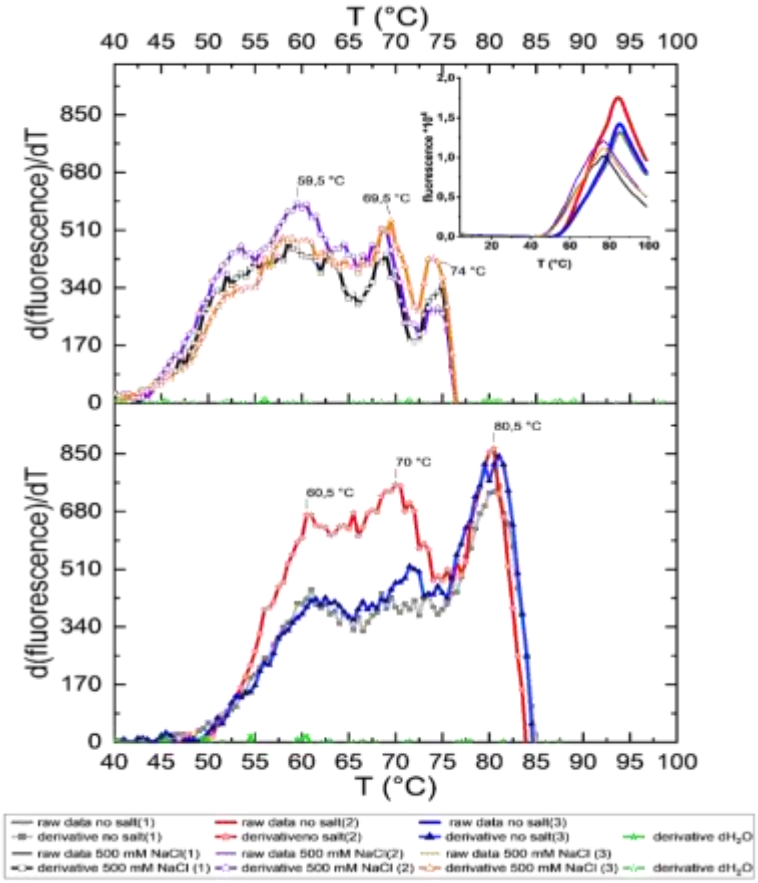

Figure 29 The raw data of the thermal shift assay (TSA) measurement (10µM sample, SYPRO orange(4x) in 30mM TRIS pH 8.00) is depicted in the top right, whereas the derivative of the measurement is split in two stacked graphs. The bottom graph contains the derivative of the measurements without additives, while the top graph contains the derivative of the measurements with 500 mM NaCl. The local maxima are marked with the respective x-values, which are the melting temperatures.

5.13.9. Copper Quantification

The Cu (II) in the protein is reduced by sodium ascorbate to Cu(I). The Cu (I) content of L-*Fv*PPO with a purity of more than 90 % was calculated as:

$$c(Cu(I)) = \frac{A_{546}(Sample)}{\varepsilon_{546} \cdot L_{opt}} \quad (6)$$

where the molar absorption coefficient ε_{546} of the bis(biquinoline)Cu(I) complex is 6300 cm^{-1} M^{-1} [78] the optical path length L_{opt} was 1 cm and the absorbance of the sample A_{546}(sample) was blank corrected. Since the type III cupper center is binuclear, a ratio of 2:1 (mol copper: mol L-*Fv*PPO) had been expected. The calculation of the ratio with the values of Table 29 revealed that each molecule L-*Fv*PPO contained 0.915 ± 0.003 Cu (I) atoms. This indicates that the protein required further preparation and stabilization in order to achieve the anticipated copper content of 2 per molecule PPO [89].

Table 29 Copper quantification of Cu(I). The absorbance at 546 nm was measured in triplicate for the blank and the sample. The amount of L-*Fv*PPO in each measurement was determined by Lowry protein quantification. The listed molecular weight of L-*Fv*PPO was used for the calculations.

A_{546} Blank (cm^{-1})	0.013	0.004	0.005
A_{546} Sample (cm^{-1})	0.093	0.098	0.102
MW L-*fx*PPO (kDa)	54.940		
Mass L-*fx*PPO per measurement (µg)	172.126 ± 12.148		

5.14. Crystallization

5.14.1. Vapor Diffusion Sitting Drop (VD-SD)

5.14.1.1. Evaluation of VD-SD Experiments

A modification of the evaluation for the sitting drop experiments was introduced, since not all of the states that were described in the model (Figure 9) could be observed in the wells. One number was assigned to a certain crystallization state according to the implemented scoring system in Table 30. The recorded observations are displayed in detail in the appendix.

Table 30 Scoring system for L-*Fv*PPO crystallization experiments utilizing vapor diffusion sitting-drop(VD-SD).

Observation	Score	Example picture	Remarks
clear drop	0		-
object	1		Observed more carefully, since small crystals could possibly form on the rim of the object and therefore the object can function as seed
turbid/ precipitation	1.5	 turbid  precipitate	In these states no further crystals were expected
light precipitation	2	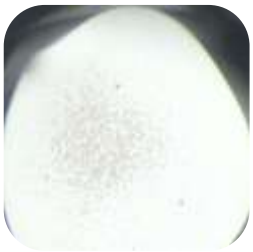	Crystal growth is assumed to happen more likely in this state
Crystalline object	4	 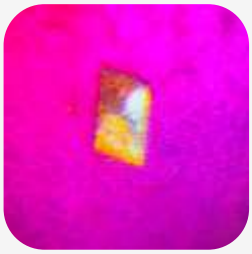	Object has refractive properties and distinct edges; further tests (5.12.4 Differentiation between Salt and Protein Crystal) are required to confirm that it is a protein crystal

5.14.1.2. Grid Screen (VD-SD)

The variation of the concentrations of $MgCl_2$, NaCl and PEG 4000, as well the pH in plate 5 led to 27 precipitations, including light precipitation, out of 288 conditions at the end of the experiment. Without the presence of salts, the variations at 50 mM TRIS buffer led exclusively to clear drops. Doubling the buffer concentration and decreasing the pH to acid conditions did not increase precipitation rates significantly. No suitable protein crystal could be produced under the tested conditions.

5.14.1.3. Sparse Matrix Screens (VD-SD)

The only promising crystal candidate, which is depicted in Table 30 (Score 4), was not confirmed to be a protein crystal with further experiments as described in chapter 4.12.4 Differentiation between Salt and Protein Crystal. No initial "hit" could be produced in this approach and due to the heavily bias of these screens towards known crystallization conditions, the obtained knowledge from these experiments is limited [64]. The complete precipitation of the protein that would block the light of the stereomicroscope as it can be seen in Figure 30 (left) was not observed. The precipitation that came closest to this property, was recorded once of the total 1839 conditions (including all VD experiments (SD+HD), and is depicted in Figure 30 (middle), while the typical observed precipitation is also depicted in Figure 30 (right) and in Table 30 (Score 1.5, precipitate). Since the number of precipitations observed was limited, the manual of the Crystallization Basic Kit for Proteins (Sigma Aldrich, Buchs, Swiss) advised, that the experiments should be repeated with higher protein concentrations or precipitant concentrations. Although the final protein concentration had been increased in between the plates to more than 150 g L^{-1} final protein concentration in the drop, too little precipitations were observed. As an alternative to the repetition of the initial screen with an increased precipitant concentration, the precipitation behavior was investigated in experiments with high precipitant and protein concentrations described in the following chapter.

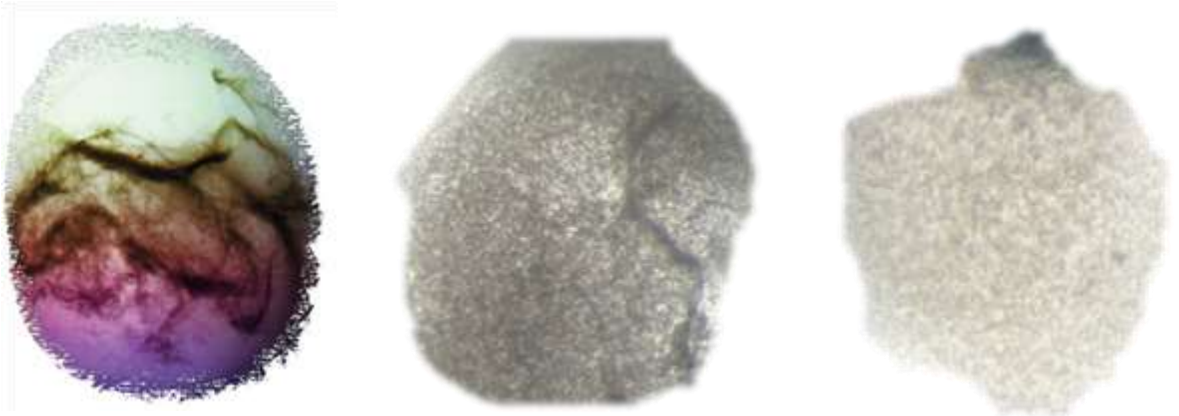

Figure 30 Comparison of precipitations (left) expectation of precipitation picture from [90] (middle) precipitation of protein with a final concentration of 34 g L^{-1} in the drop in the condition 18 % (w/v) PEG 4000, 100 mM sodium acetate, pH 4.6 on plate 2, that came closest to the expected precipitation (left) typical precipitation behavior in the performed VD-SD experiments with L-*Fv*PPO.

5.14.2. Vapor diffusion Hanging Drop (VD-HD)

5.14.2.1. Precipitation Trials with YCl_3 and TEW (VD-HD)

One of the most intriguing properties that had been observed was the lack of precipitation in the wells of the VD experiments as mentioned before. Without additives, the protein did not precipitate mainly, instead the drop turned turbid. The addition of TEW to the protein drop initiated a dense precipitation, while the addition of YCl_3 led to a flaky precipitation. However, two different PEG types PEG 2000 (50 % (v/v)) and PEG 8000 (40 % (w/v)) had been used, making it difficult to attribute precipitation solely to a certain additive. A dark grey color of the precipitate was observed before and after the addition of TEW as it can be seen in Figure 31(A) and (B) at a final L-*Fv*PPO concentration of 50 g L^{-1} in the drop. A similar behavior was observed for the higher protein concentrations in the presence of 1 mM YCl_3. Similarities between the dark precipitation in the protein drop and in well with the activated *Fv*PPO in the presence of Mg^{2+} (e.g. 500 mM) after a reaction time of 50 min can be seen (compare Figure 31 with Figure 27). Degradation of the protein could have led to accessible tyrosine, that functioned as substrate in the formation of melanin species. Tyrosine as a substrate was not tested in this work.
Nevertheless, the anticipated precipitation behavior (Figure 30 left) was not observed. These results contributed to the decision to rather focus on the further purification of the protein to more than 90 %, instead of increasing the concentration of the precipitants in the drops prepared in the sparse matrix screen VD-SD.

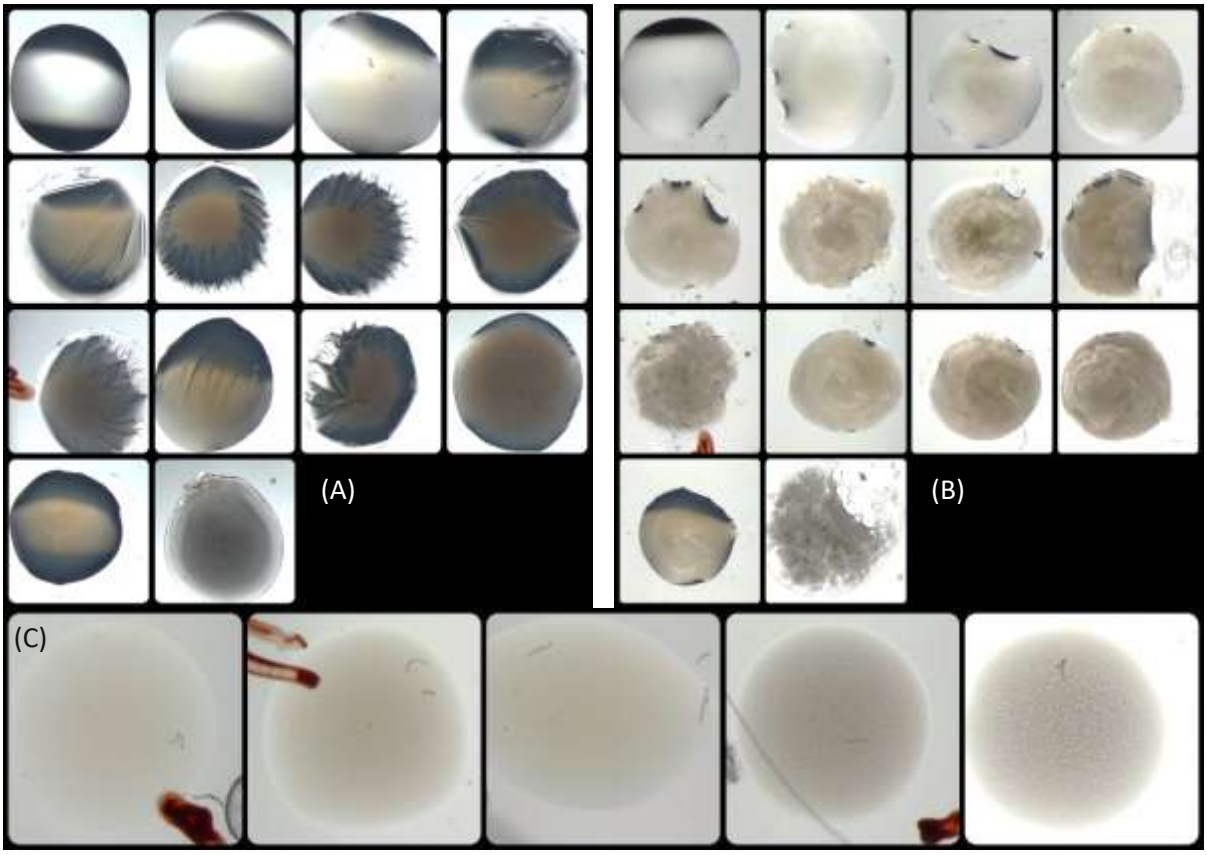

Figure 31 Precipitation of L-*Fv*PPO with a purity of more than 80 % concentrations from left to right 4,8,10,12,15,18,20,22,24,28,30,35,40 and 50 g L^{-1} in (A) after 24 hours equilibration in 50 % (v/v) PEG 2000 (B) 24 hours after the addition of 1 mM TEW final concentration; the L-*Fv*PPO concentrations from left to right 8, 32, 40, 48, and 60 g L^{-1} in (C) after 24 hours equilibration in 40 % (w/v) PEG 8000 with a final concentration of 1 mM YCl_3. Brown marker signs can be seen in the peripheral of some pictures, these were auxiliary in the course of the experiment.

5.14.2.2. Evaluation of VD-HD Experiments

The occurrence of phase separation, gelatinous protein as well as fast grown crystals were now recorded in experiments of VD-HD. Exemplary pictures of the newly observed conditions are also depicted in Table 31. The recorded observations are displayed in detail in the appendix 9.3 Crystallization).

Table 31 Scoring system for L-*Fv*PPO crystallization with VD-HD (vapor diffusion sitting-drop)

Observation	Score	Example picture	Remarks
Clear drop	0	-	-
Precipitation	3	-	Only light precipitation was observed
Gelatinous protein	4	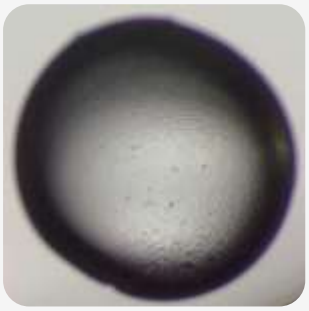	Sometimes difficult to differentiate from skin that formed at the drop´s surface
Phase separation	5		-
Fast grown crystals	6	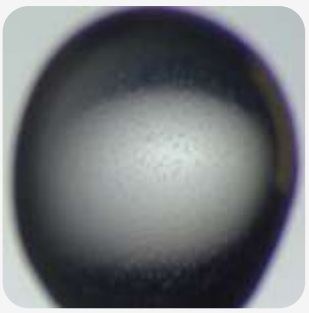	Did not show birefringence; different from precipitation due to edges
Fast grown crystals with precipitate	6.5	-	If a score of 6 had been assigned, but then the object with edges disappeared in light precipitation
Crystal	9	-	-

5.14.2.3. Literature and Grid Screen

In contrast to the other crystallization experiments, the literature screen (VD-HD) was set up on the same day of the purification of the batch with a purity of more than 90 %. After 16 days, one crystalline object could be produced which is depicted in Figure 32. The object exhibited birefringence and had distinct edges. The respective condition as well as the drop content is summarized in Table 32. According to experienced colleagues, this condition did not include precipitants or salts that would produce false positives easily. This strong indication, that a protein crystal was produced had led to an X-ray measurement attempt. However, the crystalline object was damaged during the experimental setup of the external measurement.

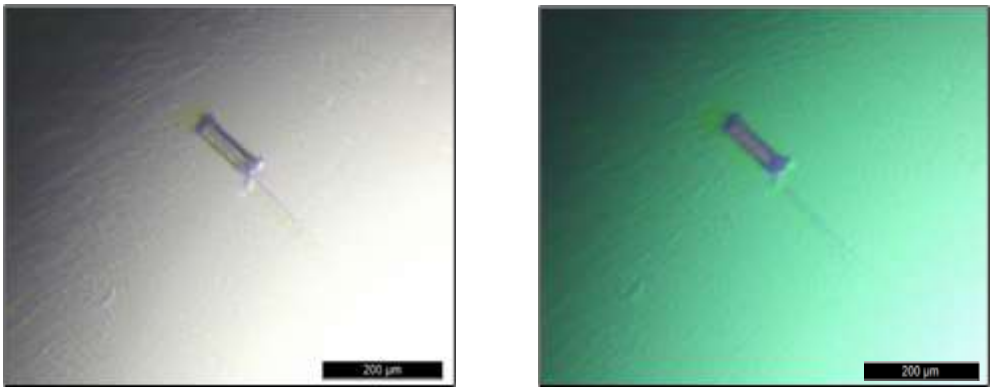

Figure 32 Possible protein crystal of L-*Fv*PPO, which was observed after 16 days due to it´s birefringence property in the condition: 50 mM sodium citrate, 13 % (w/v) PEG 8000, pH 6.77 (at 22°C). Growth temperature was 291.15 K and the final protein concentration was 5.23 g L^{-1}.

Table 32 Condition that led to a possible protein crystal of L-*Fv*PPO.

L-*Fv*PPO protein batch	More than 90 % purity
Protein concentration (g L^{-1})	5.23
Composition of reservoir	50 mM sodium citrate, 13 % (w/v) PEG 8000, pH 6.77 (at 22°C)
Volume of drop (µL)	2.00
Volume of reservoir solution in drop (µL)	1.00
Protein concentration in drop, start (g L^{-1})	2.62
Protein concentration in drop, end (g L^{-1})	5.23
Incubation temperature (K)	291.15

According to the manual of the Crystallization Basic Kit for Proteins (Sigma Aldrich, Buchs, Swiss) once ammonium sulfate is used for precipitation or in the purification, that even after further purification, trace amounts of the precipitate can be present in the sample. For the sake of reproducibility, the sample was not buffer exchanged after capturing with HIC (batch concentrated with HIC). Immediately after the addition of the protein solution, containing the chaotropic ammonium sulphate, to the drop, the formation of crystalline precipitate was observed in some conditions. They did not show any birefringence properties (condition:100 mM sodium citrate 30% (w/v) PEG 4000, pH 5.61 (at 22°C), protein concentration 8.82 g L^{-1}). The possible crystallization condition for L-*Fv*PPO could not be recreated nor were similar results produced during the systematic variation of the pH, protein, and PEG concentration in the grid screen.

6. Discussion

In the course of this work the heterologous expression of the latent form of wild strawberry PPO was successful. Significant losses during purification led to small quantities of the target protein. Nevertheless, a potential crystallization condition for the PPO without the affinity tag could be identified, but not confirmed due to the experimental framework conditions.

The molecular cloning of the GST-tagged fusion protein and its heterologous expression could be reported as successful, but the purification was not. In contrast to that, for the His6-tagged fusion protein L-*Fv*PPO a purification to more than 90 % could be achieved.
Polyphenol oxidase is in general prone to degradation before and after purification [91]. This was fostered by the results of the thermal shift assays, in which multiple melting points were identified, by the SDS-PAGE samples that contained multiple bands after the stability test, by the DLS measurement, in which polydispersity was present and by the copper quantification, in which the copper content per L-*Fv*PPO molecule was calculated to be approximately half of the expected amount. Sodium chloride had been added as stabilizer to the storage buffer, until results of the thermal shift assay revealed that the stability was not increased. The activation of strawberry PPO has been initiated at 350 mM sodium chloride in the presence of dopamine. The activation of PPO in fuji apple with sodium chloride and the NaCl concentration dependant conformational change are well described phenomena [92].
The activation of the protein could be achieved in accordance with literature with proteinase K [24], in the presence of SDS [13] and activation was observed with the bivalent ions Mg^{2+} and Ca^{2+} at concentrations of 350 mM too. The activation of PPOs with Mg^{2+} has also a possible application in biosensors, due to the linearity of the sensors in Mg^{2+} concentration of 0.5 to 7.5 mM with catechol as substrate. Other bivalent ions such as Cu^{2+}, Zn^{2+} and Mn^{2+} can also exert activation of polyphenol oxidases [93]. Only 0.8 mg copper and 1.7 mg zinc per 100 mg fresh weight are present in strawberries compared to 11 mg magnesium and 16 mg calcium per 100 mg fresh weight [94]. The introduction of Ni^{2+} ions to the protein solution does not lead to an activation of the proenzyme [93], but makes the protein less active and more fragile [95]. The usage of ammonium sulphate in the HIC buffer also decreased the activity of the protein significantly.

The LC-MS results showed that the band at 130 kDa weight in reduced SDS-PAGE, that represents the difference between the L-*Fv*PPO batch with more than 80 % and more than 90 %, contained the target tyrosinase besides another protein species of the expression system, including the chaperone DnaK. The identification of this chaperone supported the idea of removing the periplasm membrane of the expression system, since up to 40 % of this chaperone can be separated with osmotic shock [96]. This also decreases column bleeding [72]. Although combined with a chaperone wash, the band could only be removed with AEX. The idea, that the protein has already been partially activated in IMAC 1 in the presence of 500 mM NaCl in the mobile phase, which led to the formation of multimers or reaction products that resemble the 130 kDa impurity, requires further investigation. Especially, since the Western Blot has not indicated the presence of a His6-tag above the size of L-*Fv*PPO.
It was determined that the absorption maximum at 480 nm with an ε_{480} of 3300 M^{-1} cm^{-1} is time dependant for the measurement of the detectable species DOPAchrome, if the measurement is performed in a buffer different to the one Munoz et al. [34] has used. Therefore, a certain error is present in the obtained activity results.

A promising crystallization condition for the latent form of *Fv*PPO with a purity of more than 90 % was identified, presumably due to the immediate crystallization after purification. Repeating the condition and varying it in the grid screen VD-HD has not led to reproducible results. Stability of the protein could be a problem in crystallization of this protein. Also, the complete precipitation of the protein was not achieved.

7. Outlook

For further crystallization experiments, the purification approach of the His6 tagged protein should be reconsidered. It should be investigated whether further metal ions are introduced to the PPO in the course of the purification and whether this can be prevented. A characterisation of the purified PPO, including pH and temperature optima can indicate crystallization conditions that can be tested.

A change of the metal in IMAC can be considered, due to the destabilization of the protein with Ni^{2+} ions. Another metal ion that can be used in IMAC is Co^{2+}, which has a very high specificity, and it is claimed that the purity of the protein solution is sufficient for crystallization. Cobalt comes with the downfall that another metal would be introduced to the protein, due to leakage of the column [97]. For this reason Cu^{2+} ions, which are also present in the active center of the PPO, could be a possible option, even though the activation of the protein is possible with copper [93] and also its specificity in IMAC is low [97]. In order to prevent further introduction of metal ions the purification of the GST tagged fusion protein should be further investigated. Also, a buffer that stabilizes the protein sufficiently, during purification and storage should be evaluated by testing different buffers, pH values and salt concentrations in thermal shift assays.

In this purification approach with AEX the elution profile contains a steep gradient, that requires excellent pump performances. To overcome the reliance on this external parameter and eventually to increase the purification yield, purification methods based on cation exchange or size exclusion should be approached. However, cation exchange should only be performed, when it is confirmed, that the protein exerts activity at lower pH values, which are required for this method. This can be combined with the characterisation of the kinetic parameters. Pretzler et al. [13] recommends for the characterisation of the PPOs the usage of buffer systems that overlap at the respective pH-limits and at least the substrates: L-tyrosine, tyramine, tyrosol, phenol, L-DOPA, dopamine, catechol and 4-tert-butylcatechol should be tested. The dependency of the absorption coefficient in the different buffers that utilize DOPAchrome as a measurable species should also be considered. It must be added that NaCl can act as an inhibitor for PPO at pH values below 5 [98].

As an alternative for further purification after the proteolytic digestion of the His6-tag ultracentrifugation with a filter that has a cut-off of 100 kDa, could eventually separate the high molecular weight species of L-*Fv*PPO. The success can be evaluated again with SDS-PAGE and with DLS. DLS is a powerful inline tool, that can be used regularly in stability tests, that are performed in cuvettes. The formation of aggregates in the solution during storage can be monitored and this can provide additional information for crystallization. While aggregates or dimers may be concentration dependant, changing the concentration, applying long centrifugation or ultrasonication can eventually get rid of these fault states [87]. Also, stability tests with DLS and SDS PAGE should be performed for all used crystallization temperatures, which are 4°C and 20°C historically [62].

For crystallization, the presence of buffer in the protein solution drop initially stabilizes the protein. This influence should ideally be minimalized, if possible, with dialysis of the protein solution against deionized water before crystallization [62]. This could eventually lead to full protein precipitation. In general, low reproducibility of crystallization experiments has been reported by Newman et al. [99], and they also recommend that replications whilst screening can potentially increase the success rate. Utilizing an automated approach for initial screens and expanding the crystallization conditions provided by different manufacturers in different concentrations, can potentially lead to initial hits.

It must be highlighted that there is no unique condition, that leads to crystallization [62]. The access of oxygen contributes not only to the protein oxidation [100] ,but for PPO also to it´s reactivity, making anaerobic crystallization an appealing method. Apart from this advanced technique other methods like micro-dialysis, micro-batch and free-interface diffusion would influence the crystallization behavior of the protein [101].

As an alternative to the mainly destructive methods to determine a false positive crystallization hit, UV imaging can be applied. This non-destructive method requires a certain tryptophane content in the protein for the measurement of the intrinsic fluorescence of the crystal. This theoretical tryptophan requirement would be met in L-*Fv*PPO with a content of 1.4 % [73], [102].

If extensive trials, preferable automated, would eventually not lead to hits, then crystallization with an intact affinity tag like His6 tag can be considered, since of all structures published in PDB in only approximately 10 % electron density can be measured for the tag [62]. The successful crystallization of the apo-form of *Solanum lycopersicum* polyphenol oxidase provided further insight into the gate keeper residues [25]. This would also make the apo-form of *Fv*PPO appealing for crystallization.

8. Abbreviations

A_{280}	Absorption at 280 nm
AEX	Anion exchange chromatography
AP	Alkaline phosphatase buffer
APS	Ammonium persulphate
BSA	Bovine serum albumin
EC	Enzyme Commission number
EDTA	Ethylenediaminetetraacetic acid
ελ	Molar absorption coefficient at a certain wavelength
f	Titration factor
FL	Forward long
FPLC	Fast Protein liquid chromatography
FS	Forward short
HEPES	(4-(2-hydroxyethyl)-1-piperazineethanesulfonic acid
HIC	Hydrophobic interaction chromatography
HRP	Horse radish peroxidase
HRV3C	Human Rhinovirus 3C (Protease)
IMAC	Immobilized affinity chromatography
kDa	Kilo Dalton (Molecular weight)
LC-MS	Liquid chromatography coupled with mass spectrometry
LFQ	Label free quantification
L-*Fv*PPO	Latent polyphenol oxidase of *Fragaria vesca*
Lopt	Optical path length
NaN	Not a number
NTA	Nitrilotriacetic acid
OD_{600}	Optical density at 600 nm
PBS	Phosphate buffer saline
PCR	Polymerase chain reaction
pH	Potential of hydrogen or power of hydrogen
PMSF	Phenylmethylsulfonylfluoride
POM	Polyoxometalate
PPO	Polyphenol oxidase
RL	Reverse long
RS	Reverse short
RT	Room temperature
SDS	Sodiumdodeclysulphate
SOC	Super optimal broth with catabolite repression
TCEP	Tris(2-carboxyethyl)phosphine
TEMED	N,N,N',N'-Tetramethylethan-1,2-diamine
TEV	Tobacco Etch Virus (Protease)
TEW	Hexatungstotellurate $[TeW_6O_{24}]^{6-}$
TRIS	Tris(hydroxymethyl)aminomethane
TSA	Thermal shift assay
U	Unit(s)
VD-HD	Vapor diffusion hanging drop
VD-SD	Vapor diffusion sitting drop
λ	Wavelength

9. Appendix

9.1. Recipes

The PBS (1x) solution was available in the laboratory and it was not required to prepare a fresh solution according to the recipe in Table 33 in the course of the work.

Table 33 Recipe for 1 x PBS.

	concentration (mmol L^{-1})
NaCl	137
Na_2HPO_4	10
KCl	2.7
KH_2PO_4	1.67
pH 7.4 (RT)	

The AP (1x) solution was available in the laboratory and it was not required to prepare a fresh solution according to the recipe in Table 33 in the course of this work.

Table 34 Recipe for 1 x AP solution.

	concentration (mmol L^{-1})
NaCl	150
$MgCl_2$	1
TRIS	100
pH 9.0 (RT)	

The preparation of LB medium started with dissolving of NaCl, Peptone and Yeast extract in approximately 900 mL water. Then the pH value was adjusted with a 10 M and 1 M NaOH solution to 7.00 at 25 °C and the solution was filled to a final volume of 1 L. Once the glycerol was added and the solution filled to a flask, it was autoclaved at 121 °C for 20 min. After cooling it down to room temperature the sterile filtrated $MgSO_4$ solution was added. The recipe of the LB medium is shown in Table 35.

Table 35 Recipe for Luria-Bertani (LB) Medium.

	amount
Glycerol (50 %)	4 mL
$MgSO_4$ (1M)	1 mL
NaCl	10 g
Peptone	10 g
Yeast Extract	5 g
pH = 7.00 (25°C)	
filled to a final volume of 1 L with distilled Water	

The TB medium and the KP_i buffer were prepared according to Table *36* and Table 37. Glycerol was measured with a measure cylinder, that was rinsed with water multiple times in order to transfer the glycerol as complete as possible. Once both solutions were autoclaved and cooled down to room temperature, they were added together in a ratio of 1:1. This was facilitated if either of the solutions was prepared in a 1 L flask. The respective antibiotics were added before usage.

Table 36 Recipe for Terrific Broth (TB) Medium.

	amount
Glycerol (50 %)	16.0 mL
Tryptone	12.0 g
Yeast Extract	24.0 g
filled to a final volume of 0.5 L with distilled Water	

Table 37 Recipe for KP_i medium.

	amount (g)
KH_2PO_4	8.80
K_2HPO_4	37.6
filled to a final volume of 0.5 L with distilled Water	

The Lysis buffer was prepared according to Table 38 without adding lysozyme, DNase I, benzamidine and PMSF. If necessary, the pH was adjusted either by a 1 M NaOH or diluted HCl solution in order to reach the pH of 8.00. The remaining required chemicals were weighted in and DNase I and Lysozyme were dissolved directly in the lysis buffer under agitation. A benzamidine solution was prepared in water, as well as a PMSF solution in EtOH. The solubility of PMSF in EtOH could be increased if the solution was heated with the warmth of the hand. Both solutions were added, but the PMSF solution was added last, because of it´s instability in water.

Table 38 Recipe for Lysis buffer (without periplasm membrane removal).

	concentration
Benzamidine	1.0 mM
DNase I	0.04 g L^{-1}
Lysozyme	0.7 g L^{-1}
$MgCl_2$	1.0 mM
NaCl	500 mM
TRIS	100 mM
Triton 10 % (v/v)	0.02 % (v/v)
PMSF	1.0 mM
pH 8.00 (22°C)	

The periplasm buffer was prepared according to Table 39. The pH was adjusted with a NaOH or HCl solution to a final pH of 7.9 at 22 °C.

Table 39 Recipe for periplasm buffer.

	concentration
HEPES	50.0 mM
EDTA	1.00 mM
Sucrose	200 g L^{-1}
pH 7.90 (22 °C)	

The running buffers and elution buffers used in this work were prepared according to the recipes listed in Table 40 - Table 47. The final pH was reached either with a concentrated HCl or 10 M NaOH solution.

The buffers were filtered and degassed according to chapter 4.5.2 Fast Protein Liquid Chromatography (FPLC) before usage.

Table 40 Recipe for Buffer A1, IMAC Ni-NTA.

	concentration (mmol L^{-1})
NaCl	500
TRIS	30
pH 8.00 (22°C)	

Table 41 Recipe for Buffer A2, AC.

	concentration (mmol L^{-1})
NaCl	200
TRIS	50
pH 8.00 (22°C)	

Table 42 Recipe for Buffer A3 AEX.

	concentration (mmol L^{-1})
TRIS	30
pH 8.35 (25°C), 9.00 (4°C)	

Table 43 Recipe for Buffer A4 HIC.

	concentration (mmol L^{-1})
$(NH_4)_2SO_4$	1500
TRIS	30
pH 7.99 (22°C)	

Table 44 Recipe for Buffer B1 IMAC Ni-NTA.

	concentration (mmol L^{-1})
Imidazole	500
NaCl	500
TRIS	30
pH 8.00 (22°C)	

Table 45 Recipe for Buffer B2 AC GST.

	concentration (mmol L^{-1})
L-Glutathione	15
NaCl	200
TRIS	50
pH 8.00 (22°C)	

Table 46 Recipe for Buffer B3 AEX.

	concentration (mmol L^{-1})
TRIS	30
NaCl	1000
pH 8.34 (25°C)	

Table 47 Recipe for B4 HIC.

	concentration (mmol L^{-1})
TRIS	30
pH 8.00 (22°C)	

For the preparation of the agar plates according to Table 48 the required amounts of NaCl, yeast extract and tryptone were dissolved in 1 L water in an Erlenmeyer flask. After the pH was adjusted to 7.00 at room temperature, the solution was filled in a flask containing solid agar-agar. The solution was autoclaved at 121 °C for 20 min. Once the solution reached a final temperature of approximately 60 °C (can be touched), the respective antibiotic was added and subsequently the Petri dishes were filled.

Table 48 Recipe for LB Agar plates with ampicillin or kanamycin.

	concentration (g L^{-1})
Agar-agar	15
Ampicillin/Kanamycin	0.050
NaCl	10
Tryptone	10
Yeast extract	5
pH 6.94 (RT)	

The chaperone wash buffers were prepared according to Table 49 and Table 50 by dissolving the respective chemical in water and adjusting the pH with either a NaOH or HCl solution. Only the ATP · 2Na was added after the pH was adjusted. The washing buffers were filtered and degassed according to chapter 4.5.2 Fast Protein Liquid Chromatography (FPLC) before usage.

Table 49 Recipe for Chaperone wash buffer 1

	concentration (mmol L^{-1})
ATP · 2Na	5
KCl	200
$MgCl_2$	10
TRIS	50
pH 8.0 (4°C)	

Table 50 Recipe for Chaperone wash buffer 2

	concentration (mmol L^{-1})
NaCl	200
TRIS	50
Urea	2000
pH 8.0 (25°C)	

9.2. Sequences

9.2.1. *Fv*PPO-His6

Table 51 Codon optimized sequence of *L*-Fv*PPO* with His6 tag (Accession number: XP_004293563.1).

L*-Fv*PPO with His6 Tag
ATGGCAGCACCTGTTCCGCCTCCGGATCTGGCAACCTGTGGTCCGGCAGATAAACCGGATGGCACCACCATTGATTGTT GTCCGCCTAAAACCACCACGATCATTGATTTTAAACTGCCTGATCCGGGTCCGATGCGTACCCGTCTGGCAGCACAGAA TGTTGCAAAAGATCCTGTGTATCTGGCCAAGTATAAAAAGGCAATTGAACTGATGCGTGCACTGCCGGATGATGATCC GCGTAGCCTGGCACAGCAGGCAATGGTTCATTGTAGCTATTGTGATGGTGGTTATCCGATGGCAGGTTTTAGCGATCT GGAAATTCAGGTGCATTTTAGCTGGCTGTTTTATCCGTGGCATCGTCTGTATCTGTATTTCTACGAGAAAATCATGAGCA AGCTGATCGATGATCCGACCTTTGCGCTGCCGTTTTGGAATTGGGATGCACCGGCAGGTATGTATATTCCGAGCATTTT TACCGATACCACCAGTAGCCTGTATGACCAGTATCGTAATGCAGCACATCAGCCTCCGAAACTGCTGGATCTGAATTAT GGTGGCACCGATGATGATACCGATGATAAAACCCGTATTCGTGAAAATCTGACCACCATGTATCAGCAGATGATTAGC AAAGCAACCAGCCACCGTCTGTTTTTCGGTGAACCGTATAGTGCCGGTGATGAACCGAATCCTGGTGCAGGTAATATTG AAAGCATTCCGCATAACAACATTCATCTGTGGACCGGTGATCCGACACAGACCAATGGTGAAGATATGGGTGCCTTTTA TAGCGCAGGTCGTGATCCGATCTTTTATAGTCATCATGCAAATGTGGATCGCATGTGGTCAATCTATAAAGCACGTGGT GGTACAGATATCACCAAAAAGGATTGGCTGGATACCGAATTCCTGTTCTATGATGAAAACAAAAATCTGGTGCGTGTG AAAGTTCGTGATAGCCTGGATGAAAGCAAACTGGGTTACAAATATCAGGATGTTGAAATTCCGTGGCTGAATAGCAAA CCGACCGCACGTAAAAGCAAAAACAAACGTAAAGCAGCAGTTAGCAGCGCAGATCTGACCAGCAAATTTCCGGCAACA CTGAGCGAAACCATTAGCGTTGAAGTTGCACGTCCGAGCGCAGCAAAACGTACCACCGCAGAGAAAACCAAAGAAGA AGAAGTTCTGGTTATTAGCGGCATTGAATTTGCAGGTAGCGAAATGCTGAAATTCGATGTGTATGTTAACGATGATGCG GATGAAGTTAGCGGTAAAGATAAAGCAGAATTTGCCGGTTCATTTGTTCATGTTCCGCATCGTGCCAACAAAAAGATTA AAACCAATCTGCGTCTGGGCATTACAAATCTGCTGACCGATCTGGGTGCAGAAGAAGATAATAGCGTTGTTGTTACCCT GGTTCCGAAATTTGGTAAAGGTGCAATTATTGGTGGCTTCAAAATCGAACTGATTAGCACCACCGGATCCCTGGAAGTT CTGTTTCAGGGTCCGCTCGAGCACCACCACCACCACCACTGA

9.2.2. Primer sequences

Table 52 Sequences of the forward and reverse primers (5´-> 3´) utilized in sticky-end-PCR for ligation into pGEX-6P-1 digested with BamHI and EcoRI. Utilized in molecular cloning of *Fv*PPO with GST tag.

Fv*PPO-FL*
GATCCATGGCAGCACCTGTTCCGCCT
Fv*PPO-FS*
CATGGCAGCACCTGTTCCGCCT
Fv*PPO-RL*
AATTCTCAGGTGGTGCTAATCAGTTCGATTTTG
Fv*PPO-RS*
CTCAGGTGGTGCTAATCAGTTCGATTTTG

9.3. Crystallization

9.3.1. Plate diameters VD-SD

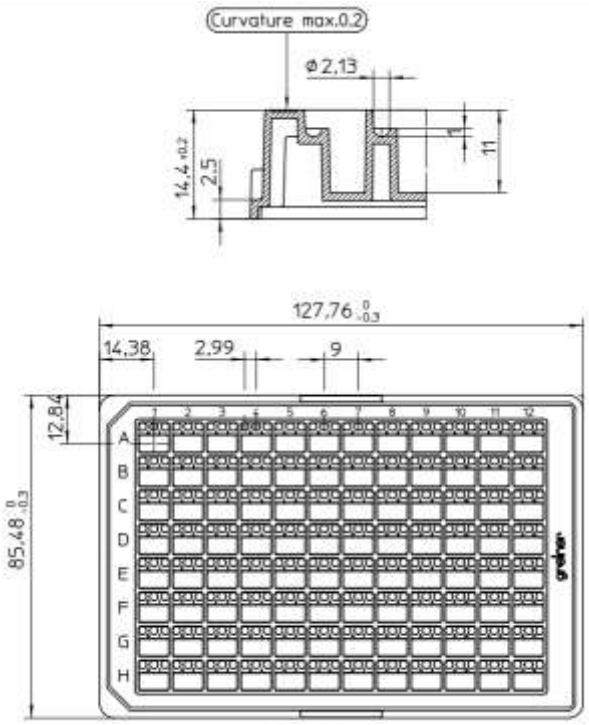

Figure 33 CRYSTALQUICK RW PLATE, 96 WELL, COC, LBR (RW: round wells; COC: concave bottom; LBR: low birefringence) (Greiner Bio-One GmbH, Frickenhausen, Germany) Dimensions of one well (top) and of the plate of the VD-SD experiments (bottom).

9.3.2. Recorded observations

Table 53 Color code for the recorded observations in the crystallization experiments performed in vapor diffusion sitting drop set up.

Score	0 (clear drop)	1.0 (object)	1.5 (precipitation/turbid)	2 (light precipitation)	4 (crystal with birefringence)
Color	Red	Orange	Yellow	Green	Dark Green

9.3.2.1. VD-SD

Table 54 Plate 1 VD-SD, Observations at day 0.

Day 0		1	2	3	4	5	6	7	8	9	10	11	12
A	I	0	0	0	1	2	1	0	0	0	0	1	0
	II	0	0	0	0	0	1	0	0	2	0	1	0
	III	2	0	0	0	1.5	1	0	0	2	1	0	0
B	I	0	0	0	0	2	0	0	0	2	1	0	0
	II	0	0	0	0	2	1	2	0	2	0	0	0
	III	0	0	0	0	2	0	2	1	2	0	0	0
C	I	0	0	2	0	1	0	0	0	0	0	0	0
	II	0	2	2	0	0	0	0	0	0	0	0	0
	III	1.5	1.5	1.5	0	1	0	2	0	0	0	0	0
D	I	0	0	0	0	0	0	0	0	0	2	0	0
	II	0	2	0	0	2	2	0	0	0	2	0	2
	III	0	2	0	0	1.5	2	2	0	0	1	0	1.5
E	I	0	0	0	0	0	1.5	0	0	0	0	2	0
	II	0	0	1	0	0	1.5	1.5	0	0	2	2	0
	III	0	0	0	0	1	1	1	0	1	1	1	1
F	I	2	0	0	0	0	0	0	0	1	0	0	0
	II	2	0	0	2	2	2	0	0	2	2	0	0
	III	2	0	0	2	1	1	1	1	1	1	0	1
G	I	0	0	0	0	2	0	0	0	0	0	0	0
	II	0	0	0	0	2	0	0	0	0	0	0	0
	III	0	0	0	0	0	0	0	0	1	0	0	0
H	I	0	0	0	0	0	0	2	0	0	0	0	2
	II	0	0	0	0	0	0	2	0	0	0	0	2
	III	1	0	0	0	0	0	0	0	0	0	0	0

Table 55 Plate 1 VD-SD, Observations at day 57. Crystal (score 4) could not be confirmed.

Day 57		1	2	3	4	5	6	7	8	9	10	11	12
A	I	1.5	0	0	0	1.5	1	1.5	2	0	0	0	1
	II	1.5	0	1.5	1.5	1.5	1	1.5	1.5	0	0	0	1
	III	1.5	1.5	2	1	1.5	1	1.5	1.5	1	1	0	1
B	I	0	2	0	0	1.5	1.5	2	2	2	1	0	0
	II	0	0	0	0	1.5	0	1.5	0	1.5	0	0	0
	III	0	1	1.5	0	1.5	2	1.5	1	1.5	0	0	0
C	I	1	1.5	1.5	0	2	1	2	0	0	2	0	0
	II	1.5	1.5	1.5	0	2	1	2	0	1	1.5	1	0
	III	1.5	1.5	1.5	1	2	1	2	0	2	1.5	0	2
D	I	0	2	2	0	2	2	0	1	0	0	2	2
	II	0	1.5	1.5	2	1.5	1.5	0	1	2	1	1	1.5
	III	2	1.5	2	0	1.5	1.5	1.5	1.5	1.5	2	4	1.5
E	I	0	0	0	0	0	1.5	1.5	0	0	1.5	1.5	0
	II	0	0	1	1	0	1.5	1.5	1	1.5	1.5	1.5	1.5
	III	0	0	1	0	1.5	1	1	1	0	1.5	1.5	0
F	I	1.5	2	0	0	0	0	0	0	1	0	0	2
	II	1.5	1	0	2	1.5	0	0	2	1.5	1.5	2	0
	III	0	0	1	1	1	1	1	1	1	1.5	1.5	2
G	I	0	0	0	0	0	2	1.5	0	0	0	0	0
	II	0	0	0	0	0	1.5	1	0	0	1	0	0
	III	0	0	0	0	0	0	0	0	0	0	0	0
H	I	0	1.5	0	0	0	0	0	1	0	0	0	1.5
	II	1	1.5	0	1.5	0	0	1	0	0	1	0	1.5
	III	0	0	0	0	0	0	1	0	0	0	0	0

Table 56 Plate 2 VD-SD, Observations at day 0.

Day 0		1	2	3	4	5	6	7	8	9	10	11	12
A	I	0	0	0	0	0	0	0	1	0	0	0	0
	II	0	0	0	0	0	0	0	0	0	0	0	0
	III	0	0	0	0	0	0	1	0	0	0	0	0
B	I	0	0	0	0	0	0	0	0	0	0	0	0
	II	0	0	0	0	0	0	1.5	0	1.5	0	0	0
	III	0	0	0	0	1	0	1.5	0	1.5	0	0	0
C	I	0	0	2	0	0	1.5	0	0	0	0	0	0
	II	0	0	2	0	1.5	1.5	0	1	0	2	0	0
	III	0	0	1.5	0	2	0	0	0	1	0	0	0
D	I	1.5	1.5	0	0	0	0	0	0	0	0	0	0
	II	0	1.5	0	0	0	2	0	0	0	0	0	0
	III	0	1.5	0	0	0	2	0	0	0	0	0	2
E	I	0	0	0	0	0	0	0	0	0	0	0	0
	II	0	1	0	1	0	2	2	2	0	2	2	0
	III	2	2	0	1	0	0	2	2	2	2	2	2
F	I	0	0	0	0	1	0	0	0	0	0	0	0
	II	0	0	0	0	2	0	1	0	2	2	2	0
	III	1	1	1	1	2	2	1	1	2	2	2	2
G	I	0	0	0	0	0	0	0	0	0	0	0	0
	II	0	0	0	0	2	0	0	0	0	0	0	0
	III	1	1	1	1	1	0	0	0	0	0	0	0
H	I	0	0	0	0	0	0	0	0	0	0	0	2
	II	0	0	0	0	0	1	0	0	0	0	0	2
	III	0	0	0	0	0	0	1	0	0	0	0	0

Table 57 Plate 2 VD-SD, Observations at day 57.

Day 57		1	2	3	4	5	6	7	8	9	10	11	12
A	I	0	0	0	0	0	0	0	1.5	0	0	0	0
	II	0	0	0	0	0	0	0	1.5	0	0	0	0
	III	0	0	0	0	0	0	0	1.5	1	0	0	0
B	I	0	0	0	0	0	0	1.5	0	0	0	0	0
	II	0	0	0	1.5	0	0	0	0	1	1.5	1.5	0
	III	0	0	0	0	0	0	0	0	1.5	0	0	0
C	I	0	0	0	0	0	0	0	0	0	0	0	0
	II	0	0	0	0	0	1	0	0	0	0	0	0
	III	1.5	1.5	1.5	0	0	1	0	0	0	0	0	0
D	I	0	0	0	1.5	1.5	1.5	0	0	0	0	2	1.5
	II	0	1	0	0	1.5	1.5	0	0	0	0	2	1.5
	III	0	0	0	0	1.5	1.5	0	0	0	0	0	1.5
E	I	0	1	0	0	0	0	1.5	0	0	0	0	0
	II	0	1	0	0	0	1.5	1.5	0	0	1.5	1.5	1
	III	0	1	0	0	0	0	1.5	0	0	1.5	1.5	1
F	I	0	0	0	0	0	0	0	0	1.5	1.5	0	0
	II	1.5	0	0	0	1.5	0	0	0	1.5	1.5	1	0
	III	1	0	1	1.5	1.5	1.5	1	0	1	1	1.5	1
G	I	0	0	0	0	0	0	0	0	0	0	0	0
	II	1	1	0	0	1.5	0	0	0	0	0	0	0
	III	1	0	0	0	0	0	0	0	0	0	0	0
H	I	0	0	0	0	0	0	0	0	0	0	0	2
	II	0	0	0	0	0	0	0	1	0	0	0	1.5
	III	1	0	0	0	0	0	0	0	0	0	0	0

Table 58 Plate 3 VD-SD, Observations at day 27.

Day 27		1	2	3	4	5	6	7	8	9	10	11	12
A	I	0	0	0	1	0	0	0	0	0	0	0	0
	II	0	0	0	1	0	0	0	0	0	0	1	0
	III	0	0	0	1	0	0	0	0	0	1	0	0
B	I	0	0	0	0	0	0	0	0	0	0	0	0
	II	0	0	0	0	0	0	0	0	0	0	0	0
	III	0	0	0	0	0	0	0	0	0	0	0	0
C	I	0	0	2	1.5	0	0	1.5	0	2	1.5	1.5	1.5
	II	0	0	2	2	0	0	2	0	2	0	2	2
	III	0	0	2	2	2	1	2	0	2	2	2	0
D	I	0	0	2	1.5	0	1.5	0	0	0	0	0	0
	II	0	0	2	2	0	0	2	0	0	0	0	0
	III	0	0	2	2	0	2	0	0	0	1	0	0
E	I	0	0	0	0	0	0	0	0	0	0	0	0
	II	0	0	0	0	0	0	0	0	0	0	0	0
	III	0	0	1	0	0	0	0	0	2	0	0	0
F	I	0	2	0	0	0	0	0	0	2	0	0	0
	II	2	2	1	0	1	0	2	1	2	2	2	2
	III	1	2	2	0	1	0	2	2	2	1	2	0
G	I	0	0	0	0	0	1.5	1.5	0	0	2	2	0
	II	1	0	0	0	1	2	1	0	2	2	2	2
	III	1	0	0	0	0	1	0	0	0	0	1	0
H	I	0	0	0	0	2	0	0	0	1.5	2	2	2
	II	1	0	0	2	1	0	0	0	2	1	0	2
	III	2	2	2	0	0	0	0	2	2	1.5	0	0

Table 59 Plate 4 VD-SD, Observations at day 2.

Day 2		1	2	3	4	5	6	7	8	9	10	11	12
A	I	0	0	1.5	0	1	0	0	0	0	0	1.5	0
	II	0	0	1.5	0	0	0	1	0	0	0	1.5	0
	III	0	0	1.5	0	0	0	1	0	0	0	1.5	0
B	I	0	0	0	0	0	0	0	0	0	0	0	0
	II	0	0	2	1	1	0	0	1	0	0	0	0
	III	0	2	2	2	2	2	2	2	0	2	2	0
C	I	0	0	0	0	0	0	0	0	0	0	0	0
	II	0	0	0	1	1	0	0	0	0	1	1	1
	III	1.5	1.5	0	0	1.5	0	0	0	0	0	0	0
D	I	2	0	0	0	0	0	2	2	2	2	2	0
	II	2	0	1	1	1	2	2	2	2	2	2	0
	III	1.5	0	1	1	2	1.5	1.5	1.5	1.5	1.5	1.5	0
E	I	0	2	0	0	0	0	0	1	0	2	0	0
	II	0	2	0	1	1	1	1	1	1	2	1	2
	III	0	1.5	0	1	1	1	1	1	2	1.5	2	1.5
F	I	0	0	0	0	0	0	0	1	0	0	0	0
	II	0	0	0	0	2	1	0	1	0	1	0	0
	III	0	0	0	0	0	1	0	1	0	0	0	0
G	I	0	0	0	0	0	0	0	0	2	0	0	0
	II	0	0	0	0	0	0	0	0	2	0	0	0
	III	0	0	0	0	0	0	0	0	0	0	0	0
H	I	0	0	0	0	0	0	0	0	2	0	0	0
	II	0	0	0	0	0	0	0	0	2	0	0	0
	III	0	0	0	0	0	0	0	0	0	0	0	0

Table 60 Plate 5 VD-SD, Observations at day 3. Crystal (score 4) could not be confirmed.

Day 3		1	2	3	4	5	6	7	8	9	10	11	12
A	I	0	0	0	0	0	0	0	0	0	0	0	0
	II	0	0	0	0	0	0	0	0	0	0	0	0
	III	0	0	0	0	0	0	0	0	0	0	0	0
B	I	0	0	0	0	0	0	0	0	0	0	0	0
	II	0	0	0	0	0	0	0	0	0	0	0	0
	III	0	0	0	0	0	0	0	0	0	0	0	0
C	I	0	0	0	0	0	0	0	0	0	0	0	0
	II	0	0	0	0	0	0	0	0	0	0	0	0
	III	0	0	0	0	0	0	0	0	0	1	0	0
D	I	0	0	0	0	0	0	0	0	0	0	0	0
	II	0	0	0	0	1	0	0	0	0	0	0	1.5
	III	2	2	2	0	0	0	0	0	0	0	0	0
E	I	1	0	0	0	0	0	0	0	0	0	0	0
	II	0	0	0	0	0	0	0	0	0	0	0	0
	III	2	1	0	0	0	2	2	0	2	2	2	0
F	I	0	0	0	0	0	0	0	0	0	0	0	0
	II	0	0	0	0	0	0	0	0	0	0	0	4
	III	2	0	0	0	1	2	1	1	1	1	0	0
G	I	0	0	0	0	0	0	0	0	0	0	0	0
	II	0	0	0	0	0	0	0	0	0	0	0	0
	III	1	2	1	1	0	1	0	0	0	0	0	0
H	I	0	0	0	0	0	0	0	0	0	0	0	0
	II	0	0	0	0	0	0	0	0	0	0	0	0
	III	0	0	0	0	0	0	0	0	0	0	0	0

Table 61 Plate 5 VD-SD, Observations at day 5.

Day 5		1	2	3	4	5	6	7	8	9	10	11	12
A	I	0	0	0	0	0	0	0	0	0	0	0	0
	II	0	0	0	0	0	0	0	0	0	0	0	0
	III	0	0	0	0	0	0	0	0	0	0	0	0
B	I	2	0	0	0	2	0	0	0	0	0	0	0
	II	0	0	0	1	0	0	0	0	0	0	0	0
	III	0	0	0	0	0	0	0	0	0	0	0	0
C	I	0	0	2	0	0	0	1.5	0	0	2	2	0
	II	0	0	0	0	0	0	0	0	2	0	0	0
	III	0	0	0	0	0	0	0	0	0	1	0	0
D	I	1	0	2	2	2	0	0	0	0	2	0	0
	II	0	0	0	0	0	0	0	0	0	0	0	0
	III	0	0	2	2	2	0	2	0	0	0	0	0
E	I	1	0	1	0	0	0	0	0	0	0	0	0
	II	0	0	0	0	0	0	0	0	0	0	0	0
	III	0	2	0	1.5	1.5	1.5	1.5	1.5	1.5	1.5	1.5	1.5
F	I	0	0	0	0	0	0	0	0	0	0	0	0
	II	0	0	0	0	0	0	0	0	0	0	0	0
	III	1.5	2	2	2	2	2	0	2	2	1	0	0
G	I	0	0	0	0	0	0	0	0	0	0	0	0
	II	0	0	0	0	0	0	0	0	0	0	0	0
	III	2	2	1	1	0	0	2	0	0	0	0	0
H	I	0	0	0	0	0	0	0	0	0	0	0	0
	II	0	0	0	0	0	0	0	0	0	0	0	0
	III	0	0	0	0	0	0	1.5	1.5	0	0	0	2

Table 62 Plate 5 VD-SD, Observations at day 7.

Day 7		1	2	3	4	5	6	7	8	9	10	11	12
A	I	0	0	0	0	0	0	0	0	0	0	0	0
	II	0	0	0	0	0	0	0	0	0	0	0	0
	III	0	0	0	0	0	0	0	0	0	0	0	0
B	I	1	0	0	0	2	2	2	0	0	0	0	0
	II	0	1	0	0	1	1	0	0	1	0	0	0
	III	0	1	0	0	0	0	0	0	0	0	0	0
C	I	1	0	2	0	0	0	2	0	0	0	0	0
	II	2	0	0	0	1	0	1	0	1	0	0	2
	III	0	0	0	0	0	0	1	0	0	0	0	0
D	I	0	0	2	0	0	0	0	0	0	0	0	0
	II	0	0	1	1	0	0	1	0	0	0	0	0
	III	1.5	1.5	0	0	0	0	0	0	0	0	0	0
E	I	0	0	0	0	0	0	0	0	0	0	0	0
	II	0	0	0	0	1	1	0	0	0	0	0	0
	III	1.5	2	0	0	1.5	1.5	0	0	1.5	1.5	1.5	1.5
F	I	2	0	0	0	0	0	0	0	0	0	0	0
	II	0	0	0	0	0	0	0	0	0	0	0	0
	III	1.5	0	0	0	1.5	1.5	1.5	1.5	1.5	1.5	0	0
G	I	0	1.5	0	0	0	0	0	0	0	0	0	0
	II	0	0	0	0	0	0	0	0	0	0	0	0
	III	0	0	0	0	0	0	0	0	0	0	0	0
H	I	0	0	0	0	0	0	0	0	0	0	0	0
	II	0	0	0	0	0	0	0	0	0	0	0	0
	III	0	0	0	0	0	0	0	0	0	0	0	0

Table 63 Plate 6 VD-SD, Observations at day 1.

Day 1		1	2	3	4	5	6	7	8	9	10	11	12
A	I	0	0	0	0	0	1	0	0	1.5	0	1.5	1.5
	II	0	1	0	0	0	0	0	0	1	0	0	0
	III	0	0	0	0	0	0	0	2	0	0	0	0
B	I	0	0	0	0	0	0	0	0	0	0	0	0
	II	0	0	0	0	0	0	0	2	2	0	2	0
	III	0	0	0	0	0	0	2	2	2	2	0	0
C	I	0	0	1.5	0	0	0	0	0	0	0	0	0
	II	0	0	2	2	0	0	0	0	2	0	0	0
	III	0	0	0	0	0	0	2	0	0	0	0	2
D	I	0	0	0	0	0	0	0	0	0	0	0	0
	II	0	0	0	0	0	0	0	0	0	0	0	0
	III	2	2	0	2	2	2	2	0	2	2	0	2
E	I	0	0	0	0	0	0	0	1.5	1.5	1.5	0	0
	II	1.5	0	0	0	0	2	0	1.5	1.5	1.5	0	0
	III	1.5	0	0	0	0	1.5	0	1.5	1.5	1.5	0	0
F	I	0	0	0	0	0	0	0	0	0	1.5	0	0
	II	0	0	0	0	0	0	0	0	0	1.5	0	1.5
	III	0	0	0	2	2	0	0	2	0	2	0	1.5
G	I	0	0	0	1.5	1.5	0	0	1.5	0	0	0	0
	II	1.5	0	0	1.5	1.5	0	0	1.5	0	0	0	0
	III	0	1.5	0	0	0	0	0	0	0	0	0	0
H	I	0	1.5	0	0	0	0	0	0	0	0	0	0
	II	0	1.5	0	1.5	1.5	0	1.5	2	1	0	1.5	0
	III	0	0	0	0	0	0	0	0	0	0	0	0

Table 64 Plate 6 VD-SD, Observations at day 3.

Day 3		1	2	3	4	5	6	7	8	9	10	11	12
A	I	0	0	0	0	0	1.5	1	1.5	1.5	0	1.5	1.5
	II	0	1	2	0	0	0	0	0	0	0	2	0
	III	0	0	2	0	0	0	2	0	0	0	0	0
B	I	0	0	0	0	0	0	0	0	0	0	0	0
	II	0	0	0	0	0	0	0	2	1.5	0	2	2
	III	0	0	0	0	0	0	2	2	1.5	0	0	0
C	I	0	0	1.5	2	0	0	0	0	0	2	2	2
	II	0	0	0	0	0	1	0	0	2	2	2	2
	III	0	0	0	2	0	0	2	0	0	0	0	2
D	I	0	0	0	0	0	0	0	0	0	2	0	0
	II	0	0	0	0	0	0	0	0	0	0	0	0
	III	2	2	2	2	2	2	1.5	0	1.5	0	0	0
E	I	0	0	0	0	0	0	0	0	1.5	1.5	0	0
	II	0	0	0	0	0	1.5	0	2	1.5	1.5	0	0
	III	1.5	0	0	0	0	1.5	0	1.5	1.5	1.5	0	0
F	I	0	0	0	0	0	0	0	0	0	1.5	0	0
	II	0	0	0	0	2	0	0	0	0	1.5	0	0
	III	0	0	0	0	1.5	0	0	0	0	1.5	0	0
G	I	0	0	0	0	0	0	1.5	0	0	0	0	0
	II	0	1.5	0	1.5	1.5	0	1.5	0	0	0	1.5	0
	III	0	0	0	0	0	0	0	0	0	0	0	0
H	I	0	1.5	0	0	0	0	0	0	0	0	0	0
	II	0	1.5	2	1.5	1.5	0	1.5	1.5	1.5	0	0	0
	III	0	0	0	0	0	0	0	0	0	0	0	0

9.3.2.2. VD-HD

9.3.2.2.1. Literature screen

Table 65 Literature screen VD-HD, Observations at day 0

Day 0	Protein concentration c1<c2<c3	Condition					
		1	2	3	4	5	6
more than 90% purity	c1	0	0	0	0	0	0
	c2	0	0	0	0	0	0
	c3	0	0	0	0	0	0
concentrated with HIC	c1	3	0	0	0	5	0
	c2	3	0	0	0	5	0
	c3	0	0	0	0	5	0

Table 66 Literature screen VD-HD, Observations at day 16

Day 16	Protein concentration c1<c2<c3	Condition					
		1	2	3	4	5	6
more than 90% purity	c1	5	0	0	0	5	3
	c2	5	0	0	9	5	3
	c3	5	0	0	0	5	3
concentrated with HIC	c1	0	0	0	5	5	0
	c2	0	0	5	5	5	0
	c3	0	0	5	5	5	0

Table 67 Literature screen VD-HD, Observations at day 38

Day 38	Protein concentration c1<c2<c3	Condition					
		1	2	3	4	5	6
more than 90% purity	c1	5	3	3	*	5	3
	c2	5	0	0	*	5	3
	c3	5	0	3	*	5	3
concentrated with HIC	c1	5	3	3	3	0	0
	c2	4	3	3	3	5	0
	c3	0	3	3	3	3	0

*One united drop with light precipitation. For better access to the crystalline object, the drops were united when the crystal was taken.

9.3.2.2.2. Grid screen

Table 68 Grid screen VD-HD, Observations at Day 8.

Protein concentration (g L^{-1})	PEG 8000 concentration (%)	Sodium citrate 50mM				
		pH				
		6.36	6.61	6.86	7.11	7.36
2	11	6	0	2	0	0
3		2	0	2	0	2
5		2	0	0	0	2
6		2	0	2	0	2
10		2	6	6.5	0	2
2	13	6	0	0	0	0
3		0	0	0	0.5	0
5		0	0	0	6	0
6		0	0	0	0	0
10		0.5	0	0.5	9	0
2	15	0	0	0	0	0
3		0	0	0	0	0
5		0	0	0	0	0
6		0	0	0	0	0
10		0	6	0	0	0

Table 69 Grid screen VD-HD, Observations at Day 13.

Protein concentration (g L^{-1})	PEG 8000 concentration (%)	Sodium citrate 50mM				
		pH				
		6.36	6.61	6.86	7.11	7.36
2	11	6	0	0	6	5
3		0	2	2	6	0
5		0	0	6	6	0
6		6	0	6	2	6
10		0	0	0	0	0
2	13	6	0	0	0	6
3		5	0	0	6	2
5		0	0	0	6	2
6		5	6	6	6	6
10		6	0	6.5	0	0
2	15	0	6.5	0	2	6
3		0	6	0	0	0
5		0	6	0	0	0
6		0	2	0	0	6
10		0	0	0	0	0

10.References

[1] L. Yu-Feng and S. Hongzhe, *Applied Metallomics From Life Sciences to Environmental Sciences Edited by Yu-Feng Li and Hangzhe Sun*., 69469 Weinheim, Germany: WILEY-VCH GmbH, 2024.

[2] N. R. C. (US) C. on D. and Health, 'Trace Elements', in *Diet and Health: Implications for Reducing Chronic Disease Risk*, National Academies Press (US), 1989. Accessed: Oct. 08, 2024. [Online]. Available: https://www.ncbi.nlm.nih.gov/books/NBK218751/

[3] M. Moustakas, 'The Role of Metal Ions in Biology, Biochemistry and Medicine', *Materials*, vol. 14, no. 3, Art. no. 3, Jan. 2021, doi: 10.3390/ma14030549.

[4] 'Introduction to metalloenzymes: From bench to bedside', in *Metalloenzymes*, Academic Press, 2024, pp. 3–5. doi: 10.1016/B978-0-12-823974-2.00038-3.

[5] Jitesh A. Soares, 'Metals in Biology'. Accessed: Oct. 08, 2024. [Online]. Available: https://pubs.acs.org/page/acbcct/thematic/metals-biology.html

[6] E. D. Harris, 'Copper, Biological Functions', in *Encyclopedia of Metalloproteins*, R. H. Kretsinger, V. N. Uversky, and E. A. Permyakov, Eds., New York, NY: Springer, 2013, pp. 718–723. doi: 10.1007/978-1-4614-1533-6_128.

[7] C. J. Coates and H. Decker, 'Immunological properties of oxygen-transport proteins: hemoglobin, hemocyanin and hemerythrin', *Cell. Mol. Life Sci. CMLS*, vol. 74, no. 2, Art. no. 2, Aug. 2016, doi: 10.1007/s00018-016-2326-7.

[8] B.-E. Kim, T. Nevitt, and D. J. Thiele, 'Mechanisms for copper acquisition, distribution and regulation', *Nat. Chem. Biol.*, vol. 4, no. 3, Art. no. 3, Mar. 2008, doi: 10.1038/nchembio.72.

[9] J. M. Berg, J. L. Tymoczko, G. J. Gatto jr., and L. Stryer, 'Die oxidative Phosphorylierung', in *Stryer Biochemie*, J. M. Berg, J. L. Tymoczko, G. J. Gatto jr., and L. Stryer, Eds., Berlin, Heidelberg: Springer, 2018, pp. 613–660. doi: 10.1007/978-3-662-54620-8_18.

[10] 'Coordination chemistry of copper proteins: How nature handles a toxic cargo for essential function', *J. Inorg. Biochem.*, vol. 107, no. 1, Art. no. 1, Feb. 2012, doi: 10.1016/j.jinorgbio.2011.11.024.

[11] F. Aguilera, C. McDougall, and B. M. Degnan, 'Origin, evolution and classification of type-3 copper proteins: lineage-specific gene expansions and losses across the Metazoa', *BMC Evol. Biol.*, vol. 13, p. 96, May 2013, doi: 10.1186/1471-2148-13-96.

[12] S. Zhang, 'Recent Advances of Polyphenol Oxidases in Plants', *Molecules*, vol. 28, no. 5, Art. no. 5, Feb. 2023, doi: 10.3390/molecules28052158.

[13] M. Pretzler and A. Rompel, 'What causes the different functionality in type-III-copper enzymes? A state of the art perspective', *Bioinorg. Bio-Inspired Chem. Copp.*, vol. 481, pp. 25–31, Sep. 2018, doi: 10.1016/j.ica.2017.04.041.

[14] B. Cherinka *et al.*, 'Marvin: A Tool Kit for Streamlined Access and Visualization of the SDSS-IV MaNGA Data Set', *aj*, vol. 158, no. 2, p. 74, Aug. 2019, doi: 10.3847/1538-3881/ab2634.

[15] L. T. Tran, J. S. Taylor, and C. P. Constabel, 'The polyphenol oxidase gene family in land plants: Lineage-specific duplication and expansion', *BMC Genomics*, vol. 13, no. 1, Art. no. 1, Aug. 2012, doi: 10.1186/1471-2164-13-395.

[16] C. Kaintz *et al.*, 'Cloning and functional expression in E. coli of a polyphenol oxidase transcript from Coreopsis grandiflora involved in aurone formation', *FEBS Lett.*, vol. 588, no. 18, Art. no. 18, Sep. 2014, doi: 10.1016/j.febslet.2014.07.034.

[17] A. M. Mayer, 'Polyphenol oxidases in plants and fungi: Going places? A review', *Phytochemistry*, vol. 67, no. 21, Art. no. 21, Nov. 2006, doi: 10.1016/j.phytochem.2006.08.006.

[18] I. Mazziotti, G. Petrarolo, and C. La Motta, 'Aurones: A Golden Resource for Active Compounds', *Molecules*, vol. 27, no. 1, Art. no. 1, Dec. 2021, doi: 10.3390/molecules27010002.

[19] H. Jia *et al.*, 'Overexpression of Polyphenol Oxidase Gene in Strawberry Fruit Delays the Fungus Infection Process', *Plant Mol. Biol. Report.*, vol. 34, no. 3, Art. no. 3, Jun. 2016, doi: 10.1007/s11105-015-0946-y.

[20] S. Zhang, 'Recent Advances of Polyphenol Oxidases in Plants', *Molecules*, vol. 28, no. 5, Art. no. 5, Jan. 2023, doi: 10.3390/molecules28052158.

[21] M.-A. McLarin and I. K. H. Leung, 'Substrate specificity of polyphenol oxidase', *Crit. Rev. Biochem. Mol. Biol.*, vol. 55, no. 3, Art. no. 3, May 2020, doi: 10.1080/10409238.2020.1768209.

[22] A. Bijelic, M. Pretzler, C. Molitor, F. Zekiri, and A. Rompel, 'The Structure of a Plant Tyrosinase from Walnut Leaves Reveals the Importance of "Substrate-Guiding Residues" for Enzymatic Specificity', *Angew. Chem. Int. Ed Engl.*, vol. 54, no. 49, Art. no. 49, Dec. 2015, doi: 10.1002/anie.201506994.

[23] F. Panis, I. Kampatsikas, A. Bijelic, and A. Rompel, 'Conversion of walnut tyrosinase into a catechol oxidase by site directed mutagenesis', *Sci. Rep.*, vol. 10, no. 1, p. 1659, Feb. 2020, doi: 10.1038/s41598-020-57671-x.

[24] M. Pretzler, A. Bijelic, and A. Rompel, 'Heterologous expression and characterization of functional mushroom tyrosinase (AbPPO4)', *Sci. Rep.*, vol. 7, p. 1810, May 2017, doi: 10.1038/s41598-017-01813-1.

[25] I. Kampatsikas, A. Bijelic, and A. Rompel, 'Biochemical and structural characterization of tomato polyphenol oxidases provide novel insights into their substrate specificity', *Sci. Rep.*, vol. 9, no. 1, Art. no. 1, Mar. 2019, doi: 10.1038/s41598-019-39687-0.

[26] N. Teribia, C. Buvé, D. Bonerz, J. Aschoff, M. Hendrickx, and A. V. Loey, 'Impact of processing and storage conditions on color stability of strawberry puree: The role of PPO reactions revisited', *J. Food Eng.*, vol. 294, p. 110402, Apr. 2021, doi: 10.1016/j.jfoodeng.2020.110402.

[27] Y. Liang, K. Luo, B. Wang, B. Huang, P. Fei, and G. Zhang, 'Inhibition of polyphenol oxidase for preventing browning in edible mushrooms: A review', *J. Food Sci.*, vol. n/a, no. n/a, Art. no. n/a, Nov. 2024, doi: 10.1111/1750-3841.17322.

[28] G. Carletti, G. Nervo, and L. Cattivelli, 'Flavonoids and Melanins: A Common Strategy across Two Kingdoms', *Int. J. Biol. Sci.*, vol. 10, pp. 1159–1170, Oct. 2014, doi: 10.7150/ijbs.9672.

[29] A. Tilley, M. P. McHenry, J. A. McHenry, V. Solah, and K. Bayliss, 'Enzymatic browning: The role of substrates in polyphenol oxidase mediated browning', *Curr. Res. Food Sci.*, vol. 7, p. 100623, Oct. 2023, doi: 10.1016/j.crfs.2023.100623.

[30] Z. Zhang, X. Pang, Z. Ji, and Y. Jiang, 'Role of anthocyanin degradation in litchi pericarp browning', *Food Chem.*, vol. 75, no. 2, Art. no. 2, Nov. 2001, doi: 10.1016/S0308-8146(01)00202-3.

[31] W. Cao *et al.*, 'Unraveling the Structure and Function of Melanin through Synthesis', *J. Am. Chem. Soc.*, vol. 143, no. 7, Art. no. 7, Feb. 2021, doi: 10.1021/jacs.0c12322.

[32] L. Le, J. Sirés-Campos, G. Raposo, C. Delevoye, and M. S. Marks, 'Melanosome Biogenesis in the Pigmentation of Mammalian Skin', *Integr. Comp. Biol.*, vol. 61, no. 4, Art. no. 4, May 2021, doi: 10.1093/icb/icab078.

[33] Y.-F. Fan *et al.*, 'Spectrophotometric Assays for Sensing Tyrosinase Activity and Their Applications', *Biosensors*, vol. 11, no. 8, Art. no. 8, Aug. 2021, doi: 10.3390/bios11080290.

[34] J. L. Muñoz, F. García-Molina, R. Varón, J. N. Rodriguez-Lopez, F. García-Cánovas, and J. Tudela, 'Calculating molar absorptivities for quinones: Application to the measurement of tyrosinase activity', *Anal. Biochem.*, vol. 351, no. 1, pp. 128–138, Apr. 2006, doi: 10.1016/j.ab.2006.01.011.

[35] C. Battistella *et al.*, 'Mimicking Natural Human Hair Pigmentation with Synthetic Melanin', *ACS Cent. Sci.*, vol. 6, no. 7, pp. 1179–1188, Jul. 2020, doi: 10.1021/acscentsci.0c00068.

[36] L. Pourcel, J.-M. Routaboul, V. Cheynier, L. Lepiniec, and I. Debeaujon, 'Flavonoid oxidation in plants: from biochemical properties to physiological functions', *Trends Plant Sci.*, vol. 12, no. 1, pp. 29–36, Jan. 2007, doi: 10.1016/j.tplants.2006.11.006.

[37] *ChemSketch Freeware*. Advanced Chemistry Development, Inc. (ACD/Labs), Toronto, ON, Canada. [Online]. Available: www.acdlabs.com.

[38] W. Liu *et al.*, 'The Flavonoid Biosynthesis Network in Plants', *Int. J. Mol. Sci.*, vol. 22, no. 23, Art. no. 23, Nov. 2021, doi: 10.3390/ijms222312824.

[39] B. J. Glover and C. Martin, 'Anthocyanins', *Curr. Biol.*, vol. 22, no. 5, Art. no. 5, Mar. 2012, doi: 10.1016/j.cub.2012.01.021.

[40] L. Y. Foo and J. J. Karchesy, 'Chemical Nature of Phlobaphenes', in *Chemistry and Significance of Condensed Tannins*, R. W. Hemingway, J. J. Karchesy, and S. J. Branham, Eds., Boston, MA: Springer US, 1989, pp. 109–118. doi: 10.1007/978-1-4684-7511-1_6.

[41] B. Alappat and J. Alappat, 'Anthocyanin Pigments: Beyond Aesthetics', *Molecules*, vol. 25, no. 23, p. 5500, Nov. 2020, doi: 10.3390/molecules25235500.

[42] M. Gössinger *et al.*, 'Effects of processing parameters on colour stability of strawberry nectar from puree', *J. Food Eng.*, vol. 90, no. 2, pp. 171–178, Jan. 2009, doi: 10.1016/j.jfoodeng.2008.06.018.

[43] F. Fang *et al.*, 'An Intracellular Laccase Is Responsible for Epicatechin-Mediated Anthocyanin Degradation in Litchi Fruit Pericarp1[OPEN]', *Plant Physiol.*, vol. 169, no. 4, pp. 2391–2408, Dec. 2015, doi: 10.1104/pp.15.00359.

[44] Y.-W. Zhao, C.-K. Wang, X.-Y. Huang, and D.-G. Hu, 'Anthocyanin stability and degradation in plants', *Plant Signal. Behav.*, vol. 16, no. 12, Art. no. 12, Jul. 2024, doi: 10.1080/15592324.2021.1987767.

[45] H. Yuan *et al.*, 'The complexity of the Fragaria x ananassa (octoploid) transcriptome by single-molecule long-read sequencing', *Hortic. Res.*, vol. 6, no. 1, pp. 1–14, Apr. 2019, doi: 10.1038/s41438-019-0126-6.

[46] K. Salas-Arias *et al.*, 'Strawberry Fragaria x ananassa cv. Festival: A Polyphenol-Based Phytochemical Characterization in Fruit and Leaf Extracts', *Molecules*, vol. 28, no. 4, p. 1865, Feb. 2023, doi: 10.3390/molecules28041865.

[47] J. A. Rothwell *et al.*, 'Phenol-Explorer 2.0: a major update of the Phenol-Explorer database integrating data on polyphenol metabolism and pharmacokinetics in humans and experimental animals', *Database*, vol. 2012, p. bas031, Jan. 2012, doi: 10.1093/database/bas031.

[48] J. A. Rothwell *et al.*, 'Phenol-Explorer 3.0: a major update of the Phenol-Explorer database to incorporate data on the effects of food processing on polyphenol content', *Database*, vol. 2013, p. bat070, Jan. 2013, doi: 10.1093/database/bat070.

[49] 'Phenol-Explorer: an online comprehensive database on polyphenol contents in foods | Database | Oxford Academic'. Accessed: Dec. 18, 2024. [Online]. Available: https://academic.oup.com/database/article/doi/10.1093/database/bap024/401207?login=true

[50] P. Nokthai, V. S. Lee, and L. Shank, 'Molecular Modeling of Peroxidase and Polyphenol Oxidase: Substrate Specificity and Active Site Comparison', *Int. J. Mol. Sci.*, vol. 11, no. 9, pp. 3266–3276, Sep. 2010, doi: 10.3390/ijms11093266.

[51] M. López-Serrano and A. Ros Barceló, 'Comparative Study of the Products of the Peroxidase-Catalyzed and the Polyphenoloxidase-Catalyzed (+)-Catechin Oxidation. Their Possible Implications in Strawberry (Fragaria × ananassa) Browning Reactions', *J. Agric. Food Chem.*, vol. 50, no. 5, pp. 1218–1224, Feb. 2002, doi: 10.1021/jf010902z.

[52] Y. Li, M. Pi, Q. Gao, Z. Liu, and C. Kang, 'Updated annotation of the wild strawberry Fragaria vesca V4 genome', *Hortic. Res.*, vol. 6, no. 1, Art. no. 1, May 2019, doi: 10.1038/s41438-019-0142-6.

[53] E. C. Meng *et al.*, 'UCSF ChimeraX: Tools for structure building and analysis', *Protein Sci.*, vol. 32, no. 11, p. e4792, Nov. 2023, doi: 10.1002/pro.4792.

[54] Bethesda (MD): National Library of Medicine (US), National Center for Biotechnology Information, 'National Center for Biotechnology Information (NCBI)'. [Online]. Available: https://www.ncbi.nlm.nih.gov/

[55] Henrik Nielsen, 'DTU Health Tech Department of Health Technology', TargetP - 2.0. [Online]. Available: https://services.healthtech.dtu.dk/services/TargetP-2.0/

[56] N. Hamdan, C. H. Lee, S. L. Wong, C. E. Fauzi, N. M. Zamri, and T. H. Lee, 'Prevention of Enzymatic Browning by Natural Extracts and Genome-Editing: A Review on Recent Progress', *Molecules*, vol. 27, no. 3, 2022, doi: 10.3390/molecules27031101.

[57] C. Queiroz, M. L. Mendes Lopes, E. Fialho, and V. L. Valente-Mesquita, 'Polyphenol Oxidase: Characteristics and Mechanisms of Browning Control', *Food Rev. Int.*, vol. 24, no. 4, pp. 361–375, Sep. 2008, doi: 10.1080/87559120802089332.

[58] Y. Jiang and J. Fu, 'Inhibition of polyphenol oxidase and the browning control of litchi fruit by glutathione and citric acid', *Food Chem.*, vol. 62, no. 1, pp. 49–52, May 1998, doi: 10.1016/S0308-8146(97)00144-1.

[59] X. Tian, Y. Lv, Z. Wang, L. Rao, and Y. Wang, 'Identification of natural inhibitors targeting polyphenol oxidase through machine learning-assisted virtual screening and investigation of molecular mechanisms using multispectral experiments', *LWT*, vol. 208, p. 116699, Sep. 2024, doi: 10.1016/j.lwt.2024.116699.

[60] 'PDB-101: Educational resources supporting molecular explorations through biology and medicine - Zardecki - 2022 - Protein Science - Wiley Online Library'. Accessed: Dec. 18, 2024. [Online]. Available: https://onlinelibrary.wiley.com/doi/10.1002/pro.4200

[61] A. Bijelic and A. Rompel, 'Polyoxometalates: more than a phasing tool in protein crystallography', *Chemtexts*, vol. 4, no. 3, p. 10, 2018, doi: 10.1007/s40828-018-0064-1.

[62] B. Rupp, *BIOMOLECULAR CRYSTALOGRAPHY Principles, Practice, and Application to Structural Biology*. 270 MadisonAvenue, New York 10016, USA and 2Park Square, Milton Park, Abingdon, OX14 4RN, UK: Garland Science, Taylor & Francis Group, LCC, 2010.

[63] J. A. Gavira, 'Current trends in protein crystallization', *Arch. Biochem. Biophys.*, vol. 602, pp. 3–11, Jul. 2016, doi: 10.1016/j.abb.2015.12.010.

[64] 'Crystallization Strategies', in *PROTEIN CRYSTALLIZATION TECHNIQUES, STRATEGIES, AND TIPS ALaboratory Manual edited by Terese M. Bergfors*, La Jolla, CA 92038-2525, USA: International University Line, 1999, pp. 69–76.

[65] 'Precipitants', in *PROTEIN CRYSTALLIZATION TECHNIQUES, STRATEGIES, AND TIPS ALaboratory Manual edited by Terese M. Bergfors*, La Jolla, CA 92038-2525, USA: International University Line, 1999, pp. 39–50.

[66] H. Tanaka, R. Utata, K. Tsuganezawa, S. Takahashi, and A. Tanaka, 'Through Diffusion Measurements of Molecules to a Numerical Model for Protein Crystallization in Viscous Polyethylene Glycol Solution', *Crystals*, vol. 12, no. 7, 2022, doi: 10.3390/cryst12070881.

[67] S. Safe, A. Jayaraman, R. S. Chapkin, M. Howard, K. Mohankumar, and R. Shrestha, 'Flavonoids: structure–function and mechanisms of action and opportunities for drug development', *Toxicol. Res.*, vol. 37, no. 2, Art. no. 2, Jan. 2021, doi: 10.1007/s43188-020-00080-z.

[68] G. Zeng, 'Sticky-End PCR: New Method for Subcloning', *BioTechniques*, vol. 25, no. 2, Art. no. 2, Aug. 1998, doi: 10.2144/98252bm05.

[69] J. Mistry *et al.*, 'Pfam: The protein families database in 2021', *Nucleic Acids Res.*, vol. 49, no. D1, pp. D412–D419, Jan. 2021, doi: 10.1093/nar/gkaa913.

[70] A. Waterhouse *et al.*, 'SWISS-MODEL: homology modelling of protein structures and complexes', *Nucleic Acids Res.*, vol. 46, no. W1, pp. W296–W303, Jul. 2018, doi: 10.1093/nar/gky427.

[71] B. Grey and T. R. Steck, 'Concentrations of Copper Thought To Be Toxic to Escherichia coli Can Induce the Viable but Nonculturable Condition', *Appl. Environ. Microbiol.*, vol. 67, no. 11, pp. 5325–5327, Nov. 2001, doi: 10.1128/AEM.67.11.5325-5327.2001.

[72] A. Magnusdottir, I. Johansson, L.-G. Dahlgren, P. Nordlund, and H. Berglund, 'Enabling IMAC purification of low abundance recombinant proteins from E. coli lysates', *Nat. Methods*, vol. 6, no. 7, Art. no. 7, Jul. 2009, doi: 10.1038/nmeth0709-477.

[73] E. Gasteiger *et al.*, 'Protein Identification and Analysis Tools on the ExPASy Server', in *The Proteomics Protocols Handbook*, J. M. Walker, Ed., Totowa, NJ: Humana Press, 2005, pp. 571–607. doi: 10.1385/1-59259-890-0:571.

[74] U. K. Laemmli, 'Cleavage of Structural Proteins during the Assembly of the Head of Bacteriophage T4', *Nature*, vol. 227, no. 5259, pp. 680–685, Aug. 1970, doi: 10.1038/227680a0.

[75] S. M. Hejazi, M. Erfan, and S. A. Mortazavi, 'Precipitation Reaction of SDS and Potassium Salts in Flocculation of a Micronized Megestrol Acetate Suspension', *Iran. J. Pharm. Res. IJPR*, vol. 12, no. 3, pp. 239–246, 2013.

[76] A. Ortega, D. Amorós, and J. García de la Torre, 'Prediction of Hydrodynamic and Other Solution Properties of Rigid Proteins from Atomic- and Residue-Level Models', *Biophys. J.*, vol. 101, no. 4, pp. 892–898, Aug. 2011, doi: 10.1016/j.bpj.2011.06.046.

[77] J. Jumper *et al.*, 'Highly accurate protein structure prediction with AlphaFold', *Nature*, vol. 596, no. 7873, pp. 583–589, 2021, doi: 10.1038/s41586-021-03819-2.

[78] P. M. Hanna, R. Tamilarasan, and D. R. McMillin, 'Cu(I) analysis of blue copper proteins', *Biochem. J.*, vol. 256, no. 3, pp. 1001–1004, Dec. 1988, doi: 10.1042/bj2561001.

[79] 'A Peptide-Induced Self-Cleavage Reaction Initiates the Activation of Tyrosinase - Kampatsikas - 2019 - Angewandte Chemie International Edition - Wiley Online Library'. Accessed: Dec. 18, 2024. [Online]. Available: https://onlinelibrary.wiley.com/doi/10.1002/anie.201901332

[80] C. Molitor, S. G. Mauracher, and A. Rompel, 'Crystallization and preliminary crystallographic analysis of latent, active and recombinantly expressed aurone synthase, a polyphenol oxidase, from Coreopsis grandiflora', *Acta Crystallogr. Sect. F Struct. Biol. Commun.*, vol. 71, no. 6, Art. no. 6, Jun. 2015, doi: 10.1107/S2053230X15007542.

[81] V. M. Virador *et al.*, 'Cloning, Sequencing, Purification, and Crystal Structure of Grenache (Vitis vinifera) Polyphenol Oxidase', *J. Agric. Food Chem.*, vol. 58, no. 2, Art. no. 2, Jan. 2010, doi: 10.1021/jf902939q.

[82] T. Klabunde, C. Eicken, J. C. Sacchettini, and B. Krebs, 'Crystal structure of a plant catechol oxidase containing a dicopper center', *Nat. Struct. Biol.*, vol. 5, no. 12, Art. no. 12, Dec. 1998, doi: 10.1038/4193.

[83] T. M. Berfors, *PROTEIN CRYSTALLIZATION TECHNIQUES, STRATEGIES, AND TIPS ALaboratory Manual edited by Terese M. Bergfors*. La Jolla, CA 92038-2525, USA: International University Line, 1999.

[84] I. Kampatsikas, A. Bijelic, M. Pretzler, and A. Rompel, 'In crystallo activity tests with latent apple tyrosinase and two mutants reveal the importance of the mutated sites for polyphenol oxidase activity', *Acta Crystallogr. Sect. F Struct. Biol. Commun.*, vol. 73, no. 8, pp. 491–499, Aug. 2017, doi: 10.1107/S2053230X17010822.

[85] K. Raghunathan, P. T. Harris, and D. N. Arvidson, 'Trial by fire: are the crystals macromolecules?', *Acta Crystallograph. Sect. F Struct. Biol. Cryst. Commun.*, vol. 66, no. 5, Art. no. 5, May 2010, doi: 10.1107/S1744309110012078.

[86] K.-D. Jany, G. Lederer, and B. Mayer, 'Amino acid sequence of proteinase K from the mold *Tritirachium album* Limber', *FEBS Lett.*, vol. 199, no. 2, pp. 139–144, Apr. 1986, doi: 10.1016/0014-5793(86)80467-7.

[87] B. Lorber, F. Fischer, M. Bailly, H. Roy, and D. Kern, 'Protein analysis by dynamic light scattering: Methods and techniques for students', *Biochem. Mol. Biol. Educ.*, vol. 40, no. 6, Art. no. 6, 2012, doi: 10.1002/bmb.20644.

[88] N. A. F. Zawawi, N. A. Md. Hazmi, M. S. How, K. Kantono, F. V. M. Silva, and A. Sulaiman, 'Thermal, High Pressure, and Ultrasound Inactivation of Various Fruit Cultivars' Polyphenol Oxidase: Kinetic Inactivation Models and Estimation of Treatment Energy Requirement', *Appl. Sci.*, vol. 12, no. 4, 2022, doi: 10.3390/app12041864.

[89] A. eddine Derardja, M. Pretzler, M. Barkat, and A. Rompel, 'Extraction, Purification, and Characterization of Olive (Olea europaea L., cv. Chemlal) Polyphenol Oxidase', *J. Agric. Food Chem.*, vol. 72, no. 6, pp. 3099–3112, Feb. 2024, doi: 10.1021/acs.jafc.3c07776.

[90] 'Hampton Research'. Accessed: Dec. 18, 2024. [Online]. Available: https://hamptonresearch.com/blog-viewing-crystal-experiments-365.html

[91] T. Kuwabara and Y. Katoh, 'Involvement of the Binuclear Copper Site in the Proteolytic Activity of Polyphenol Oxidase', *Plant Cell Physiol.*, vol. 40, no. 10, pp. 1029–1035, Jan. 1999, doi: 10.1093/oxfordjournals.pcp.a029484.

[92] M. H. FAN, M. WANG, and P. ZOU, 'EFFECT OF SODIUM CHLORIDE ON THE ACTIVITY AND STABILITY OF POLYPHENOL OXIDASE FROM FUJI APPLE', *J. Food Biochem.*, vol. 29, no. 2, pp. 221–230, Apr. 2005, doi: 10.1111/j.1745-4514.2005.00025.x.

[93] E. Akyİlmaz, Ş. H. Baysal, and E. DİnÇkaya, 'Investigation of metal activation of a partially purified polyphenol oxidase enzyme electrode', *Int. J. Environ. Anal. Chem.*, vol. 87, no. 10–11, pp. 755–761, Aug. 2007, doi: 10.1080/03067310701327816.

[94] P. Wesche Ebeling, 'Purification of Strawberry Polyphenol Oxidase and Its Role In Anthocyanin Degradation', 1983.

[95] N. Gheibi, A. Saboury, and K. Haghbeen, 'Substrate Construes the Copper and Nickel Ions Impacts on the Mushroom Tyrosinase Activities', *Bull. Korean Chem. Soc.*, vol. 27, pp. 642–648, May 2006, doi: 10.5012/bkcs.2006.27.5.642.

[96] A. el Yaagoubi, M. Kohiyama, and G. Richarme, 'Localization of DnaK (chaperone 70) from Escherichia coli in an osmotic-shock-sensitive compartment of the cytoplasm.', *J. Bacteriol.*, vol. 176, no. 22, pp. 7074–7078, Nov. 1994.

[97] R. C. F. Cheung, J. H. Wong, and T. B. Ng, 'Immobilized metal ion affinity chromatography: a review on its applications', *Appl. Microbiol. Biotechnol.*, vol. 96, no. 6, pp. 1411–1420, Dec. 2012, doi: 10.1007/s00253-012-4507-0.

[98] C. Queiroz, M. L. Mendes Lopes, E. Fialho, and V. L. Valente-Mesquita, 'Polyphenol Oxidase: Characteristics and Mechanisms of Browning Control', *Food Rev. Int.*, vol. 24, no. 4, pp. 361–375, Sep. 2008, doi: 10.1080/87559120802089332.

[99] J. Newman, J. Xu, and M. C. Willis, 'Initial evaluations of the reproducibility of vapor-diffusion crystallization', *Acta Crystallogr. Sect. D*, vol. 63, no. 7, pp. 826–832, Jul. 2007, doi: 10.1107/S0907444907025784.

[100] M. Senda and T. Senda, 'Anaerobic crystallization of proteins.', *Biophys. Rev.*, vol. 10, no. 2, pp. 183–189, Apr. 2018, doi: 10.1007/s12551-017-0345-8.

[101] A. McPherson and J. A. Gavira, 'Introduction to protein crystallization.', *Acta Crystallogr. Sect. F Struct. Biol. Commun.*, vol. 70, no. Pt 1, pp. 2–20, Jan. 2014, doi: 10.1107/S2053230X13033141.

[102] S. Desbois, S. A. Seabrook, and J. Newman, 'Some practical guidelines for UV imaging in the protein crystallization laboratory.', *Acta Crystallograph. Sect. F Struct. Biol. Cryst. Commun.*, vol. 69, no. Pt 2, pp. 201–208, Feb. 2013, doi: 10.1107/S1744309112048634.